Structure of Phospholipids in a Membrane Protein Complex Cytochrome *c* Oxidase from Bovine Heart

A Doctoral Thesis

by

Tsunehiro Mizushima

Submitted to the Graduate School

of Science, Osaka University

Japan

August, 1999

Approval

August, 1999

This thesis is approved as to

style and content by

月原昌文

Member-in-chief

松浦良樹　　後藤祐児

Member　　Member

岡久芳二

Member

Acknowledgements

This work has been carried out under the guidance of Professor Tomitake Tsukihara of the Institute for Protein Research, Osaka University. I would like to thank him heartily for his incessant guidance and encouragement through this work. I am deeply indebted to Professor Shinya Yoshikawa, Himeji Institute of Technology, for his precious guidance and discussions. I am also grateful to Dr. Kyoko Shinzawa-Ito, Himeji Institute of Technology for her technical assistance and helpful suggestion.

I am deeply grateful to Dr. Eiki Yamashita, for his stimulating and helpful advice in this work. I also sincerely thank Associate professor Yoshiki Matsuura and Associate professor Masami Kusunoki, Institute for Protein Research, Osaka University, and Dr. Hiroshi Yamaguchi, Kwansei Gakuin University, for their invaluable advice and help.

I am deeply grateful to Professor Noriyoshi Sakabe and Dr. Nobuhisa Watanabe of Photon Factory, National Laboratory for high Energy Physics for their help in data collection by means of Weissenberg camera and synchrotron radiation.

I also wish sincere thanks to Associate professor Yukio Morimoto, Himeji Institute of Technology, Associate

professor Toshifumi Takao, Institute for Protein Research, Dr. Hiroshi Aoyama, Institute for Chemical and Physical Research, Dr. Satoshi Murakami, Osaka University and Drs. Hiroaki Sakai and Genji Kurisu Institute for Protein Research, Osaka University.

I express my thanks to Dr. Ryosuke Nakashima, Osaka University, Dr. Min Yao, Hokkaido University, Miss Noriko Inoue and Miss Mingjie Fei and all the other members in Prof. Tsukihara's and Prof. Yoshikawa's laboratories for their kind assistance and encouragement.

Finally, I thank my parents for their incessant understanding and encouragement.

水島恒裕

Tsunehiro Mizushima

August, 1999

TABLE OF CONTENTS

Chapter 1. Introduction

1-1. Characterization of phospholipids in biological membranes

Phospholipids

Phospholipids are amphipathic molecules with both hydrophobic tails and hydrophilic end, and they constitute membranes in the biological organism together with such other lipids as glycolipids and cholesterol, and proteins. There are two types of phospholipids, forming the biological membrane. The first one is phosphoglycerides, where the hydroxy groups at C-1 and C-2 of glycerol are esterified by the carboxyl groups of two fatty acid chains and that of C-3 of the glycerol is esterified by a phosphate group.

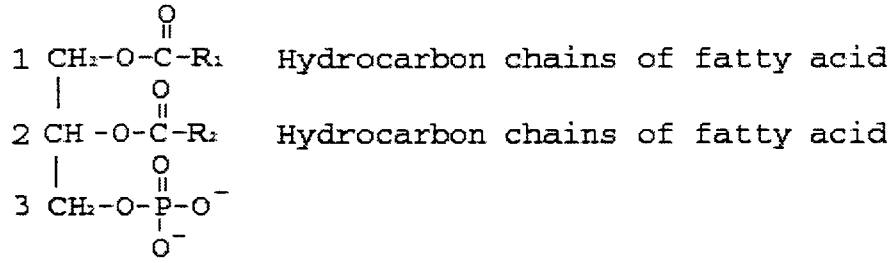

Chemical structure of phosphoglyceride

The second is a kind of sphingosine derivative. Sphingomyeline is the only phospholipid belonging to this type found in the biological membrane.

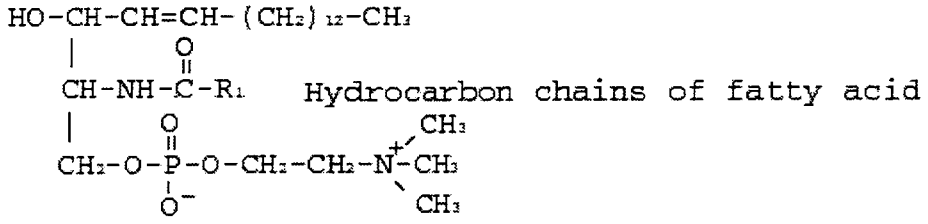

Chemical structure of sphingomyelin

The numbers of carbon and double bond in these fatty acids are different among phospholipids. One fatty acid usually has one or more *cis*-double bonds, while the other tail does not have double bond. Cis-double bonds produce kinks in the hydrocarbon chains that make them more difficult to pack tightly together, so that membrane remains fluid even at lower temperatures.

Three-dimensional structures of synthetic phospholipids have been determined by the X-ray crystal analysis. They are lysophosphatidylcholine (Hauser et al., 1980), dimyristoylphosphatidate (Harlos et al., 1984), dimyristoylphosphatidyl choline (Pearson & Pascher, 1979), dilauroylphosphatidylethanolamine (Hitchcock et al., 1974), dimyristoyl phosphatidyl glycerol (Pascher et al., 1987), and cerebroside (Pascher & Sundell, 1977), as shown in Figure 1.1. The fatty acids of these phospholipids are in trans conformations at the double bond in contrast to those of phospholipids in the biological membrane.

1,2-Dilauloyl-DL-
Phosohatidylethanolamine
(Elder, 1977)

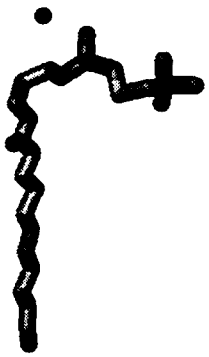

Deoxy-lysophosphatidylcholine
monohydrate
(Hause, 1980)

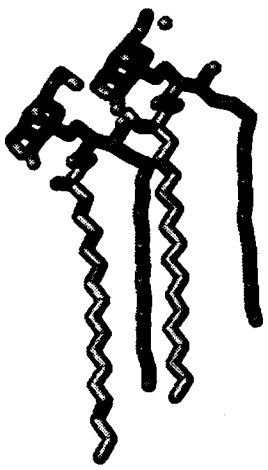

Dihydrocerebroside
(Pascher, 1977)

Figure 1.1. Three dimensional structures of phospholipids

Membranes

Main role of the cell membrane is to separate the intracellular environment from the outside and to maintain the intracellular environment by adjusting the domestic and foreign flow of nutrient, unnecessary things, ions, etc.. Moreover phospholipids in the membrane process the information such as sensory irritation. Intercellular transmission is carried out through cell membrane, while energy conversion systems are equipped in the mitochondrial and thyrakoid membranes. Proteins are the other main components of the biological membranes. The ratio lipids to proteins in the membranes varies according to their function. They are shown in Tables 1.1 and 1.2.

In mitochondria, there are two types of membranes (outer membrane and inner membrane). They form two internal compartments. The structure of outer membrane is like a sieve, which is permeable to all molecules with molecular weight of lower than 5000 daltons, including small proteins. The inner membrane is highly specialized by proteins, which are abundant in the membrane. Various transport proteins are contained in the inner membrane, which give the membrane selective permeability to those small molecules.

Cardiolipin (Hoch, 1992) is involved in critical functions on the activities of the respiratory complexes,

Table 1.1. Lipid composition of membrane preparations (in percentages)

Source	Cholesterol	PC	SM	PE	PI	PS	PG	DPG	PA	Glycolipids
RAT LIVER										
Cytoplasmic membrane	30.0	18	14.0	11	4.0	9.0	-	-	1	-
Endoplasmic reticulum (rough)	6.0	55	3.0	16	8.0	3.0	-	-	-	-
Endoplasmic reticulum (rough)	10.0	55	12.0	21	6.7	-	-	1.9	-	-
Mitochondria (inner)	3.0	45	2.5	24	6.0	1.0	2.0	18.0	0.7	-
Mitochondria (outer)	5.0	50	5.0	23	13.0	2.0	2.5	3.5	1.3	-
Nuclear membrane	10.0	55	3.0	20	7.0	3.0	-	-	1.0	-
Golgi	7.5	40	10.0	15	6.0	3.5	-	-	-	-
Lysosomes	14.0	25	24.0	13	7.0	-	-	5.0	-	-
Myelin	22.0	11	6.0	14	-	7.0	-	-	-	12
RAT ERYTHROCYTE	24.0	31	8.5	15	2.2	7.0	-	-	0.1	3
E.*coli* CYTOPLASMIC MEMBRANE	0	0	-	80	-	-	15.0	5.0	-	-

PC, phosphatidylcholine; SM, sphingomyelin; PE, phosphatidylethanolamine; PI, phosphatidylinositol; PS, phosphatidylserine; PG, phosphatidylglycerol; DPG, diphosphatidylglycerol (cardiolipin); PA, phosphatidic acid.

SOURCE: Adapted from M.K.Jain and R.C.Wagner, 1980, *Introduction to Biological Membranes*, Wiley.

Table 1.2. Chemical composition of some purified membranes (in percentage)

Membrane	Protein	Lipid	Carbohydrate
Myelin	18	79	3
Plasma membrane			
Human erythrocyte	49	43	8
Mouse liver	44	52	4
Ameba	54	42	4
Halobacterium			
Purple membrane	75	25	0
Mitochondrial			
Inner membrane	76	24	0
Chloroplast			
Spinach lamellae	70	30	0

SOURCE: Adapted from G.Guidotti, 1972, *Annu. Rev. Biochem.*

cytochrome *c* oxidase (Awasthi et al., 1971), Complex I, Complex III (Fry & Green, 1981), ATPase activity (Palatini et al., 1977), or the binding of matrix Ca^{2+} (Krebs et al., 1979), the maintenance of mitochondrial membrane permeability (Cullis et al., 1979), and the mitochondrial protein import (Endo et al., 1989; Eilers et al., 1989). Cardiolipin has been postulated to play roles in disease processes such as mitochondrial dysfunction of aging (Ames et al., 1995; Shigenaga et al., 1994).

Lipids are basic components of any biological membrane architecture, while membrane proteins provide the membrane specific functions. There are two types of membrane proteins. One is peripheral membrane proteins that do not extend into the hydrophobic interior of the lipid bilayer at all, being bound to either face of the membrane by noncovalent interactions. The peripheral membrane proteins are able to be removed from the membrane by mild treatment without detergent. The other is integral membrane protein that extends into the lipid bilayer. These transmembrane proteins are amphipathic, having both hydrophobic and hydrophilic regions. Their hydrophobic regions pass through the membrane and interact with the hydrophobic tails of the phospholipid molecules in the interior of the bilayer. Their hydrophilic regions are exposed to one or the other side

of the membrane.

The cell membrane has various functions *in vivo*, most of which are concerned with membrane proteins. However some membrane proteins require specific phospholipid in order to function. The role of phospholipid may be more complicated than what we have understood.

Several phospholipids have been found in the structure of membrane protein by the electron diffraction and X-ray method. The structure of bacteriorhodopsin from *Halobacterium halobium* has two sulfated triglycoside lipids per monomer (Grigorief et al., 1996; Essen et al., 1998). They patch the membrane proteins in oligomers. The glycolipid bridges between protein by several hydrogen bonds and an ionic bond.

In cytochrome *c* oxidase from bovine heart (Tsukihara et al., 1996) and that of *Paracoccus denifitricans* (Iwata et al., 1995), eight and one phospholipid site, respectively have been reported by X-ray diffraction methods at 2.8 Å resolution. Two phosphatidylethanolamines have been located in the structure of cytochrome bc_1 complex from chicken. However structural features of the phospholipids are not clearly shown by the X-ray analyses. Several X-ray structures of synthetic phospholipids have been known (Hitchcock et al., 1974; Pascher & Sundell, 1977; Pearson

& Pascher, 1979; Hauser et al., 1980; Harlos et al., 1984; Pascher et al., 1987), while no chemical structure of a phospholipid from living organism has been determined by the X-ray analysis.

This structural study of phospholipids is performed using cytochrome *c* oxidase. Therefore it is necessary to know the details about cytochrome *c* oxidase.

1-2. Cytochrome *c* oxidase and phospholipids

Cytochrome *c* oxidase is a multicomponent metalloprotein located in the mitochondrial inner membrane. It is the terminal enzyme in mitochondrial respiratory chain, which catalyzes the reaction, $4H^+ + 4e^- + O_2 \rightarrow 2H_2O$. Serial binding and release of four cytochrome *c* molecules to the cytochrome *c* oxidase complex take place to complete the enzyme reaction (Malmström, 1990; Babcock & Wikström, 1992).

As shown in Figure 1.2, the respiratory chain in the mitochondrial inner membrane includes three membrane protein complexes and F_1-F_0 ATP synthetase. NADH-ubiquinone oxidoreductase accepts electrons from NADH and passes them to ubiquinone, and then to cytochrome bc_1 complex. Electrons are passed to cytochrome *c* from bc_1 complex. By using the electrons from cytochrome *c*, cytochrome *c* oxidase

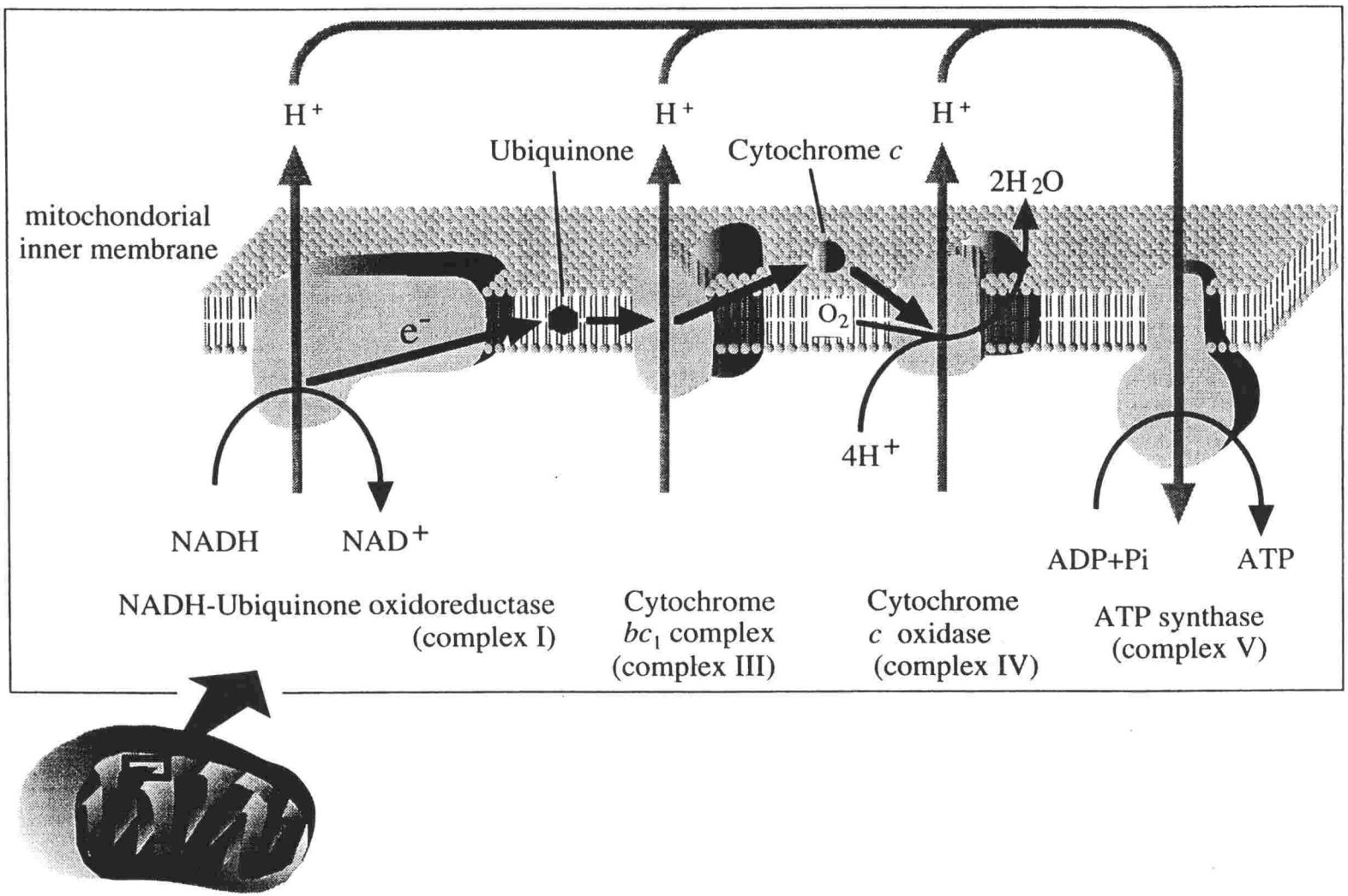

Figure 1.2. Schematic drawing of respiratory chain and ATP synthase.

reduces molecular oxygen to water. When the dioxygen reduction takes place, cytochrome *c* oxidase pumps protons from matrix space to intermembrane space. It is a kind of clean engine that uses proton and electron as fuel. F_1-F_0 ATP synthetase synthesizes ATP from Pi and ADP by using the proton gradient generated by cytochrome *c* oxidase as well as NADH-Ubiquinone oxidoreductase and cytochrome bc_1 complex.

The molecular weight of bovine heart cytochrome *c* oxidase is about 200KD. This enzyme forms a dimeric structure, with a size of 90 X 150 X 130 Å. Cytochrome *c* oxidase monomer is composed of thirteen different subunits (Figure 1.3). Subunit I, II, and III are encoded by mitochondrial DNA, while the other ten subunits (Capaldi, 1990; Kadenbach et al., 1981, 1983) are encoded by nuclear DNA codes. As shown in Figures 1.4 and 1.5 the transmembrane part of the cytochrome *c* oxidase dimer is composed of 56 α-helices. Twelve helices are in subunit I, 7 in subunit III, 2 in subunit II, and 7 in nuclear subunits IV, VIa, VIc, VIIa, VIIb, VIIc, and VIII with one helix in each subunit (Tsukihara et al., 1996).

Cytochrome *c* oxidase contains two heme a moieties (heme a, heme a_3) and two copper sites (Cu_A, Cu_B) in addition to zinc, magnesium, and sodium sites (Malmström, 1990;

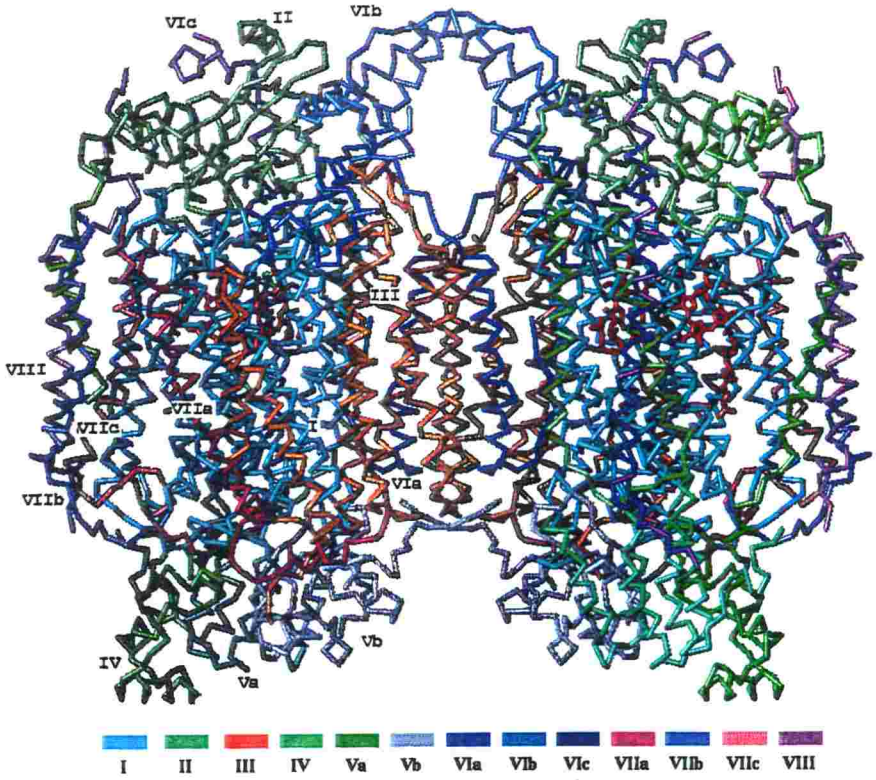

Figure 1.3. The Cα drawing of the dimer of cytochrome *c* oxidase.

A view to the transmembrane surface.

Each monomer consists of 13 different subunits. Figure contains heme a and heme a_3, three Cu atoms, one zinc atom, one magnesium atom (Red). Each subunit has different color.

I

```
                                I                                    II
MFINRWLFST NHKDIGTLYL LFGAWAGMVG TALSLLIRAE LGQPGTLLGD DQIYNVVVTA HAFVMIFFMV 70
                                       III
MPIMIGGFGN WLVPLMIGAP DMAFPRMNNM SFWLLPPSFL LLLASSMVEA GAGTGWTVYP PLAGNLAHAG 140
         IV                                                   V
ASVDLTIFSL HLAGVSSILG AINFITTIIN MKPPAMSQYQ TPLFVWSVMI TAVLLLLSLP VLAAGITMLL 210
                                       VI                                VII
TDRNLNTTFF DPAGGGDPIL YQHLFWFFGH PEVYILILPG FGMISHIVTY YSGKKEPFGY MGMVWAMMSI 280
                                       VIII                              IX
GFLGFIVWAH HMFTVGMDVD TRAYFTSATM IIAIPTGVKV FSWLATLHGG NIKWSPAMMW ALGFIFLFTV 350
                                       X                                 XI
GGLTGIVLAN SSLDIVLHDT YYVVAHFHYV LSMGAVFAIM GGFVHWFPLF SGYTLNDTWA KIHFAIMFVG 420
                                              XII
VNMTFFPQHF LGLSGMPRRY SDYPDAYTMW NTISSMGSFI SLTAVMLMVF IIWEAFASKR EVLTVDLTTT 490

NLEWLNGCPP PYHTFEEPTY VNLK  514
```

II

```
                                       I                                 II
MAYPMQLGFQ DATSPIMEEL LHFHDHTLMI VFLISSLVLY IISLMLTTKL THTSTMDAQE VETIWTILPA 70

IILILIALPS LRILYMMDEI NNPSLTVKTM GHQWYWSYEY TDYEDLSFDS YMIPTSELKP GELRLLEVDN 140

RVVLPMEMTI RMLVSSEDVL HSWAVPSLGL KTDAIPGRLN QTTLMSSRPG LYYGQCSEIC GSNHSFMPIV 210

LELVPLKYFE KWSASML  227
```

III

```
                              I                                   II
MTHQTHAYHM VNPSPWPLTG ALSALLMTSG LTMWFHFNSM TLLMIGLTTN MLTMYQWWRD VIRESTFQGH 70
                    III                                                   IV
HTPAVQKGLR YGMILFIISE VLFFTGFFWA FYHSSLAPTP ELGGCWPPTG IHPLNPLEVP LLNTSVLLAS 140
                                    V                                  VI
GVSITWAHHS LMEGDRKHML QALFITITLG VYFTLLQASE YYEAPFTISD GVYGSTFFVA TGFHGLHVII 210
                                       VII
GSTFLIVCFF RQLKFHFTSN HHFGFEAGAW YWHFVDVVWL FLYVSIYWWG S  261
```

IV

```
AHGSVVKSED YALPSYVDRR DYPLPDVAHV KNLSASQKAL KEKEKASWSS LSIDEKVELY RLKFKESFAE 70
                         I
MNRSTNEWKT VVGAAMFFIG FTALLLIWEK HYVYGPIPHT FEEEWVAKQT KRMLDMKVAP IQGFSAKWDY 140

DKNEWKK  147
```

VIa

ASAAKGDHGG TGARTWRFLT FGLALPSVAL CTLNSWLHSG HRERPAFIPY HHLRIRTKPF SWGDGNHTFF 70

HNPRVNPLPT GYE 84

VIc

STALAKPQMR GLLARRLRFH IVGAFMVSLG FATFYKFAVA EKRKKAYADF YRNYDSMKDF EEMRKAGIFQ 70

SAK 73

VIIa

FENRVAEKQK LFQEDNGLPV HLKGGATDNI LYRVTMTLCL GGTLYSLYCL GWASFPHKK 59

VIIb

IHQKRAPDFH DKYGNAVLAS GATFCVAVWV YMATQIGIEW NPSPVGRVTP KEWREQ 56

VIIc

SHYEEGPGKN IPFSVENKWR LLAMMTLFFG SGFAAPFFIV RHQLLKK 47

VIII

ITAKPAKTPT SPKEQAIGLS VTFLSFLLPA GWVLYHLDNY KKSSAA 46

Figure 1.4. Helix regions of subunits containing transmembrane parts.
Rectangles show α-helix regions as determined from the crystal structure.

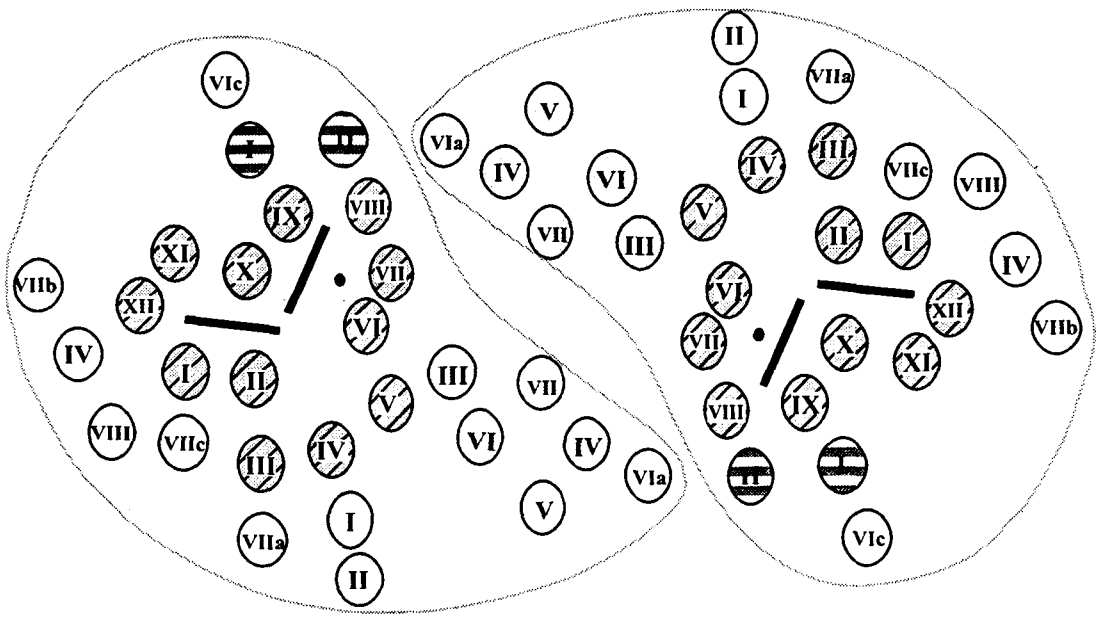

Figure 1.5. A schematic representation for location of transmembrane helices as a cross-section at the membrane surface of the cytosolic side.

Gray bars and small ball denote heme planes and Cu_B, respectively. Black Roman numbers in shaded line, dotted and crossed line circles denote the helix number of subunits I, II and III, respectively. Other numbers indicated nuclear coded subunits.

Capaldi, 1990; Yoshikawa et al., 1998). Heme a, heme a_3 and Cu_B are located in subunit I, while Cu_A and zinc are located in extramembrane subunits II and Vb, respectively. Magnesium is ligated by two amino acids of subunit I, His 368 and His 369, one amino acid of subunit II, Asp 198, and one water molecule. Cu_A is the initial electron-receiving site from cytochrome *c* (Antalis & Palmer, 1982). Two copper atoms are included in Cu_A site, of which one has four ligands in a tetrahedral geometry, and the other is in a slightly distorted trigonal pyramidal geometry. Heme a_3 and CuB form a redox center reducing molecular oxygen to water. Now, fully oxidized, fully reduced, azide-bound, and carbon monoxide-bound states structures are known from the X-ray crystal structure analysis (Yoshikawa et al., 1998). According to the structural analyses, a segment from Gly 49 to Asn 55 moves toward the cytosolic surface by about 4.5Å at the position of carboxyl group of Asp 51 on reduction of the fully oxidized enzyme. The movement indicates the aspartate as the proton pumping site, and suggested a possible mechanism for a unidirectional proton transfer by Asp 51 (Figure 1.6). Three different channels for proton pumping and one possible water channel have been reported in structural analysis of oxidized bovine cytochrome *c* oxidase at 2.3Å.

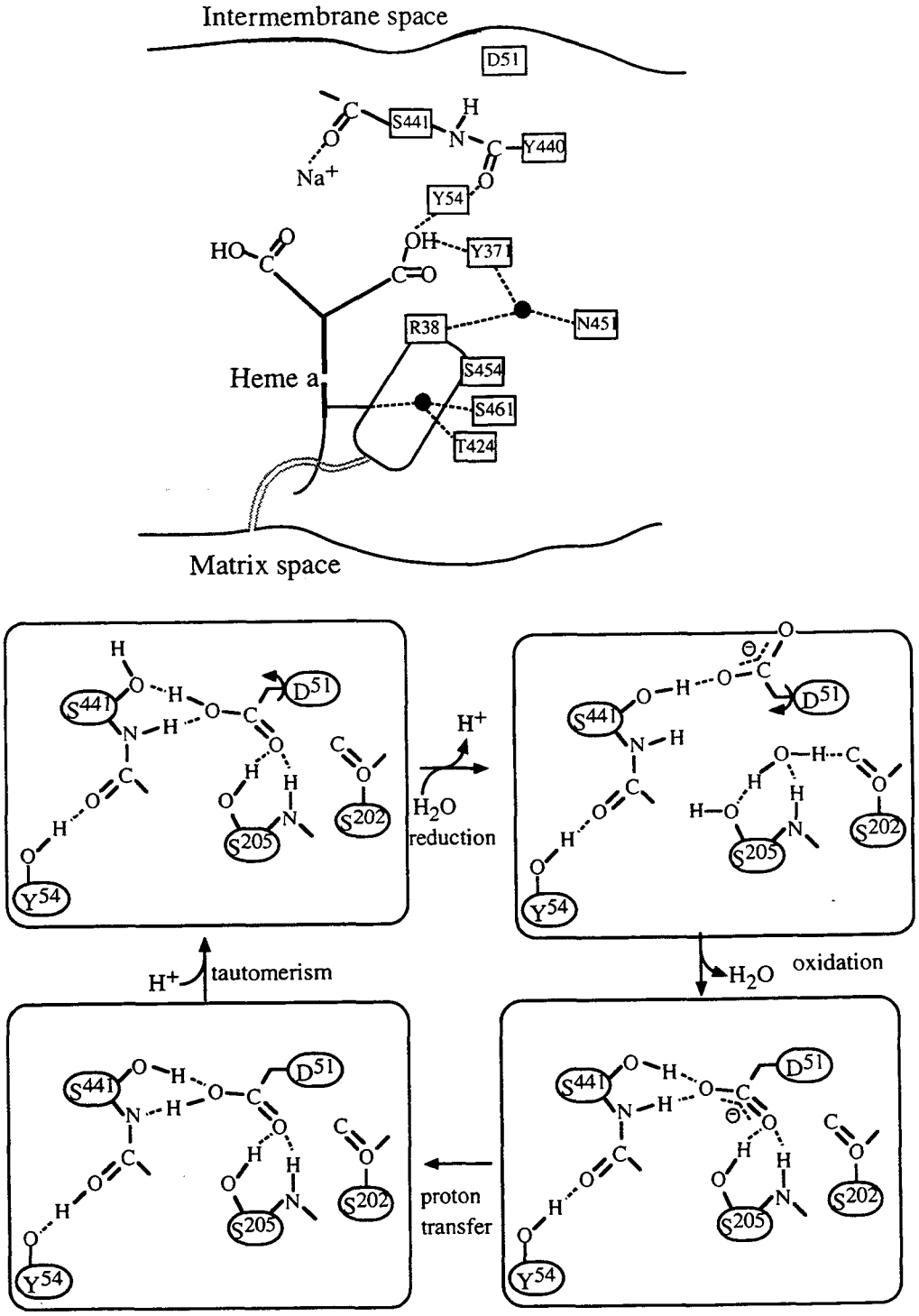

Figure 1.6. Schematic representations of the structure of the proton pumping system and a possible function of Asp51 to the matrix surface.

Cytochrome *c* is the physiological electron donor to cytochrome *c* oxidase in prokaryotes and eukaryotes. Purified mammalian cytochrome *c* oxidase binds one molecule of substrate cytochrome *c* at a high-affinity site this is the electron entry site. The enzyme can bind a second molecule of cytochrome *c* in a lower-affinity site, the function of which remains unclear (Bisson, 1980). Cytochrome *c* is bound to subunit II with negatively charged surface close to the Cu_A site. Six or seven Lys residues around the heme edge of cytochrome *c*, must make ionic pairs with complementary sets of carboxyls (Glu114, Asp112, Asp158, and Glu198 in subunit II) of cytochrome *c* oxidase (Capaldi et al., 1982; Staudenmayer et al., 1977; Reider et al., 1980). The hollow which can hold cytochrome *c* was found in the structure of the cytochrome *c* oxidase.

Purified cytochrome *c* oxidase usually contains several phospholipids (Seelig et al., 1985; Robinson 1993; Soulimane et al., 1995). They are assigned to cardiolipin, phosphatidylethanolamine, and phosphatidylcholine. Cardiolipin and phosphatidylcholine play assistant roles in combining with cytochrome *c* and cytochrome *c* oxidase (Salamon et al., 1996).

Almost all the cardiolipins of the eukaryote cell are in the inner mitochondrial membranes, making up about

one-fifth of the total lipids in the inner membrane (Hoch, 1992). Four binding sites of the cardiolipin in cytochrome *c* oxidase have been reported, of which two were tight binding sites. The binding specificity of cardiolipin indicates that the apolar tails are most important for binding, while the polar head group is not critical (Robinson et al., 1990). These cardiolipins are essential for maximal activity of the complex and could not be replaced by other phospholipids. Recently, activity of cytochrome *c* oxidase concerning to aging is also reported (Paradies et al., 1997,1998). This is due to the reduction in content of cardiolipin by aging. Moreover peroxidation of fatty acids of cardiolipin declines the cytochrome *c* oxidase activity. Cardiolipins can activate these aged cytochrome *c* oxidase. No other phospholipids have such function. Although a lot of studies concerning association of cardiolipin with cytochrome c oxidase have been reported, the binding sites and functions of the cardiolipin are still unknown.

Phospholipids contents of the enzyme used for the present study were examined by Yoshikawa et al (1999). as follows. At first phospholipids were extracted from the crystallization sample by the organic solvent (chloroform, methanol, water, and ammonia). And then they were recovered from the silica gel plate after being separated by the

thin-layer chromatography. Finally, they were analyzed by mass spectrometry. Cardiolipin (CL), phosphatidyl choline (PC), phosphatidyl ethanolamine (PE), and phosphatidyl glycerol (PG) are included in this purification sample (Figure 1.7). Not only the numbers of carbon of fatty acids that compose phospholipids but also the positions of the double bond are determined by the mass spectrometry. Four kinds of phospholipids were identified in crystallization sample of cytochrome *c* oxidase. Their contents were CL:PC:PE:PG = 5-7:1:3-5:3-4, respectively, for each monomer of cytochrome *c* oxidase.

1-3. Purposes of the present research

Phospholipids have been suggested to be necessary for the activities of not only the cytochrome *c* oxidase but also the other membrane proteins. No molecular structure of phospholipid in the membrane protein complex has been reported. Structural studies of phospholipids should allow us to understand deeply the functions of cytochrome *c* oxidase and other membrane proteins. This study is performed in order to know the followings.

1. Structure of phospholipids in the cytochrome *c* oxidase
2. Location of phospholipids in the cytochrome *c* oxidase
3. Functions of phospholipid in the cytochrome *c* oxidase

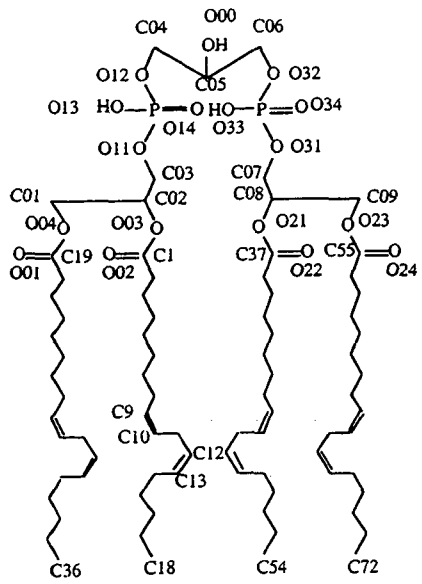

cardiolipin
(diphosphatidylglycerol)

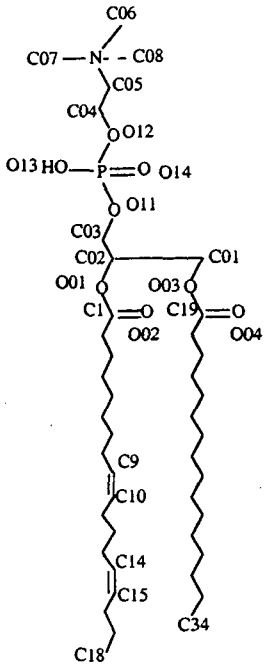

phosphatidylcholine

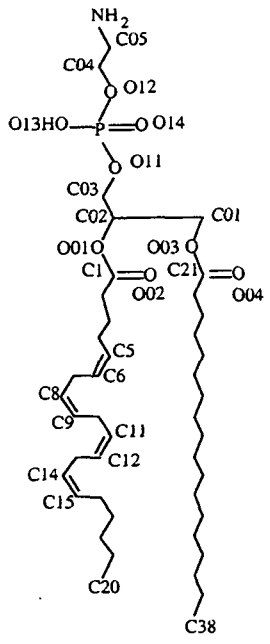

phosphatidylethanolamine

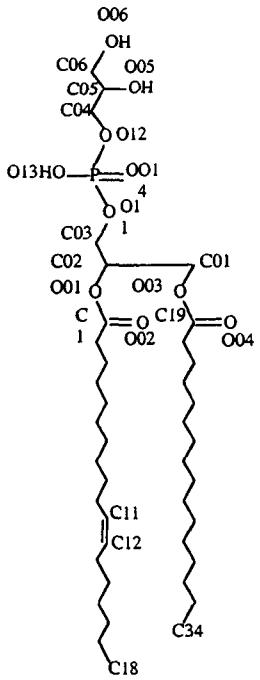

phosphatidylglycerol

Figure 1.7. Chemical structure of phospholipids.

Chapter 2. Structure analyses of cytochrome *c* oxidase

2-1. Mass spectroscopic analysis

Cytochrome *c* oxidase is composed of 13 different subunits per monomer. All the 13 subunits were found in the X-ray structural analysis (Tsukihara et al., 1996). However, several subunits have unclear electron densities at their amino-terminal or carboxyl-terminal segments. Thus the sodium dodecyl sulfate poly acrylamide gel electrophoresis (SDS-PAGE) of this enzyme was carried out to confirm the homogenity of each subunit.

2-1-1. Sample preparation from sodium dodecyl sulfate polyacrylamide gel electrophoresis (SDS-PAGE) gel

The SDS-PAGE was applied to the crystalline sample of the cytochrome *c* oxidase by using 16-22% acrylamide gradient gel. This crystalline sample gave thirteen main bands by staining with the coomassie brilliant blue (Figure 2.1). There was no major impurity detected. However minor bands were detected at two sites, a higher molecular weight of subunit IV and a lower molecular weight of subunit VIa. The ratio of minor and major bands of subunit VIa varied according to preparation of sample. Both subunits might be

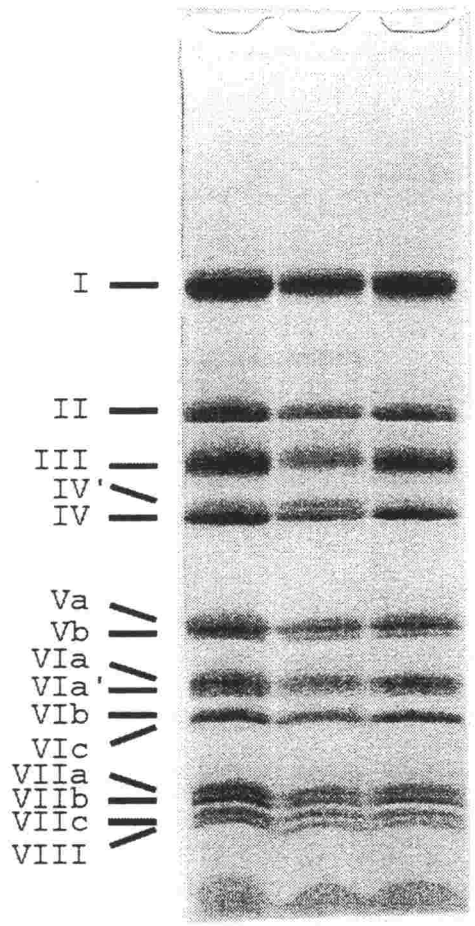

Figure 2.1. SDS-PAGE patterns of cytochrome *c* oxidase The crystalline preparation.

processed excessively after they were synthesized in the ribosome.

Thirteen subunits of cytochrome *c* oxidase and two minor bands were separated by SDS-PAGE, which were extracted from gel to perform the mass spectrometry. Since the SDS-PAGE showed minor bands, molecular masses were analyzed using extracted sample of the SDS-PAGE gel. In order to extract the each band, SDS-PAGE was carried out without staining by coomassie brilliant blue. SDS-PAGE gel was muddied by 3M Na Acetate (Maeshima et al., 1987) to recognize the bands. These bands were cut off from the gel, and were put into deionized water to remove SDS and sodium acetate from them. Since the spectra were perturbed under the existence of buffer, desalination was repeated until the pH of the deionized water became neutral. Finally each subunit was extracted from the SDS-PAGE gel by shaking with 0.4% n-octyl-β-D-glucopyranoside (β-OG) solution and they were desalted by dialyzing against 0.4% β-OG solution with membrane (MILLIPORE VSWP0025).

2-1-2. Analysis of mass spectrometry

Two types of preparations of sample were applied for the mass spectrometric analysis. One was whole complex of the cytochrome *c* oxidase. The other was each subunit that

was extracted from the SDS-PAGE gel of the enzyme complex. Sample solutions were diluted again with equal volume of the matrix solution (matrix solution: 66% saturated aqueous acetonitrile with sinapic acid). Mass spectra of this sample were measured with Voyger Elite (Perseptive Biosystems Co.).

The spectra were analyzed with the GRAMS/386 analysis program. Bovine serum albumin (MW.66431), horse apomyoglobin (MW.8476.78), and bovine insulin (MW.5734.59) were used as standard substances.

2-1-3. Results of mass spectrometry

When whole complex molecule of cytochrome *c* oxidase was applied for the measurement, the peak of subunits IV, Va, Vb, VIa, VIb, VIc, VIIa, VIIb, VIIc and VIII were detected in the mass spectrometry. However subunits I, II and III could not be detected. Molecular weights of subunit I, II and III were determined by spectra with samples cut off from the gel. Results are shown in Table 2.1.

Molecular weights obtained by the experiments for subunit Va, Vb, VIb, VIIb and VIIc were in good agreement with values calculated from the amino acid sequences. For example, molecular weight of subunit VIIb was measured as 6357 Da that was the same as the calculated molecular weight

Table 2.1. Molecular weights of subunits of bovine cytochrome *c* oxidase complex.

Subunit (Chain)		Molecular mass (Calculated mass from DNA sequence)	Molecular mass (X-ray structural analysis value)		Molecular mass (Mass spectrometry value)
I	(1-514)	57032	57060	(1-514) (formylation)	57065
II	(1-261)	26021	26049	(1-261) (formylation)	26180
III	(1-227)	29919	29919	(1-227)	30048
IV	(23-169)	17153	16887	(26-169)	Main 17186 Minor 17378
Va	(1-109)	12436	12068	(5-109)	12433
Vb	(1-98)	10670	10670	(1-98)	10667
VIa	(13-96)	9436 9206 (17-96)	9436	(13-96)	9523 9297
VIb	(1-85)	10021	9398	(7-85)	10061
VIc	(1-73)	8479	8479	(1-73)	8521
VIIa	(22-80)	6674 6243 (Meinecke)	6546	(22-79)	6674
VIIb	(33-88)	6357	5437	(38-86)	6357
VIIc	(17-63)	5441	5441	(17-63)	5438
VIII	(25-70)	4962 (K31) 4990 (R31)	4733 (K31)	(25-67)	4959 4987

from the amino acid composition.

Subunit I

Subunit I had a mass spectrometry molecular mass of 57065 Da, which was 33 mass larger than the value calculated from the sequence. Formylation of N-terminal gave the molecular weight of 57060 Da, which was 5Da smaller than the observed values.

Subunit VIc

The molecular mass of subunit VIc was 42 mass larger than calculated protein molecular weight. The difference suggested acetylation of subunits VIc.

Subunit VIIa

The primary structure of C-terminal of subunit VIIa by Seelan et al. (1991) is different from that by Meinecke et al. (1986) (Figure 2.2). The primary structure from Meinecke et al. (1986) was used for model building of subunit VIIa (Tsukihara et al., 1996). However molecular weights of subunit VIIa determined by the experiment was 6674 Da, which was consistent with that of Seelan et al (1992). After the mass spectroscopic experiment structural model was built according to Seelan et al (1992).

```
                                  62                  73    77  80
Seelan et al.          ------ GGTLYSLYCL GWASFPHKK
Meinecke et al.        ------ GGTLYSLYCL GHASKK
```

Figure 2.2. Primary structures of subunit VIIa

Subunit VIII

Two primary structures of subunit VIII have been reported. Their amino acid residues at 31 were Arg31 (Lightowlers et al., 1990; Anthony et al., 1990) and Lys31 (Meinecke et al., 1984). Present mass spectrometry of subunit VIII gave two peaks with same height, which had molecular mass of 4959 and 4987 Da (Figure 2.3). Subunit VIII, which was composed of 46 amino acids, has calculated molecular weights of 4962Da (K31) and 4990Da (R31). Molecular weights for two mass spectroscopic peaks of subunit VIII were in agreement with values calculated from the reported amino acid sequences with R31 and K31. Though the enzyme complex was purified from the same bovine heart, subunit VIII showed heterogeneous sequences.

Subunit IV

SDS electrophoresis of subunit IV gave a minor band at slightly higher molecular weight site than the main band. When a sample containing both main and minor bands was applied for the mass spectroscopic experiment, two peaks

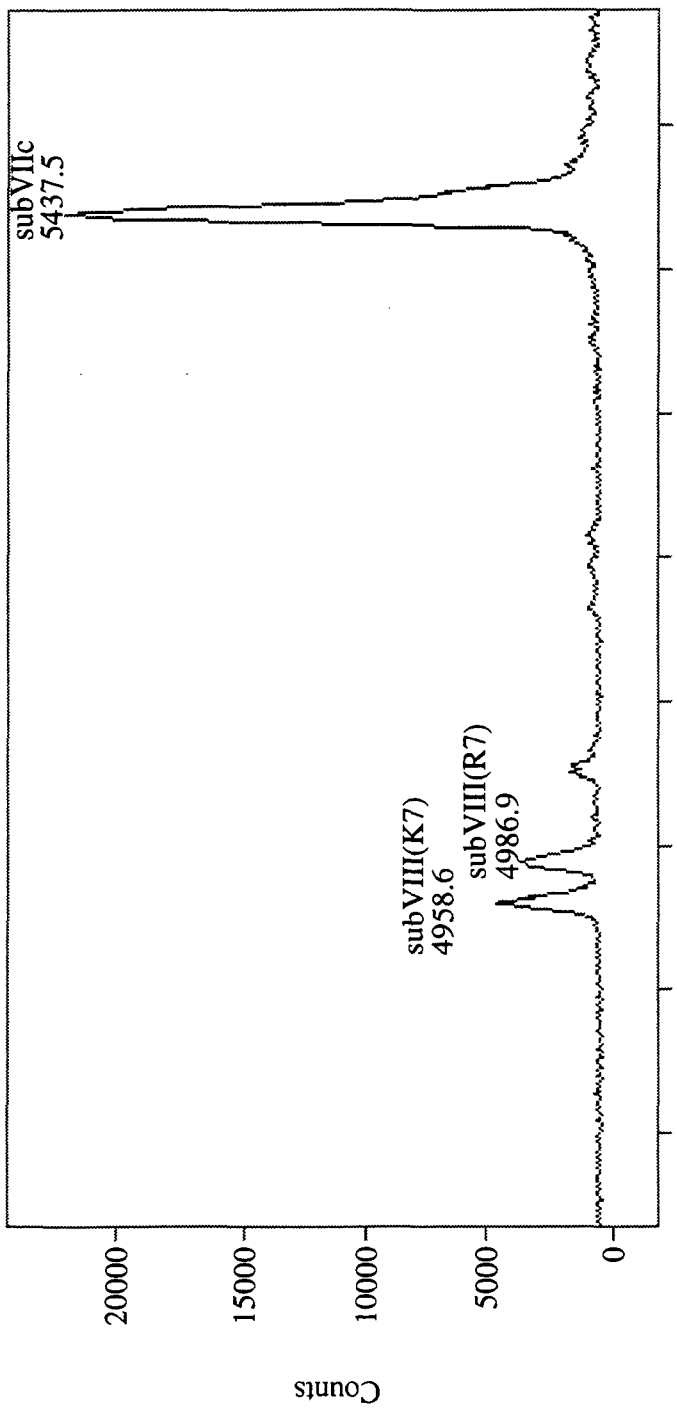

Figure 2.3. Mass analysis of subunit VIII

were detected at molecular weights of 17,186 (main peak) and 17,378 Da (minor peak), respectively (Figure 2.4). Main peak was 33 mass unit larger than the value calculated from the sequence. The molecular mass of minor peak was larger than that of the main peak by about 200Da. This was consistent with SDS electrophoresis experiment. The main peak of subunit IV exhibiting larger than the calculated value by 33 Da implicated formylation of subunit IV as was the case of subunit I. The minor peak was not correspond to the proteolysis of polypeptide. The difference in molecular weight was larger than that in either cases of acetylation and formylation. Phospholylation at two sites in addition to the formylation of N-terminal increases the mass by 190 unit. Although the larger mass by 200 suggested phospholylation at two sites, their sites were not identified by the mass spectroscopy. The subunit IV had multiple post-translational modifications.

Subunit VIa

Two or more peaks of subunit VIa were detected from the mass spectrometry. These peaks were shown in Figure 2.1. Molecular masses of these peaks were 9523 and 9297 Da (Figure 2.5), one of which was larger than the calculated values by 87 and the other was smaller than that by 139 Da,

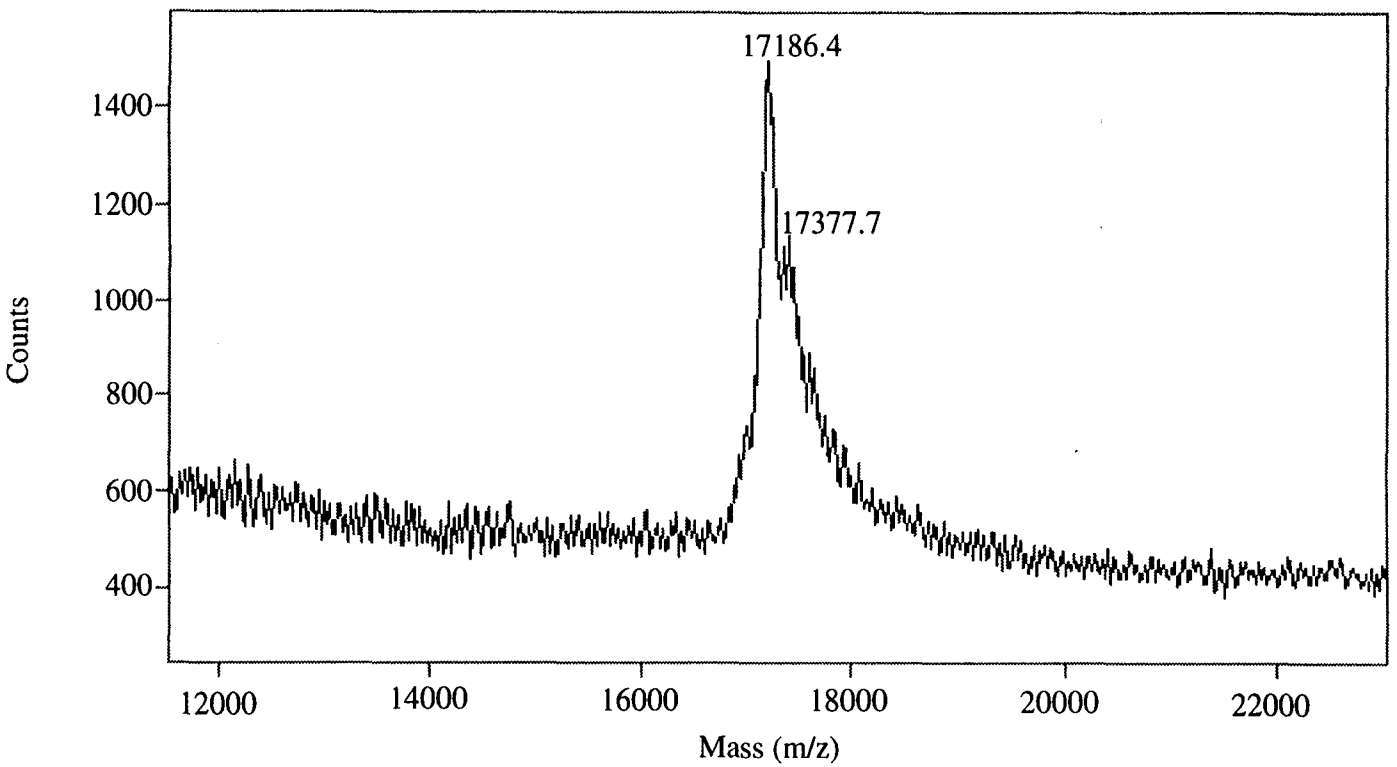

Figure 2.4. Mass analysis of subunit IV

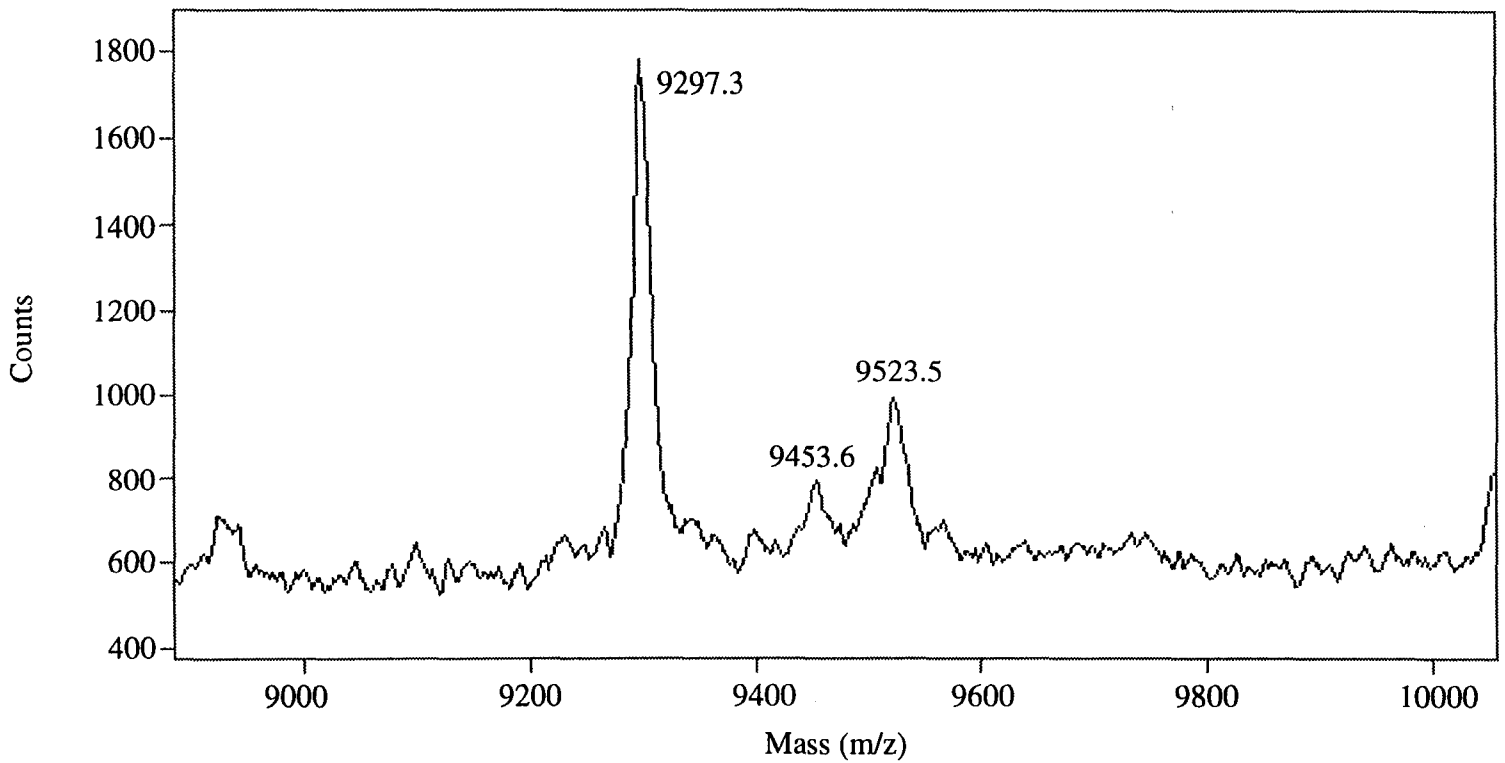

Figure 2.5. Mass analysis of subunit VIa

respectively. The difference in molecular weight between two peaks was 226 Da. According to the sequence analysis, the polypeptide at the minor peak (9257Da) was shortened by three amino acid residues of Ala-Ser-Ala with molecular weight of 230 Da. Then main peak (9523Da) was larger than the value calculated from the sequence by about 80 Da. The difference of molecular weight could be due to post-translational phospholylation. The site of post-translational modification was not at N-terminal three residues.

Subunits II and III

The molecular mass of subunits II and III were larger than estimated values from the sequences by 131 and 129 Da, respectively. The extractive efficiencies of subunits II and III from the electrophoresis were lower than that of other subunits. Thus much smaller amounts of subunits II and III were applied for the mass spectrometry. The large discrepancies were probably because of lower S/N ratio of the peak concerning subunits II and III than those of other subunits measured were.

The results of mass spectrometry were used for model building of protein subunits (Chapter 2-2-3).

2-2. Crystal structure refinement of oxidized cytochrome c oxidase at 2.3 Å resolution

Following 2.8 Å X-ray analysis of cytochrome *c* oxidase, the crystal structural analysis at 2.3 Å resolution was carried out to elucidate fine structures of proteins and phospholipids.

2-2-1. Intensity data collection

Intensity data of oxidized cytochrome *c* oxidase at 2.3 Å resolution were collected with synchrotron radiation at the Photon Factory (BL6A or BL6B), Tsukuba, Japan, by using Weissenberg camera for macromolecular crystals. The crystal was mounted in a capillary. Experimental conditions for X-ray diffraction are given in Table 2.2.a. The X-ray diffraction patterns were recorded on Fuji Film Image Plate with the size of 400 X 800 mm. The crystal of the enzyme belongs to the orthorhombic space group of $P2_12_12_1$ with unit cell dimensions of a = 189.1(4) Å, b = 210.5(3) Å, c = 178.6(3) Å. Crystallographic data is shown in Table 2.2.b.

These crystals diffracted up to 1.9 Å resolution. Since crystals were deteriorated by the synchrotron radiation X-rays, only two or three frames of diffraction were taken at the same position of a crystal. After X-rays were shot at several positions of a crystal, the crystal

Table 2.2 a. Experimental conditions for X-ray diffraction of the crystal by synchrotron radiation source.

X-ray source	Synchrotron radiation Photon Factory at BL6A2 or BL6B
Detector	Weissenberg camera for macromolecule
Collimator	0.1 mm
Wavelength	1.00Å
Camera length	573 mm
Oscillation angle	0.50°
Overlap	0.00°
Rotation speed	0.05° / second
Exposure time	180-350 seconds
Temperature	8 ± 2℃

Table 2.2 b. Crystallographic data of cytochrome *c* oxidase.

Crystal form	Orthorhombic
Space group	$P2_12_12_1$
Cell constants	a = 189.1Å
	b = 210.5Å
	c = 178.6Å
Number of molecules in the unit cell	Z = 8
Volume of asymmetric unit/molecular weight	Vm=4.4 $Å^3$/dalton
Solvent content	Vsolv = 72%

was exchanged. A total of 150 crystals or more were used for the diffraction experiments. Diffraction intensities were processed with the program DENZO (Otwinowski, 1997). One data set was obtained by merging 221 IP images from 32 crystals, which were selected among images from 150 crystals. Scaling and merging of the diffraction intensity were undertakes by the program SCALEPACK (Otwinowski, 1997) (Table 2.3).

2-2-2. Phase determination

Phase determination at 2.3 Å resolution was carried out by the multiple isomorphous replacement (MIR) method. Three heavy atom derivatives (1mM Na_2IrCl_6, 0.5mM Na_2IrCl_6 and CH_3HgCl) were prepared for MIR method. These data sets had been used for structural analysis at 2.8 Å resolution. Heavy atom sites of each derivative were confirmed by each difference Patterson map at 5 Å resolution. The coefficient of the difference Patterson function was $(F_{PH}-F_P)^2$, where F_{PH} and F_P are the structure factor amplitudes of heavy atom derivative and native crystals, respectively. The heavy atom sites were detected at the same sites as those used in the phase calculation at 2.8 Å resolution. The number of heavy atom sites for 1mM Na_2IrCl_6, 0.5mM Na_2IrCl_6 and CH_3HgCl were 9, 1 and 23, respectively. The heavy atom

Table 2.3.a. List of processing intensity data.

Crystal No.	a(Å)	b(Å)	c(Å)	α	β	γ	crysz	crysy	crysx	mosaicity
1-1	189.05	210.92	178.43	90	90	90	135.02	1.255	-86.15	0.073
	189.13	210.94	178.37	90	90	90	135.03	1.130	-86.19	0.054
1-2	189.32	211.02	178.70	90	90	90	135.03	1.061	-86.16	0.100
1-3	189.31	211.03	178.66	90	90	90	135.04	1.071	-86.16	0.100
1-4	189.09	210.96	178.49	90	90	90	135.04	1.128	-86.12	0.053
	189.19	210.96	178.38	90	90	90	135.07	1.056	-86.16	0.056
2-1	188.80	210.22	178.32	90	90	90	136.79	1.974	0.354	0.150
2-2	189.13	211.10	178.64	90	90	90	136.70	1.967	0.322	0.150
3-1	189.36	211.43	178.63	90	90	90	133.65	1.009	-179.0	0.150
3-2	188.85	210.20	178.24	90	90	90	133.75	0.979	-179.0	0.071
	188.85	210.26	178.28	90	90	90	133.83	0.958	-179.0	0.060
3-3	189.38	211.36	178.65	90	90	90	133.75	0.978	-179.1	0.150
4-1	189.06	210.64	178.44	90	90	90	-44.46	-178.9	-175.2	0.064
	189.16	210.86	178.46	90	90	90	-44.48	-178.9	-175.3	0.072
4-2	189.20	211.08	178.58	90	90	90	-44.59	-178.9	-175.3	0.093
	189.06	210.61	178.37	90	90	90	-44.56	-178.9	-175.3	0.095
4-3	189.16	210.99	178.55	90	90	90	-44.55	-178.9	-175.3	0.088
	189.17	210.96	178.51	90	90	90	-44.53	-178.9	-175.3	0.099
	189.13	210.75	178.45	90	90	90	-44.56	-178.9	-175.3	0.088
5-1	189.07	211.12	178.65	90	90	90	-47.17	0.875	1.024	0.100
6-1	189.35	211.50	178.67	90	90	90	-43.95	179.36	173.54	0.100
6-2	189.36	211.47	178.64	90	90	90	-44.05	179.29	173.56	0.100
6-3	189.17	211.07	178.54	90	90	90	-44.09	179.28	173.60	0.064
	189.23	211.14	178.54	90	90	90	-44.02	179.30	173.56	0.065
7-1	189.03	210.77	178.47	90	90	90	-44.00	0.182	-3.280	0.061
	189.16	211.02	178.50	90	90	90	-43.94	0.142	-3.338	0.065
7-2	189.28	211.10	178.64	90	90	90	-43.93	0.136	-3.298	0.100
7-3	189.07	210.91	178.52	90	90	90	-43.95	0.152	-3.283	0.070
	189.16	211.06	178.52	90	90	90	-43.94	0.146	-3.330	0.068
7-4	189.01	210.68	178.49	90	90	90	-43.89	0.091	-3.258	0.073
	189.09	210.88	178.51	90	90	90	-43.95	0.149	-3.289	0.080
	189.11	210.82	178.45	90	90	90	-43.95	0.156	-3.300	0.069
8-1	188.91	210.74	178.46	90	90	90	-44.27	178.86	-172.1	0.053
	188.97	210.82	178.45	90	90	90	-44.28	178.84	-172.2	0.072
8-2	189.20	210.78	178.64	90	90	90	-44.29	178.85	-172.1	0.120
8-3	189.16	210.79	178.66	90	90	90	-44.28	178.90	-172.1	0.120
8-4	188.93	210.79	178.46	90	90	90	-44.34	178.82	-172.1	0.085
	189.02	210.84	178.43	90	90	90	-44.26	178.93	-172.2	0.079
8-5	189.26	210.82	178.62	90	90	90	-44.29	178.87	-172.1	0.100
8-6	188.93	210.78	178.46	90	90	90	-44.32	178.87	-172.1	0.076
	189.05	210.84	178.46	90	90	90	-44.30	178.88	-172.1	0.079
8-7	189.23	210.82	178.64	90	90	90	-44.33	178.84	-172.1	0.100
8-8	189.26	211.00	178.67	90	90	90	-44.32	178.83	-172.1	0.120
9-1	190.41	211.34	179.66	90	90	90	137.39	-179.9	2.198	0.100
9-2	189.46	211.38	178.77	90	90	90	137.25	179.94	2.090	0.092
	189.47	211.41	178.77	90	90	90	137.32	-179.9	2.086	0.096
9-3	189.48	211.38	178.79	90	90	90	137.32	-179.9	2.118	0.073
	189.51	211.42	178.79	90	90	90	137.28	180.0	2.122	0.074

10-1	189.36	211.23	178.76	90	90	90	-49.20	-0.910	-2.414	0.052
	189.31	211.17	178.73	90	90	90	-49.24	-0.880	-2.434	0.050
10-2	190.23	211.01	179.64	90	90	90	-49.21	-0.929	-2.311	0.080
10-3	190.08	210.81	179.69	90	90	90	-49.18	-0.992	-2.313	0.080
10-4	189.95	210.65	179.69	90	90	90	-49.15	-1.017	-2.337	0.080
11-1	189.34	211.07	178.75	90	90	90	138.06	0.107	81.679	0.057
	189.39	211.16	178.74	90	90	90	138.19	0.202	81.685	0.065
11-2	189.30	211.21	178.76	90	90	90	138.05	-0.038	81.680	0.051
	189.34	211.21	178.74	90	90	90	138.03	0.005	81.684	0.049
11-3	189.31	211.16	178.77	90	90	90	138.00	0.044	81.696	0.045
	189.33	211.16	178.77	90	90	90	138.03	0.005	81.700	0.045
11-4	189.28	211.12	178.74	90	90	90	138.00	0.045	81.702	0.047
	189.27	211.14	178.73	90	90	90	138.10	-0.08	81.695	0.051
11-5	189.28	211.09	178.78	90	90	90	138.02	0.033	81.704	0.046
	189.27	211.09	178.74	90	90	90	138.00	0.066	81.705	0.048
12-1	189.37	211.20	178.73	90	90	90	134.12	179.93	-5.050	0.060
	189.38	211.23	178.73	90	90	90	134.12	179.98	-5.054	0.048
12-2	189.37	211.17	178.78	90	90	90	134.12	-180.00	-5.044	0.041
	189.36	211.19	178.76	90	90	90	134.06	179.93	-5.045	0.044
12-3	190.34	211.25	179.60	90	90	90	134.12	179.99	-4.949	0.080
12-4	190.30	211.19	179.62	90	90	90	134.07	179.96	-4.951	0.080
13-1	189.36	210.98	178.73	90	90	90	134.28	-1.346	-154.5	0.100
13-2	189.37	211.02	178.75	90	90	90	134.27	-1.330	-154.5	0.100
13-3	189.34	210.98	178.76	90	90	90	134.28	-1.255	-154.7	0.100
14-1	189.29	210.92	178.72	90	90	90	-42.26	1.108	-0.738	0.080
14-2	189.02	210.81	178.49	90	90	90	-42.27	1.145	-0.727	0.062
	189.06	210.88	178.51	90	90	90	-42.26	1.112	-0.759	0.057
14-3	189.28	210.95	178.72	90	90	90	-42.27	1.156	-0.728	0.080
15-1	189.19	210.93	178.44	90	90	90	-44.27	0.246	1.651	0.073
	189.19	210.98	178.55	90	90	90	-44.30	0.272	1.621	0.073
15-2	189.35	211.03	178.74	90	90	90	-44.32	0.302	1.638	0.100
15-3	189.13	210.94	178.48	90	90	90	-44.33	0.265	1.649	0.064
	189.18	211.01	178.51	90	90	90	-44.32	0.206	1.610	0.059
15-4	189.12	210.94	178.49	90	90	90	-44.33	0.180	1.656	0.063
	189.17	211.00	178.54	90	90	90	-44.34	0.265	1.625	0.061
15-5	189.15	210.94	178.50	90	90	90	-44.33	0.211	1.645	0.075
	189.15	211.01	178.53	90	90	90	-44.34	0.255	1.612	0.060
16-1	189.43	211.06	178.72	90	90	90	44.671	-0.583	6.346	0.100
16-2	189.21	210.96	178.50	90	90	90	44.675	-0.563	6.362	0.072
	189.12	211.03	178.61	90	90	90	44.700	-0.466	6.329	0.059
16-3	189.10	210.96	178.59	90	90	90	44.705	-0.525	6.375	0.058
	189.19	211.02	178.52	90	90	90	44.682	-0.572	6.343	0.063
16-4	189.17	210.96	178.51	90	90	90	44.679	-0.526	6.361	0.069
	189.24	211.02	178.49	90	90	90	44.664	-0.575	6.329	0.064
17-1	188.77	210.40	178.77	90	90	90	134.55	-1.172	-179.6	0.130
17-2	188.65	210.41	178.57	90	90	90	134.52	-1.184	-179.6	0.108
	188.63	210.39	178.53	90	90	90	134.52	-1.107	-179.6	0.095
17-3	188.98	210.55	178.74	90	90	90	134.52	-1.206	-179.6	0.130
17-4	188.71	210.46	178.55	90	90	90	134.51	-1.184	-179.6	0.110
	188.71	210.46	178.53	90	90	90	134.51	-1.153	-179.6	0.096
17-5	188.83	210.51	178.48	90	90	90	134.53	-1.143	-179.6	0.103
	188.78	210.48	178.47	90	90	90	134.53	-1.132	-179.6	0.086
17-6	188.79	210.51	178.46	90	90	90	134.53	-1.120	-179.6	0.103
	188.83	210.48	178.41	90	90	90	134.54	-1.139	-179.6	0.098
18-1	189.10	210.89	178.44	90	90	90	-46.57	179.83	176.62	0.070
	189.05	210.93	178.51	90	90	90	-46.58	179.68	176.58	0.053

18-2	189.14	210.89	178.45	90	90	90	-46.57	179.76	176.63	0.066
	189.10	210.93	178.47	90	90	90	-46.57	179.64	176.60	0.059
18-3	189.10	210.90	178.51	90	90	90	-46.58	179.66	176.62	0.061
	189.02	210.94	178.55	90	90	90	-46.59	179.69	176.59	0.059
18-4	189.06	210.89	178.54	90	90	90	-46.59	179.72	176.63	0.068
	189.01	210.90	178.46	90	90	90	-46.59	179.74	176.60	0.064
18-5	189.28	210.95	178.76	90	90	90	-46.59	179.72	176.60	0.100
18-6	189.30	210.98	178.74	90	90	90	-46.58	179.63	176.60	0.100
19-1	190.39	211.49	179.53	90	90	90	44.653	18.173	-94.07	0.080
19-2	189.22	211.09	178.55	90	90	90	-134.6	18.180	-91.68	0.049
	189.26	211.11	178.58	90	90	90	-134.6	18.160	-91.68	0.049
19-3	189.11	211.06	178.66	90	90	90	-134.5	18.175	-91.68	0.045
	189.18	211.09	178.59	90	90	90	-134.6	18.038	-91.69	0.048
19-4	190.47	211.46	179.31	90	90	90	-134.6	18.161	-91.68	0.080
19-5	190.51	211.50	179.37	90	90	90	-134.6	18.173	-91.71	0.080
19-6	190.54	211.48	179.40	90	90	90	-134.6	18.126	-91.71	0.080
19-7	190.55	211.51	179.36	90	90	90	-134.6	18.155	-91.71	0.080
20-1	188.87	210.25	178.26	90	90	90	153.15	1.658	-4.147	0.100
	189.44	211.56	178.77	90	90	90	153.09	1.667	-4.182	0.102
20-2	189.25	211.16	178.62	90	90	90	153.10	1.676	-4.154	0.077
	188.88	210.23	178.23	90	90	90	153.17	1.668	-4.129	0.087
20-3	188.86	210.21	178.24	90	90	90	153.05	1.688	-4.131	0.101
	189.38	211.44	178.73	90	90	90	153.16	1.664	-4.167	0.102
20-4	189.19	211.02	178.56	90	90	90	153.07	1.699	-4.153	0.092
	189.09	210.73	178.42	90	90	90	152.93	1.739	-4.146	0.096
21-1	189.03	210.41	178.34	90	90	90	113.26	-2.014	174.46	0.095
	189.29	211.00	178.54	90	90	90	113.39	-2.045	174.43	0.101
21-2	190.35	213.49	179.48	90	90	90	113.40	-2.004	174.37	0.080
21-3	189.29	211.02	178.57	90	90	90	113.19	-1.942	174.45	0.050
	189.29	210.98	178.53	90	90	90	113.44	-2.013	174.44	0.053
22-1	189.08	210.74	178.50	90	90	90	113.80	-1.224	176.08	0.071
	189.25	211.15	178.62	90	90	90	113.83	-1.233	176.05	0.072
22-2	189.06	210.72	178.50	90	90	90	113.77	-1.214	176.08	0.067
	189.20	211.02	178.58	90	90	90	113.74	-1.202	176.07	0.064
22-3	189.16	210.97	178.57	90	90	90	113.86	-1.245	176.10	0.066
	189.27	211.21	178.64	90	90	90	113.72	-1.188	176.09	0.067
22-4	189.22	211.13	178.63	90	90	90	113.90	-1.248	176.10	0.053
	189.16	210.91	178.54	90	90	90	113.88	-1.243	176.12	0.061
22-5	189.09	210.79	178.52	90	90	90	113.84	-1.217	176.13	0.059
	189.22	211.08	178.59	90	90	90	113.74	-1.167	176.12	0.063
22-6	189.21	211.09	178.62	90	90	90	113.80	-1.194	176.13	0.059
	189.20	210.99	178.57	90	90	90	113.85	-1.215	176.14	0.062
22-7	189.16	210.93	178.57	90	90	90	113.82	-1.211	176.17	0.065
	189.29	211.21	178.62	90	90	90	113.85	-1.224	176.15	0.066
23-1	189.29	211.11	178.59	90	90	90	-164.5	-5.903	176.63	0.151
	189.35	211.25	178.64	90	90	90	-164.4	-5.954	176.59	0.158
23-2	189.21	210.75	178.46	90	90	90	164.36	6.369	-4.146	0.183
	189.33	211.20	178.62	90	90	90	164.34	6.377	-4.194	0.179
23-3	189.10	210.55	178.37	90	90	90	164.33	6.474	-4.076	0.180
	189.28	211.07	178.57	90	90	90	164.29	6.489	-4.135	0.180
23-4	189.22	210.93	178.51	90	90	90	164.40	6.512	-4.078	0.178
	189.27	210.88	178.52	90	90	90	164.34	6.553	-4.088	0.173
23-5	189.32	211.39	178.73	90	90	90	164.31	6.625	-3.960	0.200
23-6	189.16	211.11	178.74	90	90	90	164.37	6.650	-3.919	0.200
24-1	189.92	211.11	180.10	90	90	90	109.52	-176.0	0.054	0.080
24-2	189.99	211.23	180.14	90	90	90	109.45	-176.0	0.007	0.080

24-3	190.01	211.28	180.14	90	90	90	109.47	-175.9	-0.026	0.080
24-4	190.06	211.27	180.08	90	90	90	109.48	-175.9	-0.051	0.080
24-5	190.04	211.40	180.30	90	90	90	109.34	-176.1	-0.050	0.080
24-6	189.15	210.90	178.57	90	90	90	109.47	-176.0	-0.186	0.051
	189.28	211.03	178.75	90	90	90	109.66	-175.5	-0.192	0.056
25-1	189.21	210.97	178.57	90	90	90	112.52	-0.697	176.16	0.048
	189.26	211.05	178.55	90	90	90	112.47	-0.656	176.11	0.053
25-2	189.23	211.09	178.57	90	90	90	112.52	-0.685	176.15	0.047
	189.18	210.82	178.54	90	90	90	112.47	-0.646	176.14	0.047
25-3	189.23	211.03	178.56	90	90	90	112.53	-0.667	176.16	0.048
	189.24	211.07	178.59	90	90	90	112.50	-0.646	176.14	0.065
	189.22	210.99	178.56	90	90	90	112.54	-0.673	176.13	0.054
25-4	189.16	210.83	178.57	90	90	90	112.50	-0.640	176.19	0.053
	189.27	211.16	178.57	90	90	90	112.56	-0.677	176.12	0.066
	189.23	210.98	178.55	90	90	90	112.47	-0.613	176.13	0.051
25-5	189.40	211.25	178.61	90	90	90	112.50	-0.627	176.11	0.100
26-1	189.27	211.08	178.64	90	90	90	-29.23	-1.477	-1.281	0.045
	189.24	211.09	178.61	90	90	90	-29.27	-1.397	-1.284	0.045
26-2	189.22	211.08	178.62	90	90	90	-29.31	-1.384	-1.286	0.046
	189.31	211.11	178.62	90	90	90	-29.20	-1.611	-1.283	0.044
26-3	189.28	211.08	178.64	90	90	90	-29.22	-1.653	-1.209	0.045
	189.22	211.08	178.61	90	90	90	-29.27	-1.502	-1.212	0.048
26-4	189.24	211.06	178.62	90	90	90	-29.32	-1.375	-1.203	0.046
	189.29	211.11	178.61	90	90	90	-29.25	-1.544	-1.208	0.046
27-1	189.15	211.02	178.55	90	90	90	-16.69	-0.024	-0.785	0.040
	189.16	211.08	178.58	90	90	90	-16.73	0.003	-0.824	0.064
	189.22	211.02	178.55	90	90	90	-16.65	-0.071	-0.824	0.042
27-2	189.15	210.96	178.55	90	90	90	-16.74	-0.025	-0.776	0.053
	189.21	211.10	178.59	90	90	90	-16.70	-0.064	-0.814	0.064
	189.24	211.01	178.58	90	90	90	-16.77	0.002	-0.813	0.044
27-3	189.27	211.06	178.69	90	90	90	-16.76	-0.013	-0.796	0.100
27-4	189.29	211.04	178.71	90	90	90	-16.81	-0.007	-0.791	0.100
27-5	189.43	211.23	178.69	90	90	90	-16.81	0.009	-0.796	0.100
27-6	189.12	211.03	178.55	90	90	90	-16.80	-0.030	-0.784	0.052
	189.18	211.04	178.58	90	90	90	-16.80	-0.020	-0.798	0.074
	189.24	211.00	178.57	90	90	90	-16.78	-0.037	-0.807	0.049
28-1	189.03	210.70	178.55	90	90	90	113.81	-179.0	-1.138	0.103
	189.06	210.82	178.53	90	90	90	113.83	-178.9	-1.184	0.124
	189.10	210.84	178.53	90	90	90	113.74	-179.1	-1.202	0.097
28-2	189.03	210.81	178.51	90	90	90	113.83	-178.9	-1.166	0.083
	189.05	210.88	178.44	90	90	90	113.77	-179.0	-1.222	0.067
28-3	189.05	210.83	178.45	90	90	90	113.84	-179.0	-1.196	0.103
	189.11	210.91	178.50	90	90	90	113.79	-179.0	-1.229	0.090
29-1	189.17	210.77	178.62	90	90	90	111.54	-0.775	-179.6	0.100
29-2	189.23	210.76	178.66	90	90	90	111.52	-0.901	-179.8	0.100
30-1	189.12	210.87	178.53	90	90	90	-29.69	178.33	-179.2	0.083
	189.09	210.85	178.56	90	90	90	-29.68	178.37	-179.3	0.094
30-2	188.87	210.40	178.74	90	90	90	-29.62	178.32	-179.3	0.200
30-3	188.79	210.17	178.71	90	90	90	-29.61	178.29	-179.3	0.200
31-1	189.24	211.12	178.60	90	90	90	153.74	174.61	-0.824	0.063
	189.35	211.16	178.63	90	90	90	153.73	174.50	-0.830	0.060
31-2	190.96	211.69	179.38	90	90	90	153.81	174.43	-0.763	0.080
31-3	190.93	211.70	179.38	90	90	90	153.85	174.53	-0.762	0.080
31-4	189.11	211.00	178.60	90	90	90	153.75	174.53	-0.844	0.058
	189.16	211.03	178.60	90	90	90	153.75	174.54	-0.848	0.055
31-5	189.16	210.97	178.63	90	90	90	153.73	174.58	-0.751	0.059

	189.28	211.03	178.64	90	90	90	153.75	174.63	-0.744	0.052
31-6	189.16	210.95	178.61	90	90	90	153.73	174.60	-0.748	0.058
	189.11	210.95	178.58	90	90	90	153.71	174.54	-0.755	0.054
32-1	189.19	210.82	178.58	90	90	90	-22.93	179.29	179.27	0.100
32-2	189.13	210.78	178.59	90	90	90	-22.98	179.23	179.21	0.100

Table 2.3.b. Intensity data collection.

Resolution (Å)	100-2.3Å (2.38-2.30Å)
Observed reflections	973,307 (90.077)
Independent reflections	284,634 (28,157)
I/sigma	30.9 (4.1)
Averaged redundancy*	3.3 (3.1)
Completeness (%)	90.2 (89.9)
R_{merge} (%)	6.1 (25.1)

Figures in parentheses are for the highest resolution shell.

$R_{merge} = \Sigma_h \Sigma_I |I(h,I) - \langle I(h) \rangle| / \Sigma_h \Sigma_I I(h,I)$

*Redundancy is the number of observed reflections for each independent reflection.

parameters were refined with program MLPHARE (Otwinowski, 1991) of the CCP4 program suite. The results of phase determination are shown in Table 2.4.

Although initial phase information was poor beyond 5 Å resolution, phases were extended from 5 to 2.3 Å by use of solvent flattening (Wang, 1985), histogram mapping (Zhang, 1990), and non-crystallographic symmetry (NCS) averaging (Bricogne, 1974; Schuller, 1996) by the program DM (Cowtan, 1994) of CCP4. After the phases were gradually extended from 5 to 2.8 Å in initial 200 steps, the phase extension was repeated from 3 to 2.3 Å resolution in additional 200 steps. The NCS mask and the NCS matrix were calculated using program ncsmask and program lsqkab of CCP4 (Kabsch, 1976), respectively, at the beginning of each resolution step. Atomic coordinates determined at 2.8 Å resolution were used for the initial determination of mask and matrix. Free-R factor (Brünger, 1992) calculated for 5 % of the reflection was reduced from 0.525 to 0.279, and the NCS correlation coefficient, $\{\Sigma(\rho 1-\langle\rho 1\rangle)(\rho 2-\langle\rho 2\rangle)/\Sigma[(\rho 1-\langle\rho 1\rangle)^2(\rho 2-\langle\rho 2\rangle)^2]^{1/2}\}$, was increased from 0.194 to 0.907 (Figure 2.6). The resultant map (MIR-DM map) was used for model building.

2-2-3. Structure and refinements

Table 2.4. Refinement of heavy atom parameters by MLPHARE of CCP4.

	1mM Na_2IrCl_6	0.5mM Na_2IrCl_6	CH_3HgCl
Resolution (Å)	100-3.0 (3.2-3.0)	100-3.0 (3.14-3.00)	100-3.0 (3.11-3.00)
Number of heavy atom binding sites	9	1	23
R_{iso}*	0.220 (0.541)	0.167 (0.318)	0.256 (0.531)
R_{cullis}**	0.85 (0.90)	0.87 (0.94)	0.90 (0.95)
Phasing power#	0.85 (0.57)	0.85 (0.62)	0.74 (0.44)

*R_{iso}: $\Sigma|F_{PH}-F_P|/\Sigma F_{PH}$,

**R_{cullis}: $\Sigma||F_{PH}-F_P|-F_H(calc)|/|F_{PH}-F_P|$, where $F_H(calc)$ is the calculated heavy atom structure factor.

#Phasing power is root mean square (rms) isomorphous difference divided by rms residual lack of closure.

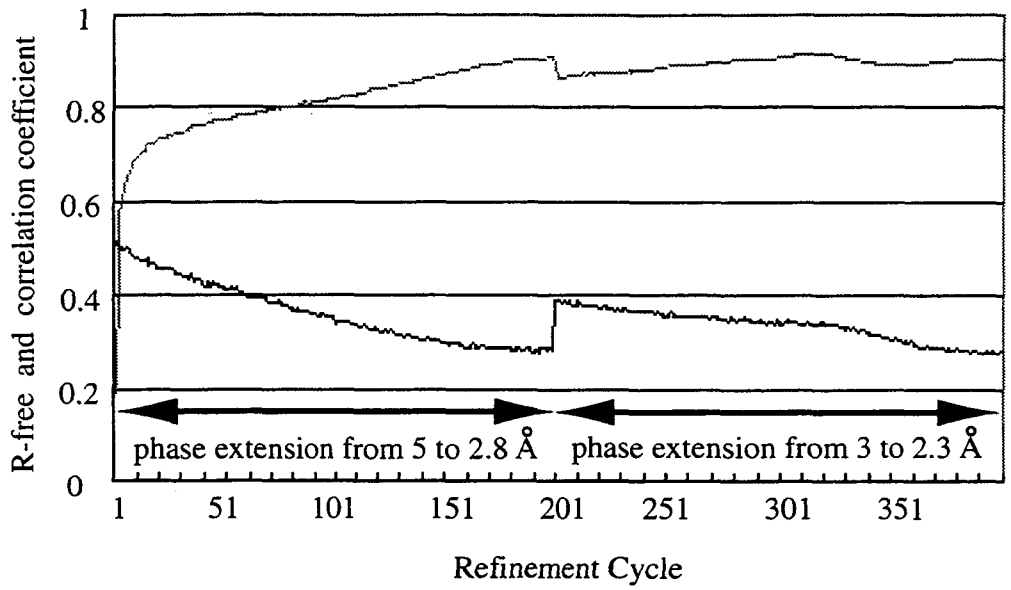

Figure 2.6. A refinement survey of DM.
Heavy and thin lines represent R-free and correlation coefficient, respectively.

Electron density map

In order to determine structures of amino acid residues and phospholipids, which were ambiguous in the MIR-DM map, three kinds of maps (Difference Fourier map, Difference Fourier omit map and SigmaA weighted map) were calculated using the refined coordinate of cytochrome *c* oxidase. These maps were calculated at every cycle of refinement to rebuild the model manually. Since the MIR-DM map does not contain the bias of the model at all, it was used for model building of most of phospholipids. However some fatty acid tails and head groups of phospholipids were not able to be located in MIR-DM map. The structure of each phospholipid was determined by inspecting these maps. In addition to 2.3 Å intensity data of oxidized form, 2.35 Å data of the reduced form was used to confirm structures of phospholipids. MIR-DM map of fully oxidized state, MIR-DM map of reduced state, omit map of fully oxidized state, and sigmaA weighted map of fully oxidized state for a cardiolipin (CL5) are shown in Figure 2.7 a, b, c and d, respectively.

(1) Difference Fourier map (Fo-Fc map)

Fo-Fc map was composed with coefficients of $(Fo-Fc)\exp(i\alpha c)$, where αc are the calculated phase angles

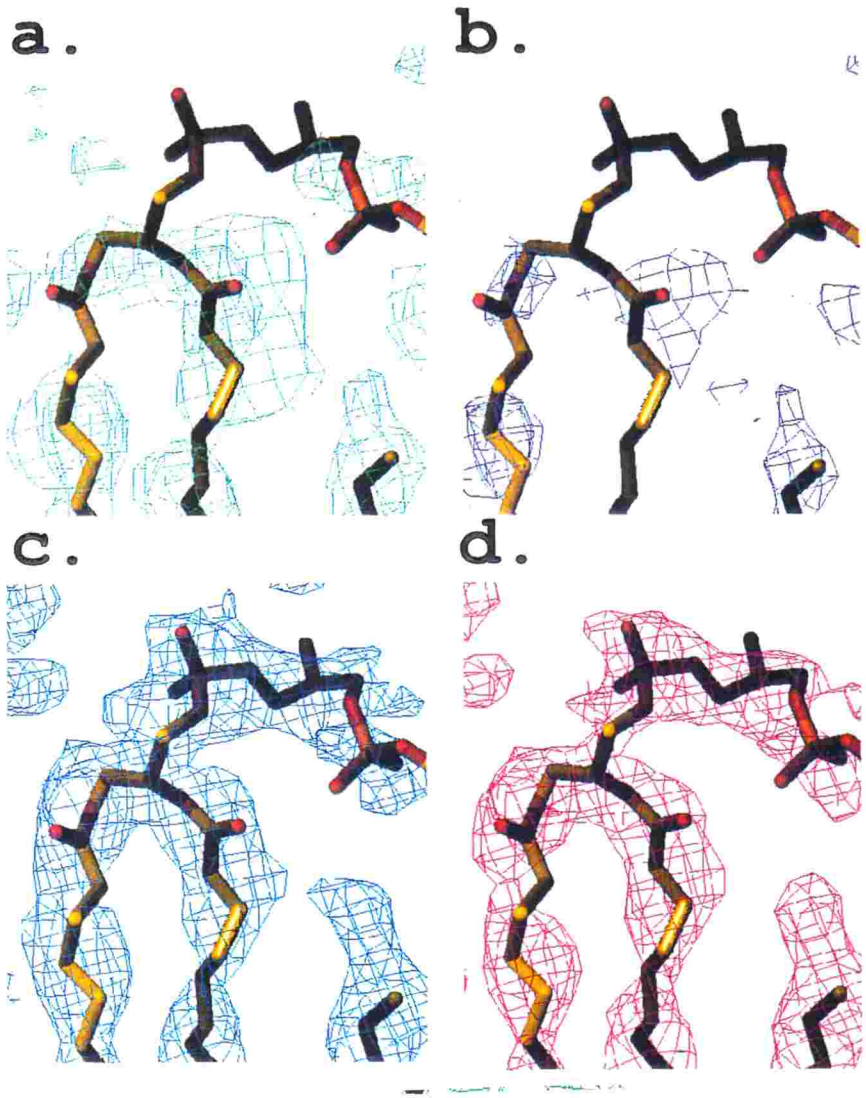

Figure 2.7. Electron density maps of CL5.

a. MIR-DM map of oxidized form

b. MIR-DM map of reduced form

c. Difference Fourier map of oxidized form

d. Sigma A weighted Difference Fourier map of oxidized form

from the refined model. This map was used to find atoms, which had not been included in the structure refinement.

(2) Difference Fourier omit map (omit map)

The omit map was calculated with coefficients of (Fo-Fc) exp(iαc) in the resolution range between 100 Å to 2.3 Å, where Fc and αc evaluated by excluding several residues of which structure should be confirmed.

(3) SigmaA weighted map (Read, 1986)

This map was calculated with coefficients of $(2m|Fo|-D|Fc|)\exp(i\alpha c)$, where m is the figure of merit and D is the estimated coordinate errors (Luzzati, 1952).

Model building of protein subunits

The initial model of cytochrome *c* oxidase was built by the rigid-body refinement of XPLOR using the structure determined at 2.8 Å resolution. The model was revised manually by using the MIR-DM map. Structural ambiguity of the cytochrome *c* oxidase has been decreased compared with 2.8 Å resolution structures. A covalent bond between $N\varepsilon_2$ of His240 imidazole group and $C\varepsilon_2$ of Tyr244 phenol group, and sodium site (Yoshikawa et al., 1998) were elucidated in 2.3 Å resolution electron density map.

Formylation of subunits I and II suggested by the mass spectroscopy were detected at their N-termini in 2.3 Å electron density. N-terminal amino acid residues (7-11) of subunit VIb and C-terminal two residues (78-79) of subunit VIIa, which were ambiguous in the 2.8 Å electron density, were assigned in 2.3 Å electron density. Electron density of C-terminal of subunit VIIa was fitted well to the sequence of Seelan et al (1992).

Acetylation of subunits VIc and VIIa were not confirmed in the 2.3 Å electron density map, probably because the electron densities of N-terminals were disordered. Although two different polypeptides (R31 and K31) were proposed for the subunit VIII by the mass spectroscopic experiment, lysine was fitted well to an electron density map at 2.3 Å resolution. Thus the model was made by assigning K31 (Figure 2.8).

Phospholylations in subunits IV and VIa were predicted by mass spectrometry. Tyr11 of subunit IV and Thr11 of subunit VIa had extra electron densities. They could be due to phosphate esters.

Model building of the phospholipids

Three phospholipids (PE1, PG1, and PG2) were detected in clear electron density of the MIR-DM map. Then four

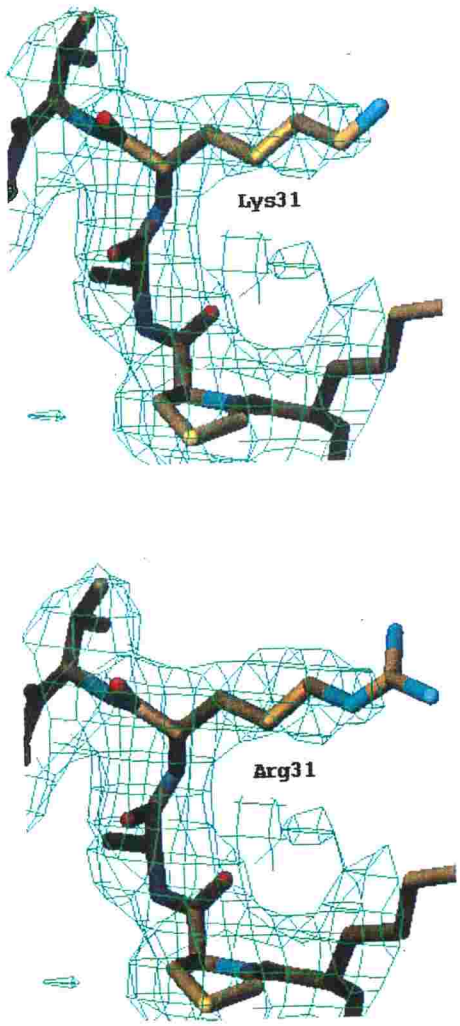

Figure 2.8. Fitting of the Lys31 and Arg31 to the MIR-DM map in subunit VIII.

cholates used for the isolation of the enzyme from the membrane and a decylmaltoside used for the crystallization were located unambiguously in the MIR-DM map. After the protein structure (with the three phospholipids, four cholates and one decylmaltoside included) was refined by using program XPLOR, Sigma A weighted (2Fo-Fc) and (Fo-Fc) maps were calculated in the resolution range 100 Å to 2.3 Å. The (Fo-Fc) map showed clear electron densities for CL1 and PG3. CL1 was ambiguous in the MIR-DM map but it had a clear electron density in the (Fo-Fc) map. Since CL1 was located in the boundary of the dimer, that electron density was not improved by the NCS averaging of DM probably because of wrong mask. The halves of fatty acid chains for each of CL2, CL3, CL4 and CL5 were hardly distinguishable from other phospholipids because of their low electron densities outside the enzyme molecule. They were, however, assigned to CLs from the sharp electron density distributions of the remaining halves of fatty acid tails residing in hollows of the molecular surface of the enzyme. The model of CL3 had been built as a phosphatidylglycerol in the structural analysis at 2.8 Å resolution. However the rest of fatty acids were clearly assigned as those of CL by 2.3 Å analysis. Although the head group of PG4 was not clear in the Fo-Fc map, the tails within the enzyme were unambiguously

identified by the difference map. After XPLOR refinement including nine phospholipids and five detergent molecules, an (Fo-Fc) synthesis was carried out to detect the remaining phospholipid molecules. The tails of PE2 and PE3 were fitted well in the cages of the (Fo-Fc) map, which were too long for PG. PC1 whose tails were hardly distinguishable by their electron density distributions from those of PG and CL, was identified by the bulky electron density corresponding to its head group. An electron density assignable to any of PG, PC or part of CL moieties remained in the (Fo-Fc) map. It was however, tentatively assigned as PG5. Most of fatty acid tails that were elucidated clearly in the electron density maps were fixed tightly in cavities or hollows of the enzyme molecule by hydrophobic interactions.

Temperature factors for phospholipids at the final stage of the refinement are given in Table 2.5. In this structural analysis, almost halves of tails and head groups of phospholipids had high temperature factors (B-factors) beyond 100 $Å^2$. Mean square displacement (σ^2) is given by the equation of $\sigma^2=B/8\pi$. σ^2 is 1.27 $Å^2$ for B-factor of 100 $Å^2$. We recognized the electron density of these structures with high B-factors by searching in the electron density drawn at a lower level. These structures took flexible conformations outside the protein complex.

Table 2.5. Average temperature factor of phospholipid.

	A molecule					B molecule				
	Head	Tails				Head	Tails			
		1	2	3	4		1	2	3	4
CL1	119.4	86.1	91.6	89.1	77.2	117.6	88.3	91.0	88.5	80.6
CL2	118.6	135.3	111.7	67.5	77.6	120.3	135.8	112.0	69.7	74.8
CL3	98.8	137.0	99.1	73.5	71.6	105.2	138.9	101.8	79.6	75.9
CL4	121.7	44.2	79.1	115.2	107.4	125.4	50.2	81.8	114.5	110.0
CL5	124.2	63.3	90.8	90.1	108.7	129.8	73.4	88.3	102.8	120.6
PC1	132.2	84.0	74.7			132.7	88.4	76.5		
PE1	31.0	63.5	38.4			39.0	66.2	47.0		
PE2	135.3	110.7	56.6			138.4	112.0	56.2		
PE3	149.5	71.5	124.2			149.8	74.4	125.6		
PG1	24.7	42.2	45.7			34.4	46.9	46.8		
PG2	31.3	45.3	40.6			36.5	48.3	44.2		
PG3	103.6	110.2	68.3			103.6	110.4	70.2		
PG4	133.2	69.9	83.7			133.9	73.8	89.0		
PG5	144.1	111.6	91.0			145.2	112.5	89.6		
Protein			37.2					46.4		

Structural refinement by XPLOR

The structural model was refined using molecular dynamics refinement (simulated annealing), positional refinement and temperature factor refinement implemented in program XPLOR (Brünger, 1988). The restraint parameters used in the XPLOR refinement for the protein were those given by Engh and Huber (1991). Those of the phosphatidyl glycerol and phosphatidyl ethanolamine were the same ones used for 2.8 Å resolution analysis of this enzyme. Parameters for cardiolipin and phosphatidylcholine were made by referring to the structures of phospholipids registered in the Cambridge Structural Database. These parameters used in this XPLOR refinement are given in Table 2.6. Non-crystallographic symmetry restrains were applied in all the refinement processes. The structures of amino acid residues and phospholipids were rebuilt manually using a program TURBO FRODO in the maps of MIR-DM, Sigma A weighted (2Fo-Fc) and (Fo-Fc). Five cardiolipins, one phosphatidylcholine, three phosphatidyl ethanolamines, and five phosphatidyl glycerols were confirmed during the alternative repetition of XPLOR refinement and model building. The final model included 3,564 amino acid residues, two hemes a, two hemes a3, six coppers, two zincs, two magnesiums, two sodiums,

Table 2.6.a. The bond length parameter of phospholipids

Bond parameter

atom type*	atom type	Energy parameter (kcal/mole Å^2)	Bond length (Å)
O=**C**-	-**C**H_2	400	1.522
-**C**=	=**O**	1500	1.220
O=**C**-	-**O**-P-	300	1.334
-H**C**-	-**C**H_2-	445	1.538
-H**C**-	-**C**H-	450	1.530
-H**C**-	-**O**-P-	680	1.430
-H_2**C**-	-**C**H_2-	445	1.530
-H_2**C**-	-**C**H_3	445	1.528
-H_2**C**-	-**N**H_3	522	1.510
-H_2**C**-	-**N**-CH_3	844	1.450
-**N**-	-**C**H_3	844	1.490
-H_2**C**-	-**O**-P-	680	1.430
O=	=**P**	1160	1.480
O-	-**P**	540	1.600
H$^+$-	-**N**H	820	1.040
-H**C**-	-**O**H	856	1.420
-H_2**C**-	-**O**H	856	1.420
H-	-**O**-	1090	0.960

*Bonding atoms are represented by bold.

Table 2.6.b. The angle parameter of phospholipids.

Angle parameter

atom type	atom type	atom type	Energy parameter (kcal/mole rad^2)	Angle (degree)
-CH_2	O=**C-**	**=O**	140.0	125.0
-CH_2	O=**C-**	**-O**=P-	110.0	109.0
=O	O=**C-**	**-O**=P-	180.0	125.9
-CH_2	**-HC-**	**-C**H_2	116.7	113.5
-O=P-	**-HC-**	**-C**H_2	151.4	110.1
O=**C-**	**-C**H_2**-**	**-C**H_2	104.0	108.0
-H**C-**	**-C**H_2**-**	**-O**=P-	151.4	110.1
-H**C-**	**-HC-**	**-C**H_2	90.0	112.5
-H**C-**	**-C**H_2**-**	-H**C-**	90.0	117.0
-CH_2	**-C**H_2**-**	-H**C-**	90.0	112.5
-CH_2	**-C**H_2**-**	**-C**H_2	116.7	113.6
-CH_2	**-C**H_2**-**	**-C**H_3	116.0	115.0
-CH_2	**-C**H_2**-**	**-N**-CH_3	135.4	110.0
-CH_2	**-N**-CH_3	**-C**H_3	120.0	109.5
-CH_3	**-N**-CH_3	**-C**H_3	120.0	109.5
-CH_2	**-C**H_2**-**	**-N**-CH_3	130.0	105.0
-CH_2	**-C**H_2**-**	**-O**=P-	151.4	110.1
-CH_2	**-N**-CH_3	**H^+-**	66.0	109.5
-CH_2	**-O-**P-	**-P**	40.0	120.0
-O-P-	**-P=**	**O=**	197.8	111.6
-O-P-	**-P-**	**-O-**P-	160.0	104.3
H^+-	**-N-**	**H-**	82.0	109.5
-CH_2	-H**C-**	**-O**H	151.4	110.1
-H**C-**	**-C**H_2**-**	**-O**H	151.4	110.1
-H**C-**	**-O**H	**-H**	115.0	106.0
-CH_2	**-O**H	**-H**	115.0	106.0

28 phospholipids, eight cholate, two decylmaltosides, two peroxides, and 1124 waters. Ten phospholipids were cardiolipins, two were phosphatidylcholines, six were phosphatidyl ethanolamines, and 10 were phosphatidyl glycerols. This model gave a crystallographic R factor of 0.204 for 973,307 of observed reflections at 2.3 Å resolution and free R factor (Brünger, 1992) of 0.242 that was calculated for a test set of 5% of the reflections not used in the refinement. The root mean square deviations from ideal values are 0.016 Å for bond length and 2.07° for bond angles. The results of structural refinement were shown in Table 2.7. The Ramachandran (ϕ,ψ) plot (Ramakrishman, 1965) for 3,564 residues are given in Figure 2.9. No residue was in the disallowed region. Out of 3,062 non-glycine and non-proline residues, only 0.8% were in the generously allowed region, and 90.1% and 9.2% were in the most favored and the favored regions, respectively. These criteria implicated soundness of the present structural determination.

2-3. High-resolution X-ray analysis of cryogenic crystal

Orthorhombic crystals diffracted up to 1.9 Å resolution at the initial stage of the diffraction experiments. However the resolution of crystal was

Table 2.7. The result of structural refinement at 2.3 Å resolution.

Resolution (Å)	15-2.3Å
R^{*} (%)	20.4
R_{free}^{**} (%)	24.2
σ_{bond} (Å)	0.016
σ_{angle} (°)	2.07
rms***	0.30

*R is conventional crystallographic R factor, $\Sigma|Fo-Fc|/\Sigma|Fo|$, **R_{free} is a free R factor of XPLOR refinement evaluated for the 5% of reflections that are excluded from the refinement. ***rms is a root mean square error of atomic coordinates estimated by the Luzatti plots.

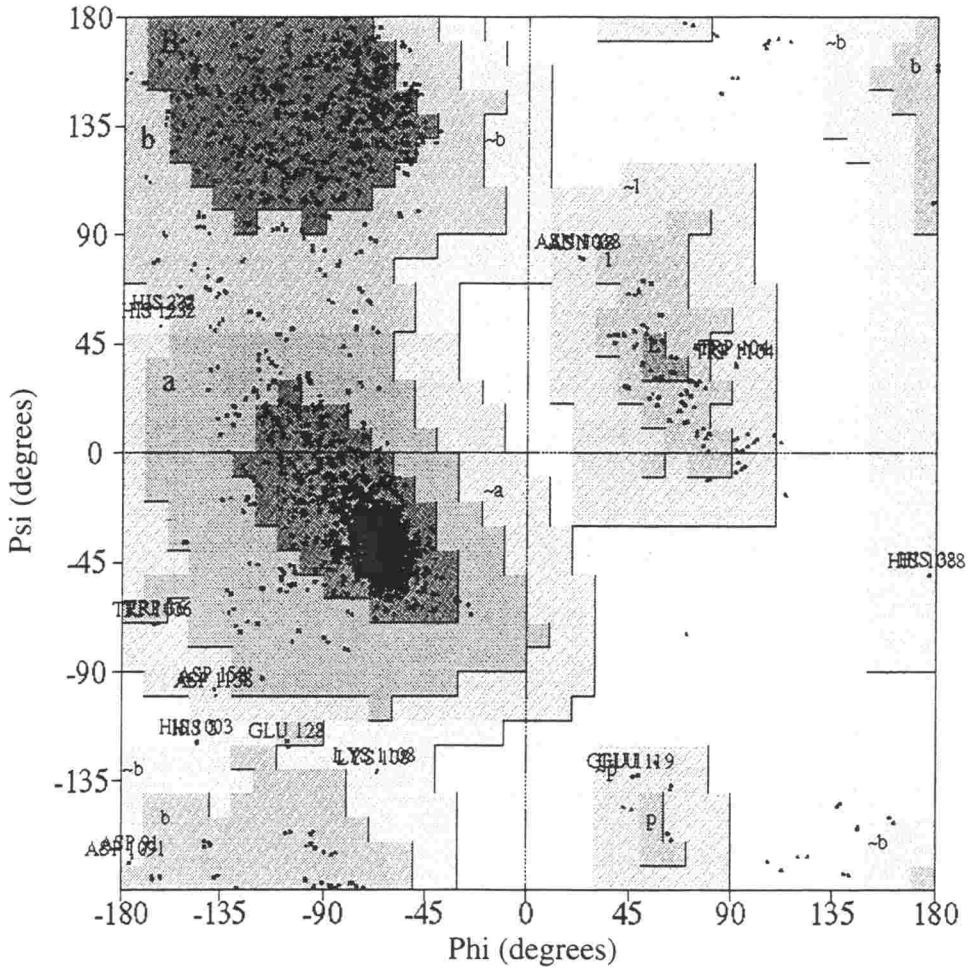

Plot statistics

Residues in most favoured regions [A,B,L]	2773	90.6%
Residues in additional allowed regions [a,b,l,p]	268	8.8%
Residues in generously allowed regions [~a,~b,~l,~p]	21	0.7%
Residues in disallowed regions	0	0.0%
	----	------
Number of non-glycine and non-proline residues	3062	100.0%
Number of end-residues (excl. Gly and Pro)	50	
Number of glycine residues (shown as triangles)	256	
Number of proline residues	196	

Total number of residues	3564	

Figure 2.9. Ramachandran plots for refined model of cytochrome *c* oxidase at 2.3 Å resolution.
Triangle represenr glycine residues and squares represent non-glycine residues, respectively.

decreased with the X-ray exposure. A complete data collection was done only at 2.3 Å resolution. Cryogenic experiment reduces the rate of X-ray radiation damage of protein crystal (Low et al., 1966). When X-ray diffraction experiment is undertaken by using third generation synchrotron radiation, the cryogenic experiment is indispensable to reduce deterioration of the crystal by strong X-ray exposure. Although successful cryogenic experiments for membrane protein were very few, the 2.0 Å data collection of this enzyme was successfully undertaken by cooling the crystal at 100 K.

Protein crystals were soaked into anti-freezing reagent prior to freezing of the crystals to prevent the formation of hexagonal ice. The hexagonal ice destroys mechanically a lattice structure of protein crystal. Glycerol was added to the crystallization buffer as an anti-freezing reagent. The glycerol concentration of the buffer was increased by 5% (v/v) in each step up to 35% (v/v).

Crystals were transformed into liquid nitrogen bath to freeze them. The crystal of cytochrome *c* oxidase had some problems in freezing. Various conditions were searched for the cooling procedure. Most of the freezing by the liquid nitrogen made the crystals cracked. Each cooling procedure produced a shrunken lattice loosing isomorphism.

After more than 20 trials, cryogenic experiment was successfully carried out by using a frozen crystal prepared by flash-cooling with synchrotron radiation at BL41 of the Spring-8. Intensity data with 94.9% completeness at 2.0 Å resolution were obtained. Experimental conditions for X-ray diffraction of the cryogenic crystal and crystallographic data is given in Table 2.8. The crystal belongs to the orthorhombic space group of $P2_12_12_1$ with the unit cell dimensions a = 184.7 Å, b = 207.5 Å, c = 178.4 Å. The cell dimensions shrank by 0.2 to 4.4 Å. R_{iso} between intensity data at room temperature and those at cryogenic temperature was 0.45. ($R_{iso}=\Sigma|F_{PH}-F_P|/\Sigma F_{PH}$, where F_{PH} and F_P are the cryogenic and normal temperature structure factor amplitudes, respectively.) The present cryogenic crystal lost the isomorphism against the crystal at room temperature.

The phase determination has been carried out by the molecular replacement (MR) method with the program XPLOR. Search model was the structure of cytochrome *c* oxidase determined at 2.3 Å resolution. The results of MR are given in Table 2.9. All procedures of MR were performed using the program XPLOR. The initial phases determined at 5.0 Å resolution were extended and improved by 200 steps of iteration to 2.0 Å resolution by non-crystallographic symmetry averaging, solvent flattening and histogram

Table 2.8 a. Experimental conditions for X-ray diffraction of the cryogenic crystal by synchrotron radiation.

X-ray source	Spring8 BL41XU
Detector	R-axis IV
Collimator	0.1 mm
Wavelength	0.708Å
Camera length	350 mm
Oscillation angle	0.65°
Overlap	0.00°
Exposure time	78 seconds
Temperature	100 K

Table 2.8 b. Crystallographic data of cytochrome *c* oxidase.

Crystal form	Orthorhombic
Space group	$P2_12_12_1$
Cell constants	a = 184.7Å
	b = 207.5Å
	c = 178.4Å
Number of molecules in unit cell	Z = 8
Volume of asymmetric unit/molecular weight	Vm=4.2 $Å^3$/dalton
Solvent content	Vsolv = 71%

Table 2.9. The results of molecular replacement.

Resolution	15-5Å
Rotation (Euler angles)	Θ_1 = 0.15 Θ_2 = -0.08 Θ_3 = -0.61
Translation (Å)	x = -1.46 y = -4.76 z = -1.90
R	0.302
R_{free}	0.349

Eulerian angles (Θ_1, Θ_2, Θ_3) as defined by Rossmann and Blow (1962)

mapping using the program DM of CCP4. This phase extension was repeated twice. The structural refinement processes were performed the same way as those of 2.3 Å resolution. The refined model included all amino acid residues determined at 2.3 Å resolution, four hemes, and all metals of dimer.

The structures of phospholipids determined at 2.3 Å resolution were confirmed by cryogenic electron densities at 2.0 Å resolution, which were clearer than that at 2.3 Å (Figure 2.10). Although halves of CL2 and CL3 tails were on the surface of the enzyme, the fatty acid tails of CL2 and CL3 were fixed in high resolution electron densities at cryogenic temperature.

The overall structure of the both enzymes was nearly same with that at normal temperature. However the number of extra water molecules were appeared in the electron density map at 100K compared with that at around 290K. The results of structural refinement were given in Table 2.10.

2-4 Quaternary structure

The X-ray crystal structure of this enzyme showed that it took dimeric structure. Ten subunits (I, II, III, IV, VIa, VIc, VIIa, VIIb, VIIc and VIII) had transmembrane α-helices. Subunit Va was at the matrix side below subunit

(a)

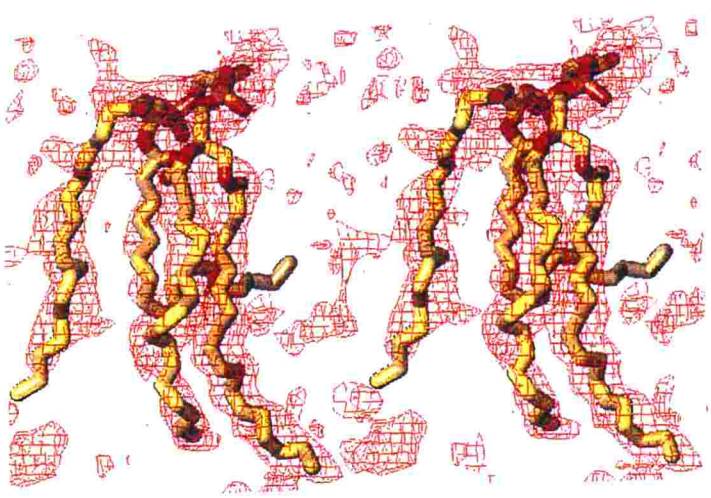

(b)

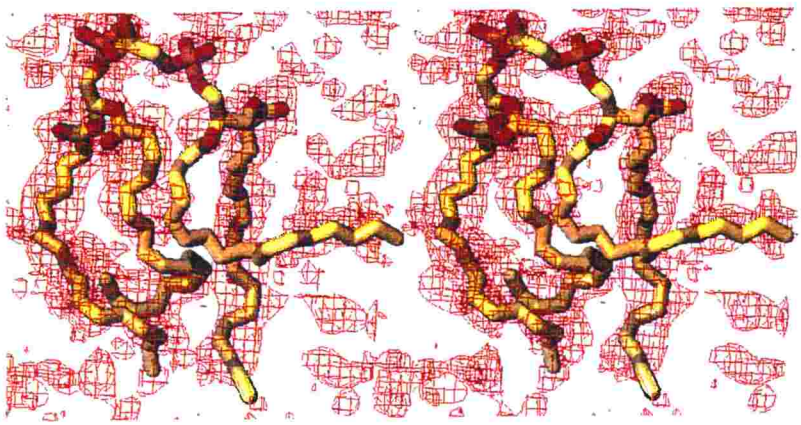

Figure 2.10. Stereoscopic drawing of CL2 (a), CL3 (b), are superposed on the Difference Fourier map of 2.3 Å resolution analysis at 2.5σ level.

Table 2.10. The results of structural refinement at 2.0 Å resolution.

Resolution (Å)	15-2.0Å
R^{*} (%)	22.6
R_{free}^{**} (%)	26.7
σ_{bond} (Å)	0.014
σ_{angle} (°)	1.731
rms***	0.30

*R is conventional crystallographic R factor, $\Sigma|Fo-Fc|/\Sigma|Fo|$, **R_{free} is a free R factor of XPLOR refinement evaluated for the 5% of reflections that are excluded from the refinement. ***rms is a root mean square error os atomic coordinates estimated by the Luzatti plots.

I. Subunit Vb at the matrix side was below subunit I and III, adjacent to subunit Va and the extramembrane domain of subunit IV. Subunit VIb was only one extramembrane subunit at the intermembrane side.

Subunits I, II, and III make a core structure, and the other subunits surround the core. Two monomer each consisting of 13 different subunits forms a dimeric structure with two-fold symmetry. The interactions among 26 subunits to form dimeric cytochrome *c* oxidase are shown in Table 2.11 listing the number of intermolecular distances shorter than 4 Å. Subunit I interacted with both subunits II and III, while subunits II and III had no direct interaction with each other. Subunit I was at the center in the core structure. The core structure made up by subunits I, II, and III interacted with eight other subunits. However subunit Va and VIIb hardly interacted with the core structure. These subunits interacted mainly with subunit IV. Interactions between monomers are mainly formed by subunits I and VIa.

Table 2.11. Intersubunit interactions with atomic contacts shorter than 4.0 Å Upper right represents interactions within monomer A. Lower left represent interactions between the two monomers A and B.

	sub I	sub II	sub III	sub IV	sub Va	sub Vb	sub VIa	sub VIb	sub VIc	sub VIIa	sub VIIb	sub VIIc	sub VIII
sub I		354	252	123		163	40	11	7	13	14	202	132
sub II				103	25			140	230		8		
sub III						134	186	25		134		1	
sub IV					216	14			47		195		22
sub Va						22			113				
sub Vb						8	1			21			
sub VIa	62							30					
sub VIb								24					
sub VIc											4		
sub VIIa												9	
sub VIIb													
sub VIIc													53
sub VIII													

Chapter 3. Structure of phospholipids

3-1. Location of phospholipids in cytochrome c oxidase

Cytochrome c oxidase included fourteen phospholipids per monomer (Figure 3.1). They were five cardiolipins, one phosphatidylcholine, three phosphatidylethanolamines, and five phosphatidyl glycerols. All phospholipids were found in the transmembrane region, five of them were at intermembrane side, and the other nine were at matrix side. Figure 3.2 shows the position of the phosphate groups of all phospholipids in a view to the transmembrane surface. Two planes at the matrix side and at the intermembrane side were separated by 38.2 Å, which was calculated using averaged position of phosphates. The maximum deviation of the phosphate position of matrix side and intermembrane side was 7.1 Å and 9.4 Å, respectively. The root-mean-square deviations of them were 2.4 Å and 2.9 Å for the matrix and intermembrane sides, respectively. The arrangement of phospholipids preserved the lipid bilayer structure. The thickness of membrane was corresponding to the width of 40.2 Å, which was calculated from the coordinates of phosphate groups in bacteriorhodopsin (2BRD) (Grigorieff et al., 1996).

All phospholipids interacted with the core structure

(a)

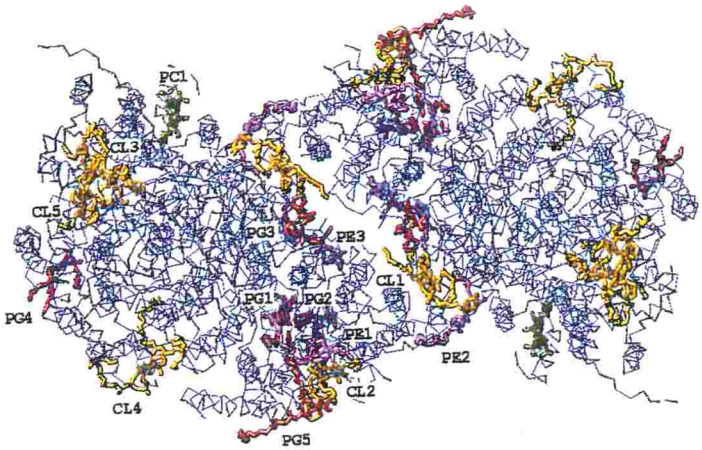

(b)

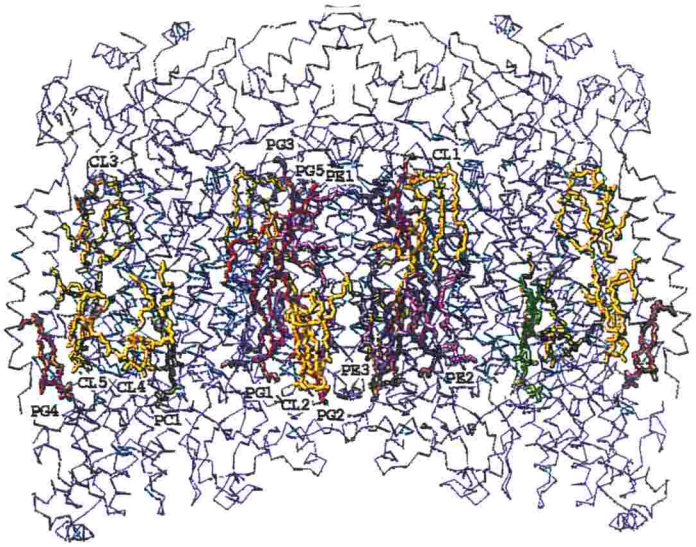

Figure 3.1. The distributions of phospholipids.

a. A view from the cytosolic side.

b. A view to the trans membrane surface.

The Cα backbone traces of dimer of bovine heart cytochrome *c* oxidase.

CL : Yellow, PC : Green, PE : Pink, PG : Red

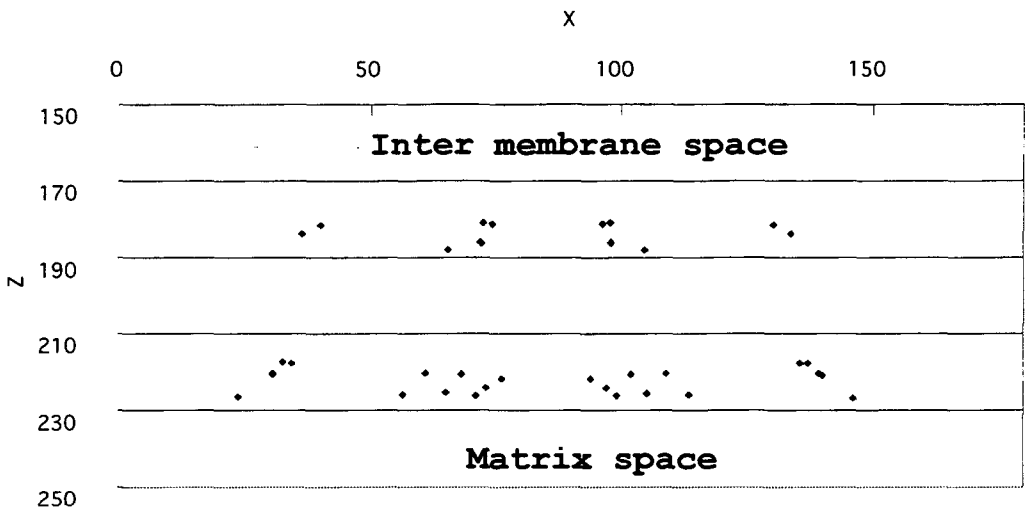

Figure 3.2. Coordinates of phosphate groups of phospholipid.

Where z is parallel to the two-fold axis of the dimer.

that was made from subunits I, II, and III (Table 3.1). PE1, PG1, and PG2 were included in subunit III. Phospholipids patch α-helices of core and nuclear coded subunits. α-helix of subunit VIa was joined to the core by six phospholipids (CL1, PE1, PE2, PE3, PG3 and PG5). CL1, PE2, PE3, and PG3 were located intermonomer cavity. CL2, CL3, CL4, CL5, PC1, PG4 and PG5 were placed at the hollows of the surface.

3-2. Structure of detergents

Cholate

Two cholate molecules were identified in 2.3 Å resolution map (Figure 3.3) in addition to two cholates that have been assigned by 2.8 Å analysis. Cholate was used as detergent for the solubilization of cytochrome *c* oxidase from the mitochondrial inner membrane. Cholate1 was on the cytosolic side between subunits I and III. Cholate2, Cholaste3 and Cholate4 were located in matrix side of subunit VIa, III and VIIa, respectively. Locations of the cholates are shown in Figure 3.4. Since the size and shape of cholate molecule resemble those of ADP, the cholate binding sites could be the binding sites for nucleotides. The nucleotide binding to subunit VIa which is proposed to control the enzyme function (Anthony et al., 1993) was replaced by cholate in the present crystal.

Table 3.1. Interaction between α-helix and phospholipids.

Helix		Phospholipid	Helix		Phospholipid
Sub I	I	CL4	Sub III	III	PE3,PG1,PG2
	II				PG3
	III	CL4,PG1		IV	CL1
	IV	PE1,PG1		V	CL2,PE1,PE2
	V	PE1		VI	CL2,PE1,PG2
	VI			VII	CL1
	VII	CL1(B)	Sub IV	I	CL5,PG4
	VIII	CL1(B),PC1	Sub Va		-
	IX	CL3,CL5	Sub Vb		-
	X	CL3,CL4	Sub VIa	I	CL1,PE1,PE2
	XI	CL3,CL5,PG4			PE3(B),PG3(B) ,PG5
	XII	CL4	Sub VIb		-
Sub II	I	CL3,PC1,CL5	Sub VIc	I	CL3,PC1
	II	CL1(B),PC1	Sub VIIa	I	CL2,PG5
Sub III	I	PG1,PG5	Sub VIIb	I	PG4
	II	CL2,PG1,PG2	Sub VIIc	I	CL4
			Sub VIII	I	PG4

Subunit Va, Vb and VIb do not have transmembrane helix.

(a)

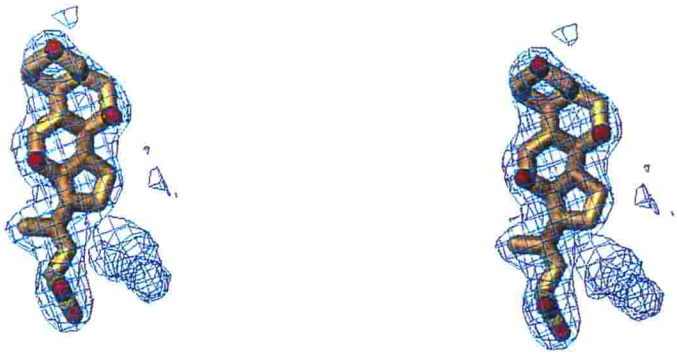

(b)

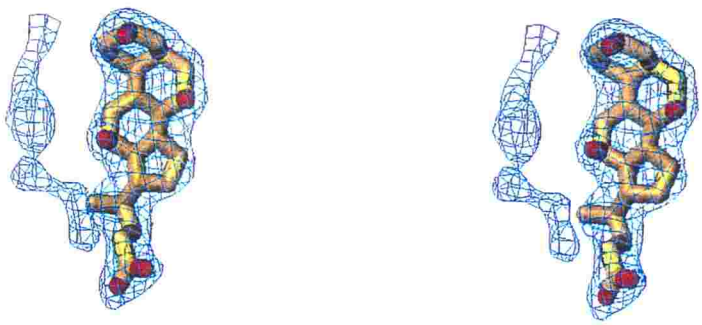

Figure 3.3. Stereoscopic drawing of three cholates (Cholate1(a), Cholate 2(b), Cholate 3(c) and Cholate4(d)) are superposed on the (Fo-Fc) difference Fourier map of 2.3 Å resolution analysis at 2.5σ level.

(c)

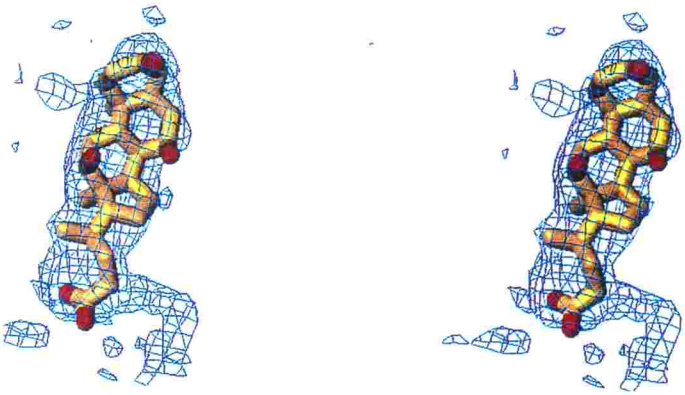

(d)

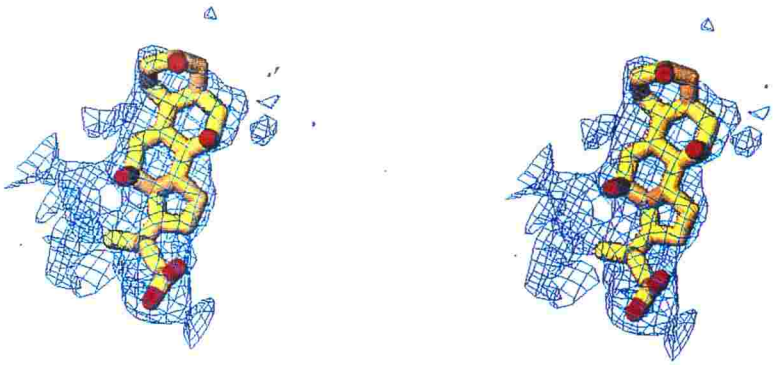

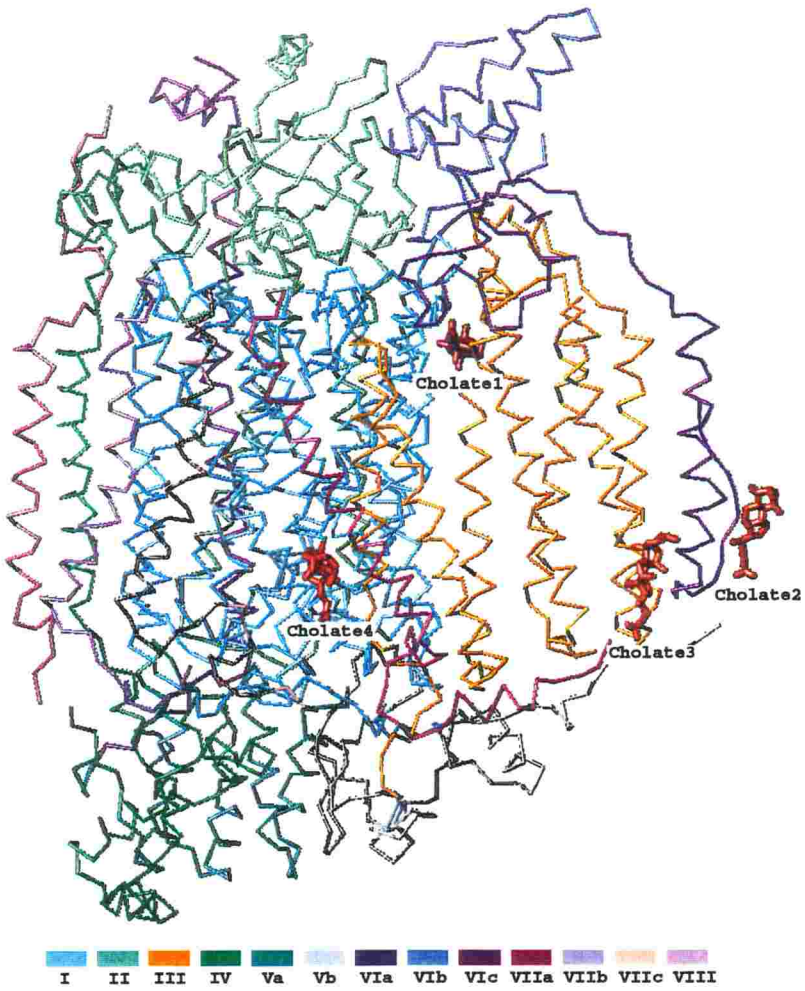

Figure 3.4. Location of cholates in the cytochrome *c* oxidase monomer. Red structures are the cholates. Each subunit has different color.

Decylmaltoside

Detergent species used for crystallization of membrane protein affect the quality of the crystal obtained. Decylmaltoside was used for the present crystallization. One decylmaltoside was found in the electron density map (Figure 3.5). It pierced between subunit IV and VIII.

The trans membrane surface of the dimer with hydrophobic natures had no inter-dimer interaction, and there was large space without any ordered structure except for the decylmaltoside around the hydrophobic surface. Decylmaltoside molecules with disordered structures might cover the transmembrane surface of dimer.

3-3. Structure of phospolipids

Cardiolipin

Five cardiolipins were in the monomeric cytochrome *c* oxidase (Figure 3.6). Cardiolipin has been known as one of the phospholipids that cannot be removed from the enzyme without loss of the enzyme activity. Cardiolipin had not been identified in the structural analysis at 2.8Å resolution. CL1 was asigned in the cytochrome *c* oxidase for the first time in 2.3 Å resolution MIR-DM and (Fo-Fc) maps. CL1 took an unusual structure with hook shape. The positions of two phosphate groups were in the different levels shifting

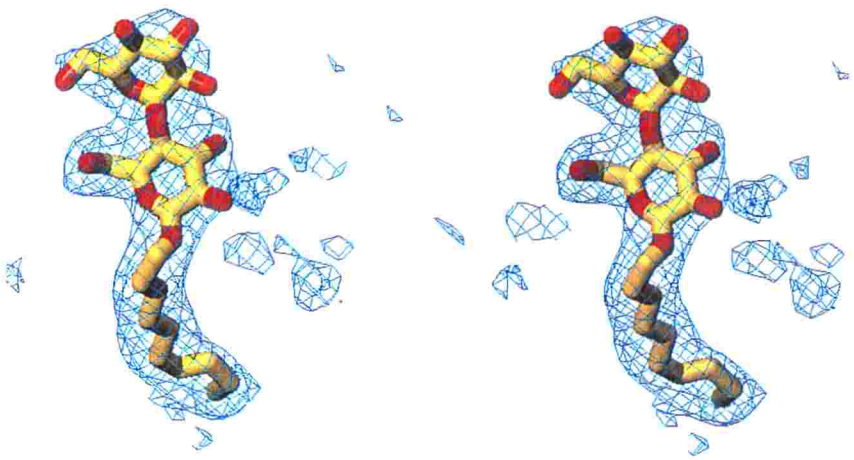

Figure 3.5. Stereoscopic drawing of decylmaltoside is superposed on the (Fo-Fc) difference Fourier map of 2.3 Å resolution analysis at 2.5σ level.

(a)

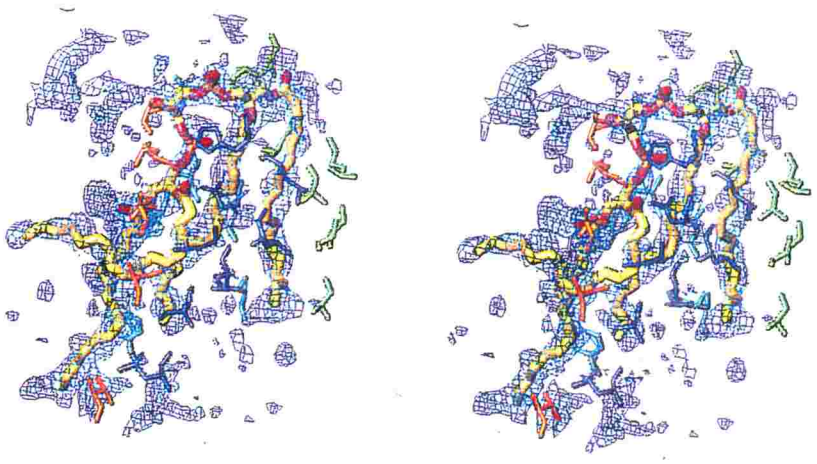

(b)

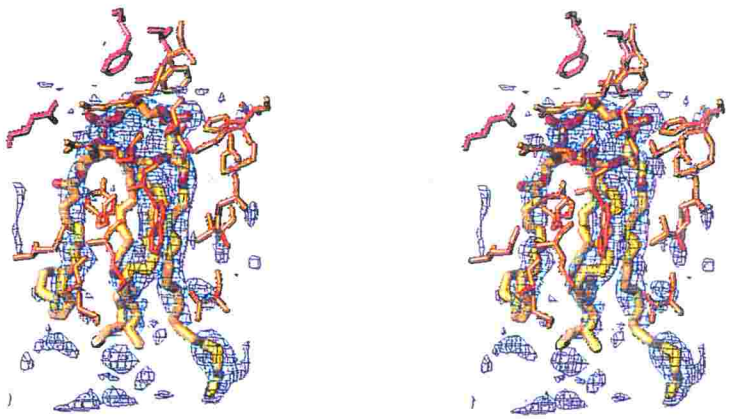

Figure 3.6. Stereoscopic drawing of CL1 (a), CL2 (b), CL3 (c), CL4 (d) and CL5 (e) are superposed on the (Fo-Fc) difference Fourier map of 2.3 Å resolution analysis at 2.5σ level.

(c)

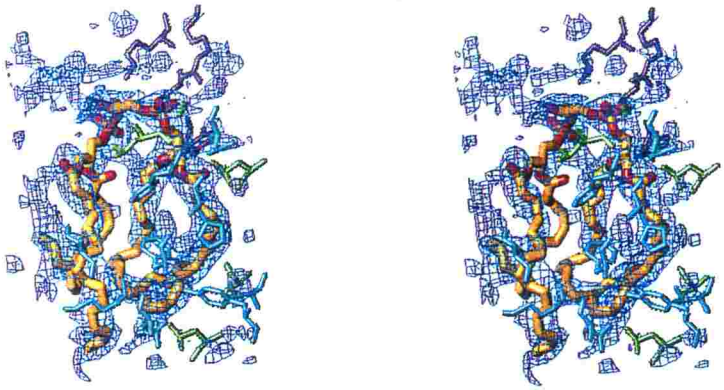

(d)

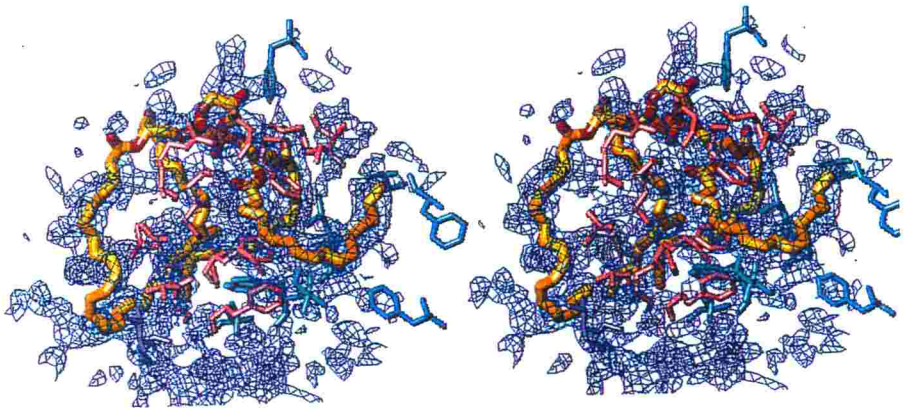

(e)

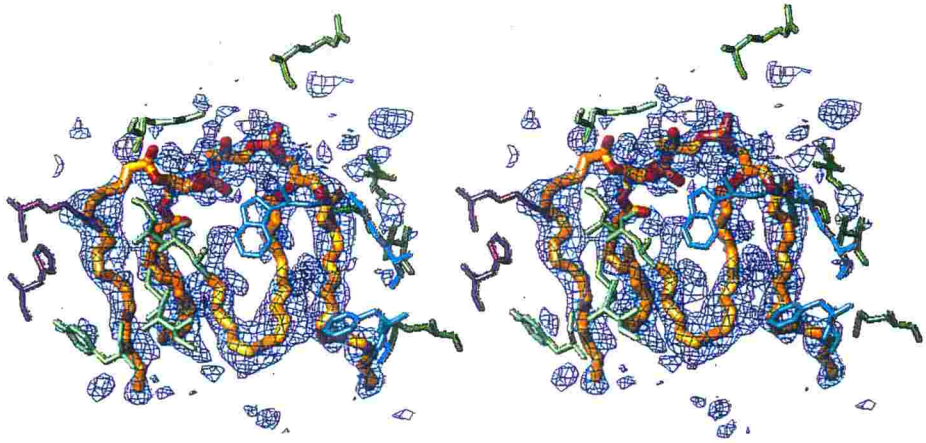

up and down.

All CLs bound to the protein mainly by the hydrophobic interaction between the fatty acids and hydrophobic amino acid residues. Number of hydrogen bonds between each phosphate groups of CL1, CL2, CL3, CL4 and CL5 and protein were 5, 5, 2, 3 and 0, respectively.

The fatty acid tails of CL4 and CL5 with curved structures were fitted well in the electron density (Figure 3.6). The curved structure of CL4 and CL5 was surrounded by several phenylalanine residues. Phe346, Phe414 and Phe418 (subunit I) were placed around the curved fatty acid of CL5. Phe393, Phe397, Phe476 (subunit I), Phe13, Phe28 and Phe29 (subunit VIIc) were placed that of CL4.

Phosphatidylcholine

The head group of this phospholipid is choline, which is the biggest one among phospholipids in this enzyme. Phosphatidylcholine (PC) was identified by the bulky electron density distribution of its head group. PC1 was located among the four subunits I, II, V, and VIc (Figure 3.7). The fatty acid tails were placed in the clear electron density distribution among the helices I and II of subunit II, and subunit VIc. The head group of PC1 was in the low electron density region near the N-terminal of subunit Va

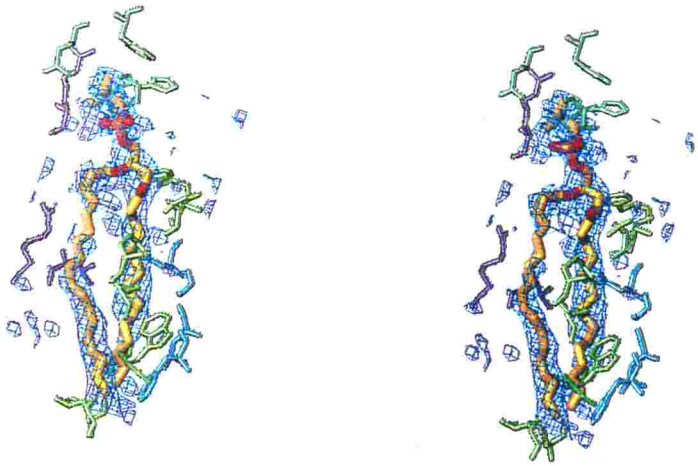

Figure 3.7. Stereoscopic drawing of PC1 is superposed on the (Fo-Fc) difference Fourier map of 2.3 Å resolution analysis at 2.5σ level.

exhibiting disordered conformation. Choline moiety of PC1 interacted with Asp8 (subunit Va) and Arg10 (subunit VIc). PC1 was the only one PC in the enzyme monomer, which is consistent with biochemical analysis, while phosphatidylcholine in the mitochondrial membranes of bovine heart is made up of about 40% of the total lipids. The discrepancy of phospholipid ratios between the enzyme and the membrane implicates that the enzyme incorporated each phospholipid with selectivity.

Phosphatidylethanolamine

Three phosphatidylethanolamines (PEs) were detected in the enzyme monomer (Figure 3.8). PE1 being in subunit III contacted with subunits I and VIa. Many amino acid residues interacted with PE1 not only at fatty acids but also at head group. The ethanolamine moiety of PE1 had hydrogen bonds with Tyr181, Tyr182, Ala184 (subunit III), Phe70 and Asn76 (subunit VIa). One fatty acid tail of PE1 exhibited a curved structure and the other was straight one. Phe203 (subunit III) prevented the fatty acid tail from extending straightly. The double bond of fatty acid was placed at the bending site. PE1, with extended and bent tails, resided in a cavity (Figure 3.9).

PE2 and PE3 were between two monomers. PE2 was located

(a)

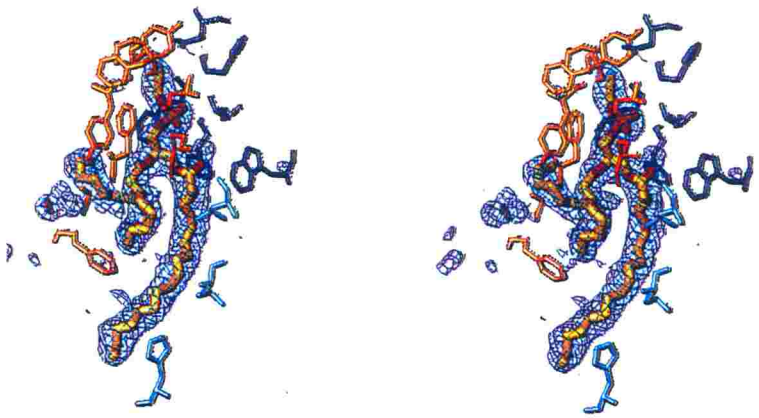

(b)

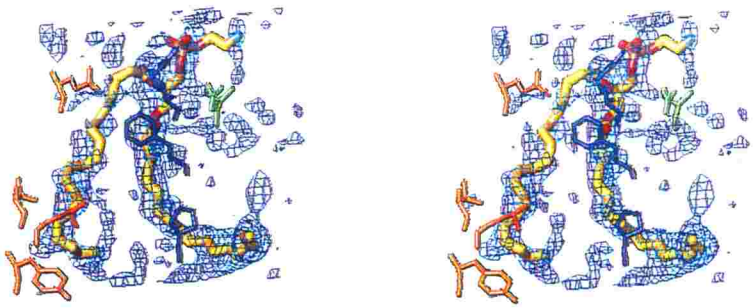

Figure 3.8. Stereoscopic drawing of PE1 (a), PE2 (b) and PE3 (c) are superposed on the (Fo-Fc) difference Fourier map of 2.3 Å resolution analysis at 2.5σ level.

(c)

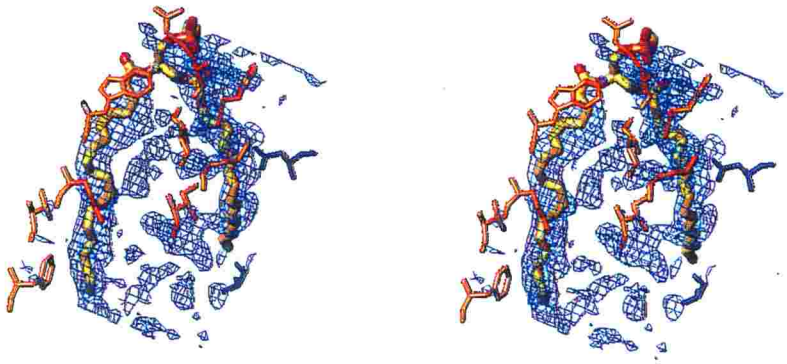

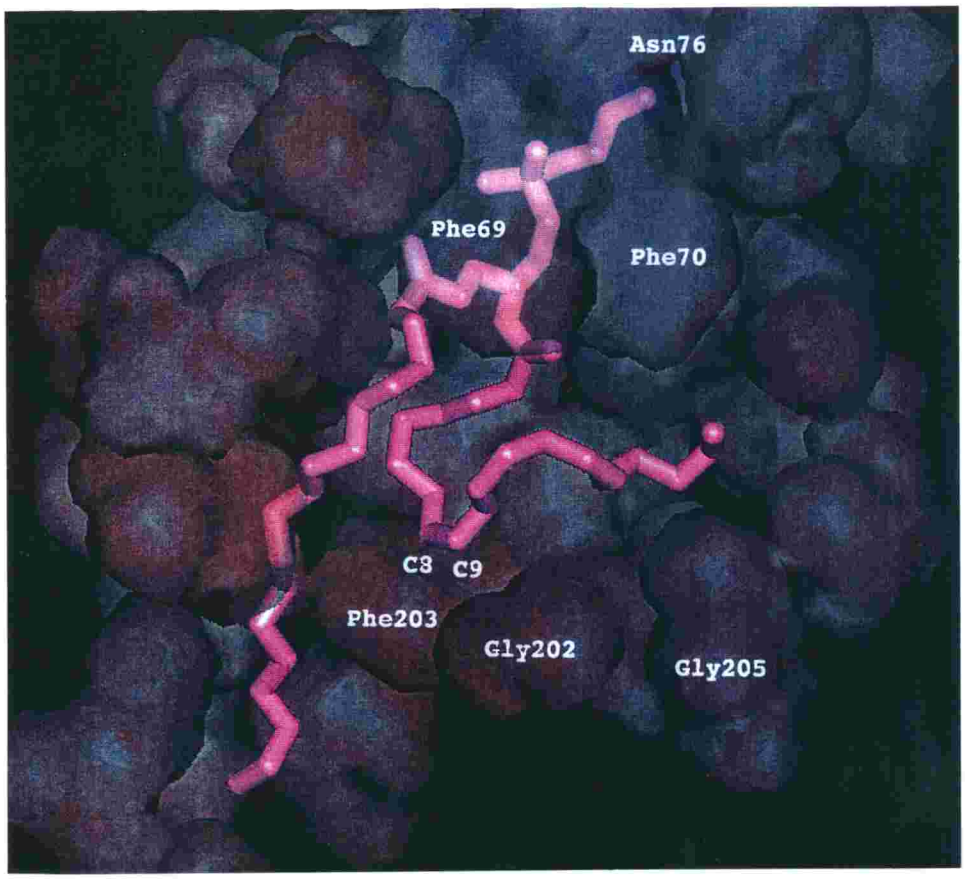

Figure 3.9. Binding site of PE1.

PE1 and amino acid residues interacting with PE1.

nearly a binding site of two monomers, which was the opposite side of CL1. PE3 was located intermonomer space. The fatty acid tails of PE2 and PE3 took straight structures on the surface of the protein complex.

Phosphatidylglycerol

Five phosphatidylglycerols (PGs) were located in the monomeric enzyme (Figure 3.10). PG1 and PG2 were placed in subunit III. They had a lot of interactions with amino acid residues. The head group of PG1 interacted with both acidic and basic amino acids (Arg96 (subunit I), Glu64 and His71 (subunit III)) by forming hydrogen bonds. Since the glycerol head is neutral, it interacted with both acidic and basic amino acids. That of PG2 had hydrogen bonds with Thr66, His226, and His231 (subunit III). PG3, PG4 and PG5 bound to the protein mainly by the hydrophobic interaction of tails. PG3 and PG5 had no hydrogen bonds with protein atoms.

3-4. Conformation of phospholipids

Hydrocarbon tails of phospholipids had high conformational variations among the molecules with the same chemical structure as shown in Figure 3.11. These conformations were strongly affected by the interactions with proteins. B-factors of tails that exposed to

(a)

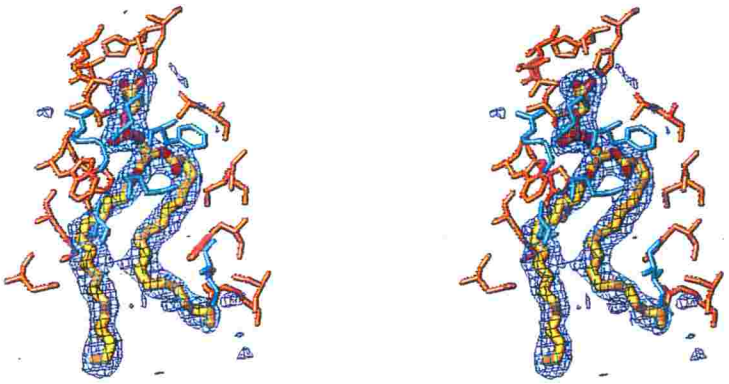

(b)

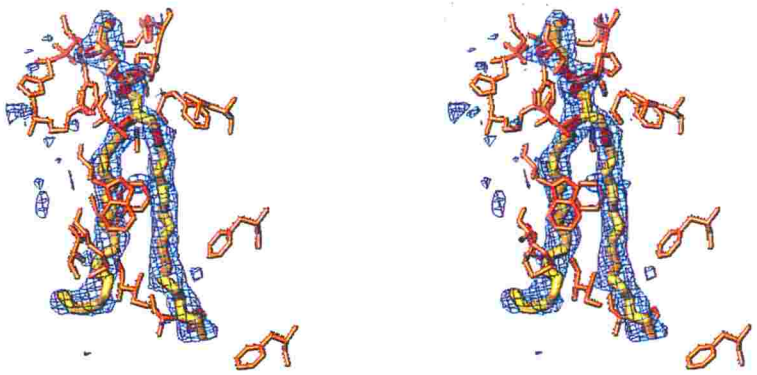

Figure 3.10. Stereoscopic drawing of PG1 (a), PG2 (b), PG3 (c), PG4 (d) and PG5 (e) are superposed on the (Fo-Fc) difference Fourier map of 2.3 Å resolution analysis at 2.5σ level.

(c)

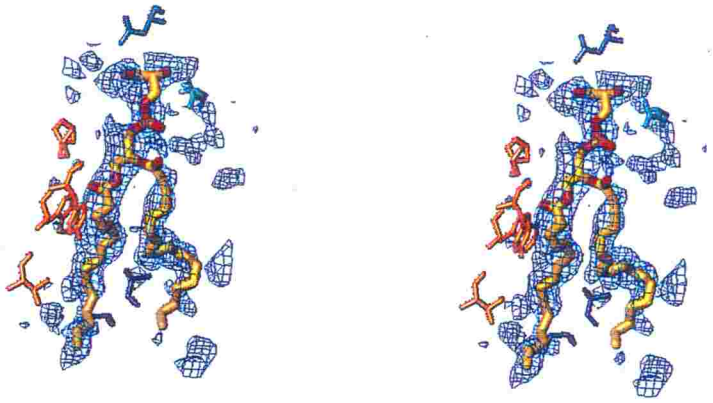

(d)

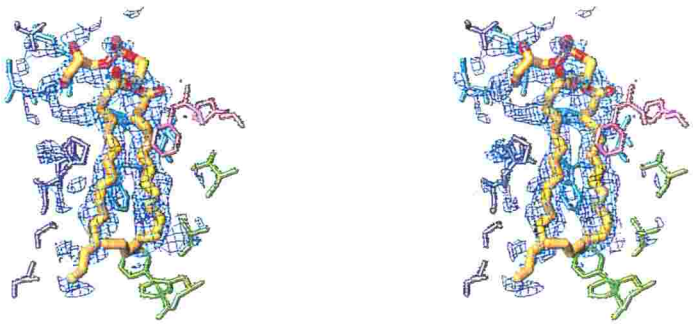

(e)

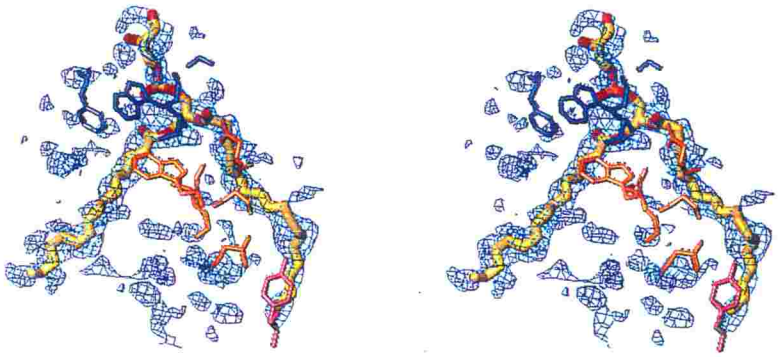

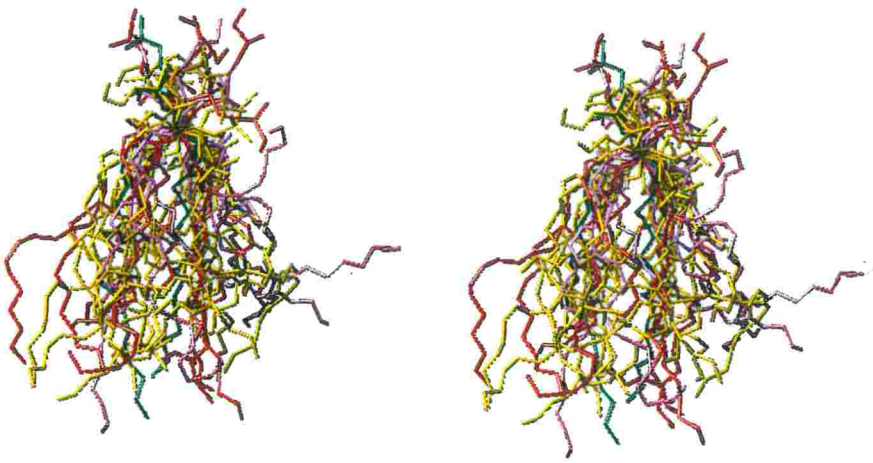

Figure 3.11. Conformational variation of phospholipids are shown by a stereoscopic drawing of 19 molecules supeposed on a standard molecule (1,2-dilauroyl-DL-phosphatidylethanolamine, Elder, 1977), where two pairs of CL tails each consisting of two tails are treated as two independent molecules. CLs, PC, Pes and PGs are colored by yellow, green, purple and red, respectively.

surrounding had significantly higher than those being inside the enzyme molecule. Since tails of phospholipids are flexible, the tails could be accommodated in cavities or cleft with both hydrophobic nature and enough space to hold them. Head groups except for those of PE1, PG1 and PG2 exhibited higher B-factors than those of tails of the same phospholipids. This suggested that head groups were flexible if they had no specific interactions with protein. The phospholipids of membrane are more flexible in conformational state than proteins. Thus phospholipids provide the membrane liquidity.

A phospholipid has an asymmetric carbon atom in glycerol moiety. The absolute configurations of the phospholipids were determined by comparing two independent refinements by the XPLOR. The bond angles and sums of them concerning to non-hydrogen atoms around each asymmetric carbon atom were given in Table 3.2. The sum of the angles for a synthetic organic phospholipid whose structure has been determined by X-ray diffraction method is 327° representing a typical tetrahedral conformation. Out of 19 asymmetric carbon atoms, the sums of three bond angles of 17 R configurations were closer to 327° than those of corresponding S configurations. The average values were 334±5° for the R configuration and 346±8° for the S

Table 3.2. Geometric analysis of asymmetric carbon of glycerol moiety

phospholipid			1*(°)	2#(°)	3§(°)	1+2+3(°)
CL1	C02	R	109.51	110.97	114.33	334.81
		S	110.61	115.00	117.84	343.45
	C08	R	108.57	121.50	108.52	338.59
		S	116.65	127.04	116.29	359.98
CL2	C02	R	114.07	113.18	112.79	340.04
		S	116.13	116.04	112.95	345.12
	C08	R	109.82	110.36	111.11	331.29
		S	118.46	119.74	120.15	358.35
CL3	C02	R	113.09	114.59	110.84	338.52
		S	116.18	116.20	112.27	344.65
	C08	R	113.82	115.20	103.85	332.87
		S	121.54	122.23	113.24	357.01
CL4	C02	R	109.37	107.94	113.70	331.01
		S	112.96	112.48	110.70	336.14
	C08	R	113.51	119.75	114.17	347.43
		S	117.53	122.89	119.58	360.00
CL5	C02	R	116.78	112.44	110.96	340.18
		S	112.52	108.13	114.06	334.71
	C08	R	108.29	111.51	109.98	329.78
		S	116.12	121.83	120.36	358.31
PC1		R	112.25	107.10	110.35	329.70
		S	113.25	113.95	115.95	343.15
PE1		R	104.66	118.77	104.33	327.76
		S	107.80	117.12	110.36	335.28
PE2		R	111.34	115.45	109.68	336.47
		S	113.69	116.17	114.46	344.32
PE3		R	113.51	111.08	107.21	331.80
		S	114.36	118.57	112.74	345.67
PG1		R	114.31	100.67	104.59	319.57
		S	121.92	100.33	106.44	328.69
PG2		R	113.10	104.27	109.84	327.21
		S	117.72	112.37	123.09	353.18
PG3		R	114.64	116.62	110.88	342.14
		S	113.84	117.42	111.18	342.44
PG4		R	106.99	113.97	111.57	332.53
		S	113.04	116.06	113.89	342.99
PG5		R	109.35	113.12	111.58	334.05
		S	111.81	124.16	117.22	353.19

*#§Angle were defined between the C(02)-O(01) bond and the C(02)-C(03)bond, that between C(02)-C(01) bond and the C(02)-C(03) bond and C(02)-O(01) bond and the C(02)-C(01) bond, respectively.

configuration. These angles indicated that the structure with the R configuration was refined with fewer errors than in the case of the S configuration, which exhibited a rather flattened conformation around the asymmetric carbon atoms. Consequently the asymmetric carbon atoms of phospholipids were in the R configuration.

3-5. Interactions of phospholipids and proteins

Intermolecular interactions of phospholipids in the enzyme complex together with evolutional conservatism of amino acid residues are summarized in Table 3.3. Hydrophilic head groups including esters of phospholipids were stabilized by hydrogen bonds with hydrophilic amino acids. Hydrocarbon tails of phospholipids interacted with not only aliphatic hydrophobic amino acids but also aromatic amino acids. Numbers of amino acids interacting with the phospholipids were shown in Table 3.4. The figures in parentheses show the number of amino acids in the extramembrane region. Phe and Leu were the two most amino acid residues among the amino acids interacting with the hydrocarbon tails of the 14 phospholipids, the sum of which reached almost one third of the total residues interacting with tails.

Hydrophobic residues that composed α-helices of the

Table 3.3. Intermolecular interactions of phospholipids within the enzyme dimer and evolutional variation of amino acid residues interacting with phospholipids.

Phospholipid[$]	Subunit*	Amino acid	No. of identical residues[#]	Amino acid	No. of identical residues[#]
CL1					
Tail	(I)	Phe282	21/30	Tyr304	29/30
		Ser307	28/30	Ile311	30/30
	(II)	Ala70	21/30	Ile74	27/30
		Leu78	30/30	Leu81	30/30
	III	Leu131	30/30	Ser135	19/30
		Val142	30/30		
	VIa	Leu23	4/4	Ser27	3/4
		Leu30	4/4	Cys31	4/4
		Leu33	3/4	Asn34	4/4
		Leu37	2/4		
Head	(I)	Asp300	30/30		
	VIa	His38	4/4		
CL2					
Tail	III	Met51	1/30	Leu52	29/30
		Met54	28/30	Tyr55	24/30
		Trp58	30/30	Arg59	30/30
		Ile62	19/30	Thr174	30/30
		Thr213	24/30	Val217	27/30
		Phe220	2/30		
Head	III	Arg63	30/30	His226	30/30
	VIIa	Asp28	3/3		
CL3					
Tail	I	Val350	25/30	Tyr379	30/30
		Phe418	30/30	Asn422	30/30
		Met423	11/30	Phe426	30/30
		His429	30/30	Phe430	30/30
	II	Phe32	24/30	Ser35	24/30
		Leu39	27/30		
Head	II	Gly8	30/30		
	VIc	Arg43	3/3		
CL4					
Tail	I	Thr17	30/30	LEU21	19/30
		Phe22	30/30	Trp25	30/30
		Leu113	28/30	Phe393	30/30
		Phe400	27/30	Ile472	26/30
	VIIc	Ile11	1/3	Phe13	3/3
		Ala23	3/3	Met25	3/3
		Thr26	2/3	Leu27	2/3
		Phe28	1/3	Phe29	3/3
		Ser31	3/3		
	VIII	Val21	2/3	Ser25	1/3
Head	VIIc	Met24	2/3		

CL5					
Tail	I	Trp334	30/30	Phe414	30/30
		Ala415	3/30		
	II	Tyr40	30/30	Ile42	24/30
		Ser43	13/30	Leu46	23/30
		Thr47	21/30		
	IV	Trp78	4/4	Val81	4/4
		Met86	4/4		
	VIc	Arg16	3/3	His20	3/3
PC1					
Tail	I	Phe321	30/30	Leu324	28/30
		Ala325	30/30	His328	28/30
	II	Leu37	30/30	Ile41	22/30
		Met56	17/30	Glu60	30/30
		Val61	20/30	Trp65	30/30
	VIc	Leu17	3/3	Arg18	2/3
Head	Va	His5	3/4	Asp8	4/4
	VIc	Arg10	2/3		
PE1					
Tail	I	His151	29/30	Thr207	30/30
		Leu210	30/30	Leu215	25/30
	III	Tyr181	30/30	Phe198	30/30
		Gly202	30/30	Phe203	30/30
		Gly205	30/30		
	VIa	Trp62	4/4	Phe69	1/4
Head	III	Tyr181	30/30	Tyr182	22/30
		Ala184	22/30	Ile188	29/30
	VIa	Thr68	4/4	Phe70	4/4
		Asn76	4/4		
PE2					
Tail	III	Gln161	27/30	Thr168	1/30
		Leu169	30/30	Tyr172	30/30
	VIa	Arg17	4/4	Phe21	4/4
		Pro26	4/4		
PE3					
Tail	III	Tyr81	30/30	Ile84	30/30
		Leu85	30/30	Ile88	10/30
		Trp240	30/30	Phe244	30/30
		Val47	29/30	Phe251	29/30
	(VIa)	Ala3	4/4	Lys5	4/4
		Asp7	3/4		
PG1					
Tail	I	Met100	30/30	Ile158	30/30
	III	Asn50	18/30	Met54	28/30
		Trp57	30/30	Trp58	30/30
		Leu79	29/30	Gly82	29/30
		Met83	30/30	Phe86	30/30
		Ser89	30/30	Glu90	30/30
Head	I	Phe94	30/30	Pro95	30/30
		Arg96	30/30	Met97	30/30
	III	Trp57	30/30	Glu64	29/30
		His71	30/30		
PG2					
Tail	III	Met54	28/30	Trp58	30/30
		Phe86	30/30	Glu90	30/30

		Phe93	30/30	His207	29/30
		Ile210	30/30	Thr213	24/30
		Phe214	30/30		
Head	III	Thr66	29/30	Arg221	30/30
		His226	30/30	His231	30/30
		Phe233	30/30	Gly234	30/30
PG3					
Tail	III	Thr95	29/30	Trp99	30/30
	(VIa)	Ala1	4/4	Ser2	4/4
PG4					
Tail	I	Asn406	12/30	Thr408	25/30
		Trp409	28/30		
	IV	Thr80	4/4	Ala84	1/4
		Phe87	4/4	Phe88	4/4
	VIIb	Phe9	3/3		
	VIII	Pro12	1/3	Gln15	3/3
		Ala16	3/3	Ser20	3/3
Head	I	Arg480	30/30		
	VIII	Ala6	3/3		
PG5					
Tail	III	Trp34	30/30	Asn38	19/30
		Ser39	27/30	Met40	9/30
		Thr41	11/30		
	VIa	Phe69	1/4		
	VIIa	Tyr45	3/3		

[$]Head represents a head group of phospholipid including esters, and tail, hydrocarbon chain. *Subunit names of the monomer A and B are given without and with parenthesis, respectively. [$]Amino acids each with a residue number cytochrome *c* oxidase which have the same amino acid residue as the bovine heart enzyme in the aligned sequences. Thirty cytochrome *c* oxidase were compared for subunits I, II and III, three or four cytochrome *c* oxidase for the other subunits.

Table 3.4. Numbers of amino acids interacting with phospholipids, where atomic contacts are shorter than 4.0 Å.

Amino acid	Numbers of amino acids interacting with phospholipid	Numbers of amino acids at trans membrane region	Numbers of amino acids in cytochrome *c* oxidase
Phe	35 (11)	74	114
Leu	26 (6)	112	189
His	17 (10)	25	65
Ser	15 (4)	48	115
Thr	15 (5)	57	122
Arg	13 (2)	19	62
Ile	12 (2)	63	100
Tyr	12 (3)	33	72
Trp	11 (2)	30	57
Met	11 (2)	46	76
Ala	10 (4)	66	128
Val	9 (0)	63	113
Asn	8 (5)	14	60
Asp	6 (4)	13	66
Lys	6 (4)	14	81
Gly	6 (2)	56	127
Glu	4 (0)	16	81
Pro	4 (1)	23	98
Gln	3 (1)	11	38
Cys	1 (0)	5	18

The number in parentheses show the number of amino acids in the extramembrane region.

transmembrane part interacted with tails of the phospholipids. Structures of hydrocarbon tails were stabilized by van der Waals contacts and C-H···π bonds, which have been found in organic crystals containing both aliphatic and aromatic groups (Kobayashi, 1993; Hunter, 1994). C2, C5, C25 and C26 of CL4 formed C-H···π bonds to Phe28 (subunit VIIc), Phe13 (subunit VIIc), Trp25 (subunit I) and Trp25 (subunit I), respectively, as shown in Figure 3.12. Other C-H···π interactions are shown in Table 3.5.

Head groups of PE1, PG1 and PG2 were fixed tightly by hydrogen bonds with various amino acid residues conserved during molecular evolution (Table 3.3) and their B-factors were lower than those of protein atoms, and the B-factors of their tails were similar to those of proteins. This implied that high binding specificities of PE1, PG1 and PG2 were effected by the specific hydrogen bonds with amino acid residues as well as by the hydrophobic interactions of their hydrocarbon tails and amino acid residues.

Around the phosphate sites of CL1, CL2, CL3, PC1, PG1 and PG2, a lot of basic amino acid residues such as His and Arg were located (Table 3.6). Ionic interactions contributed in part to hold their structures in the enzyme complex. Each of other phospholipids was mainly fixed by hydrophobic interaction of their tails with proteins.

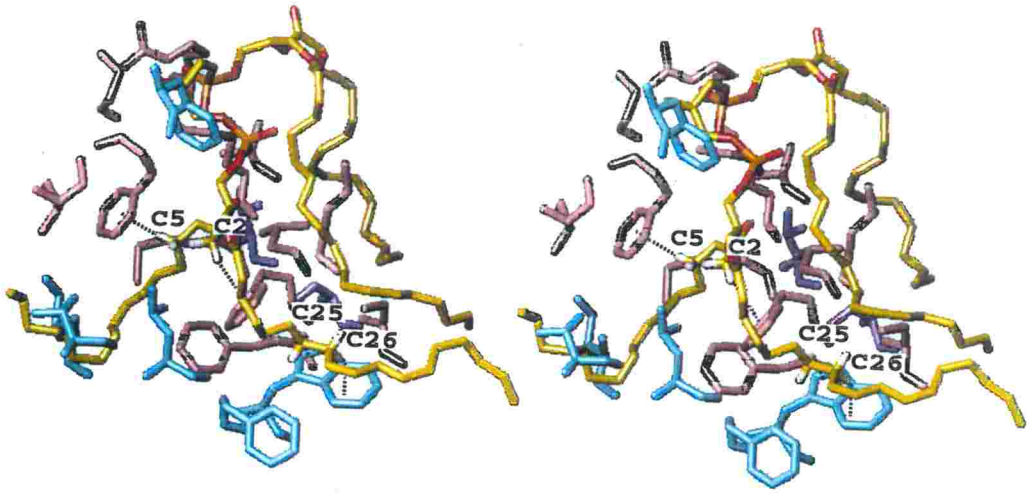

Figure 3.12. C-H···π hydrogen bonding model of the fatty acid of CL4 with aromatic residues of cytochrome *c* oxidase.

Table 3.5. Geometric parameters for CH···π interactions.

	C···π	H···π	Angle (°)
CL2			
C23···Tyr55 (Sub III)	4.11	3.25	152
CL3			
C47···Phe426 (Sub I)	3.34	2.93	115
CL4			
C2 ···Phe28 (Sub VIIc)	3.71	2.91	139
C5 ···Phe13 (Sub VIIc)	3.51	2.81	134
C25···Trp25 (Sub I)	3.50	3.03	119
C26···Trp25 (Sub I)	3.55	2.68	152
CL5			
C2 ···Trp334 (Sub I)	3.50	2.51	175
PE1			
C35···His151 (Sub I)	3.60	3.10	120
PE3			
C17···Phe251 (Sub III)	3.41	3.38	92
PG1			
C21···Trp57 (Sub III)	3.55	2.60	165
PG4			
C8···Trp409 (Sub I)	3.56	2.73	147

C···π: Perpendicular distance of the carbon atom to the ring. H···π: Predicted perpendicular distance of the hydrogen atom to the ring. Angle: Angle between the C-H bond and the perpendicular from the hydrogen atom to the ring plane.

Table 3.6. Protein phospholipid hydrogen bonds.

Amino acid residue			Phospholipid		Distance (Å)
Phosphate group					
His38	ND1	Sub VIa	CL1	O33	3.31
His38	NE2			O12	3.29
				O32	3.30
				O33	3.37
Asp300	OD1	Sub I (B)		O13	3.43
Arg63	NE	Sub III	CL2	O12	3.40
Arg63	NH2			O12	3.02
				O13	3.25
His226	NE2			O33	2.76
Asp28	OD1	Sub VIIa		O13	3.45
Gly8	N	Sub II	CL3	O33	3.23
Arg43	NH1	Sub VIc		O34	2.48
Met24	SD	Sub VIIc	CL4	P02	3.37
				O31	3.46
				O34	2.62
His5	N	Sub Va	PC1	O13	3.45
Ile188	N	Sub III	PE1	O13	2.89
Thr68	OG1	Sub VIa		O14	2.89
Phe70	N			O14	2.66
Phe94	O	Sub I	PG1	O13	3.35
Pro95	N			O13	3.40
Arg96	N			O13	2.88
Arg96	NE			O14	2.88
Arg96	NH2			O12	3.12
				O14	3.46
Met97	N			O13	2.97
Trp57	NE1	Sub III		O14	2.86
Arg221	NH1	Sub III	PG2	O13	3.00
Arg221	NH2			O12	3.30
His231	NE2			O14	3.30
Phe233	N			O14	3.03
Gly234	N			O13	3.03
Head group					
Asp8	OD1	Sub Va	PC1	C07	3.38
Arg10	NE	Sub VIc		C06	3.23
Arg10	NH1			C06	3.16
Tyr181	O	Sub III	PE1	N	2.93
Tyr182	O			N	3.39
ALA184	O			N	3.26
Phe70	O	Sub VIa		N	2.85
Asn76	OD1			N	2.94
Glu64	OE2	Sub III	PG1	O06	2.71
His71	NE2			O06	2.68
Thr66	OG1	Sub III	PG2	O05	2.56
His226	O			O05	2.60
His231	ND1			O06	3.31
Arg480	OG	Sub I	PG4	O06	3.30
Arg480	NE			O06	3.21
Arg480	NH2			O06	2.88

ALA6	N	Sub VIII		O05	3.32
Ester group					
Tyr55	OH	Sub III	CL2	O22	3.47
Lys411	NZ	Sub I	CL5	O03	3.35
Thr47	O			O21	3.47
Glu77	OE2	Sub IV		O04	3.37
Trp78	N			O04	3.26
Asp57	N	Sub II	PC1	O04	3.35
Trp58	NE1	Sub III	PG1	O04	2.55

Based on the distance criteria 2.5 Å < distance < 3.5 Å

Chapter 4. Function of the phospholipids in cytochrome c oxidase

4-1. Roles in structural organization of the enzyme

Phospholipid interactions with protein subunits were shown in Table 4.1. In cytochrome *c* oxidase, all the phospholipids interacted with several subunits except for PG2, which was buried in subunit III to stabilize the subunit structure (Figure 4.1). When the surface structure of the enzyme was examined without any phospholipids present, there were many deep clefts or cavities between protein subunits. Phospholipids filled these inter-subunit spaces to stabilize the complex structure.

PG1, lying in a V-shaped cavity of subunit III, contacted partly with subunit I and its head group formed highly ordered hydrogen bonds with subunits I and III. A hydrocarbon tail of PE1 in the V-shaped cavity of subunit III contacted with subunit I. Thus, both PG1 and PE1 contributed toward making tight connections between subunit I and III. The hydrophilic head of PE1 surrounded by subunits III and VIa formed hydrogen bonds with amino acids of both subunits.

Thus PC1 and PG4 connected four subunits together. PC1 had interactions with subunits I, II, Va and VIc at four,

Table 4.1. Location of phospholipids in the crystal structure.

Phospholipids	Subunits	Helices interacting with hydrocarbon		Level
		Subunit	helix	
CL1	III, VIa	III	IV	I
	I, II (B mol)	I	VII, VIII	
		II	II	
CL2	III, VIIa	III	II, V, VI	M
CL3	I, II, VIc	I	IX, X, XI	I
		II	I	
CL4	I, VIIc, VIII	I	I, III, X, XII	M
CL5	I, II, IV	I	IX, XI	M
		II	I, II	
PC1	I, II, Va, VIc	I	VIII	M
		II	I, II	
PE1	I, III, VIa	I	IV, V	I
		III	V, VI	
PE2	III, VIa	III	V	M
	II (B mol)	II	II	
PE3	III	III	III, VII	M
	VIa (B mol)			
PG1	I, III	I	III, IV	M
		III	II, III	
PG2	III	III	II, III, VI, VII	M
PG3	III	III	III	I
	VIa (B mol)			
PG4	I, IV, VIIb, VIII	I	XI	M
PG5	III, VIa, VIIa	III	I	I

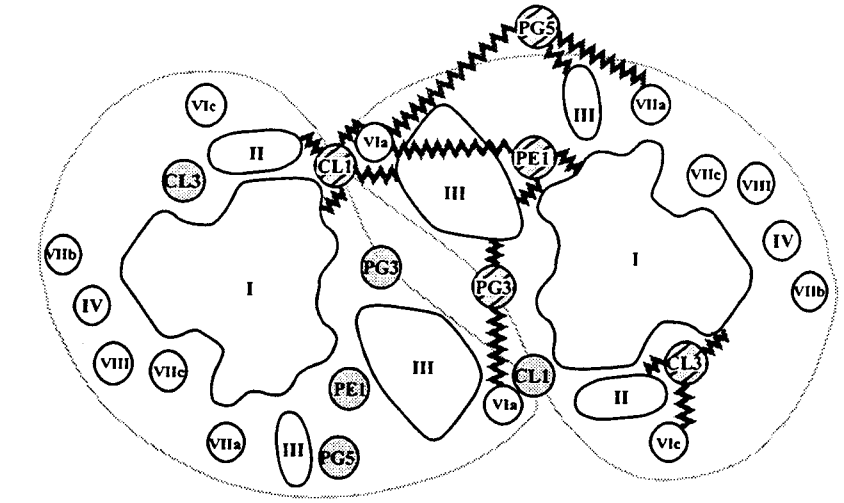

(a) Intermembarne half

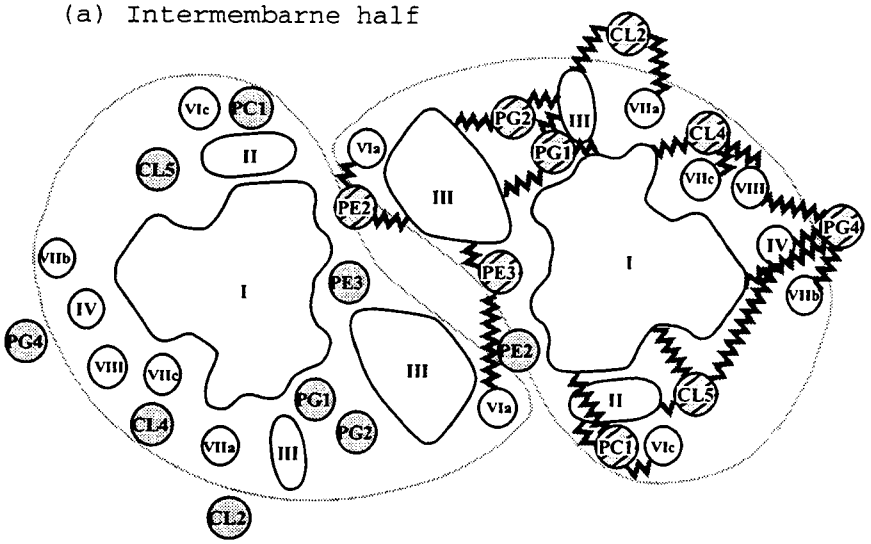

(b) Matrix half

Figure 4.1. Schematic representations of inter molecular bonds among protein subunits as a cross section at the membrane surface.

(a) Intermembrane half

(b) Matrix half

Black letters indicated subunits and phospholipids, respectively. Inter molecular bonds depicted by a notched line.

six, two and three sites, respectively. PG4 had interactions with subunits I, IV, VIIb and VIII at four, four, one and five sites, respectively. Number of hydrophobic interactions of PC1 and PG4 were 12 and 11, respectively. They contacted with these subunits mainly by the hydrophobic interaction. The head of PC1 formed hydrogen bonds with subunits II, Va and VIc. Glycerol group of PG4 bridged subunits I and VIII with hydrogen bonds.

Phosphate groups of CL2 and CL3 bridged two subunits by forming hydrogen bonds with Arg63, His226 (subunit III) and Asp28 (subunit VIIa). CL3 made hydrogen bonds with Gly8 (subunit II) and Arg43 (subunit VIc).

All phospholipids interacted with core subunit (subunit I, II and III). Each nuclear coded subunit of subunit IV, VIa, VIc, VIIa, VIIb, VIIc and VIII that had a transmembrane α-helix, contacted with at least one phospholipids. Phospholipids served to strengthen the interactions between core subunits and nuclear coded subunits surrounding the core subunits.

Cytochrome *c* oxidase from bovine heart takes the dimeric structure not only in the orthorhombic crystal but also the hexagonal and tetragonal crystals (Lee et al., 1999). It suggests that the dimer is a physiologically active form.

Only PE2 had been between monomers in the previous

X-ray structure of cytochrome *c* oxidase at 2.8 Å resolution. Structural analysis of phospholipid at 2.3 Å resolution revealed four phospholipids interacting with both A and B monomers. They were CL1, PE2, PE3, and PG3. CL1 and PE2 were located near an interaction site of two monomers. CL1 at the intermembrane side and PE2 at the matrix side faced to each other with their tails. CL1 bridged the two monomers by interactions with subunits III and VIa of monomer A and with subunits I and II of monomer B. Fatty acid tails of CL1 interacted with monomer A at 10 sites, and with monomer B at eight sites. Head group of CL1 had a salt bridge to His38 of subunit VIa of monomer A. One of the hydrocarbon tail of PE2 contacted both subunits III and VIa of the same monomer, while the other tail filled the inter-monomer space between subunit VIa of monomer A and subunits I and II of monomer B.

PE3 and PG3 were located at the intermembrane side in the inter-monomer space, which was large enough to contain several phospholipids. PE3 interacted with subunit III of monomer A at eight sites, and with subunit VIa of monomer B at three sites. PG3 contacted with subunit III of monomer A at two sites, and with subunit VIa of monomer B at two sites.

N-terminal of subunit VIa makes inter monomer

interaction at the matrix side to stabilize dimeric structure of cytochrome *c* oxidase (Lee et al., 1999). CL1, PE3, and PG3 were involved in the formation of the dimeric structure at both the intermembrane and the matrix sides.

4-2. A pool of oxygen molecule

Three phospholipids, PE1, PG1 and PG2 were included in the V-shape space of subunit III of the cytochrome *c* oxidase from bovine heart as described previously. They were fixed tightly in the subunit by hydrogen bonds around head groups (Figure 4.2) and by hydrophobic interaction around tails. PE1 and PG1 contacted with subunit I. They form hydrophobic space accessible to the hydrophobic part of lipid bilayer via CL2 and PG5 as shown as Figure 4.3. The hydrophobic cavity has higher affinity to dioxygen molecules with hydrophobic nature than protein part. Thus dioxygen molecules should be accumulated in the cavity. Since the fatty acid space had an open space to the hydrophobic part of the lipid bilayer, it might function as a funnel to introduce dioxygen molecules efficiently from the membrane to the dioxygen reduction center. A clear electron density corresponding to a dioxygen molecule was located between PG1 and PG2 in the lipid pool. The dioxygen molecules stored in the cavity were transferred to the active

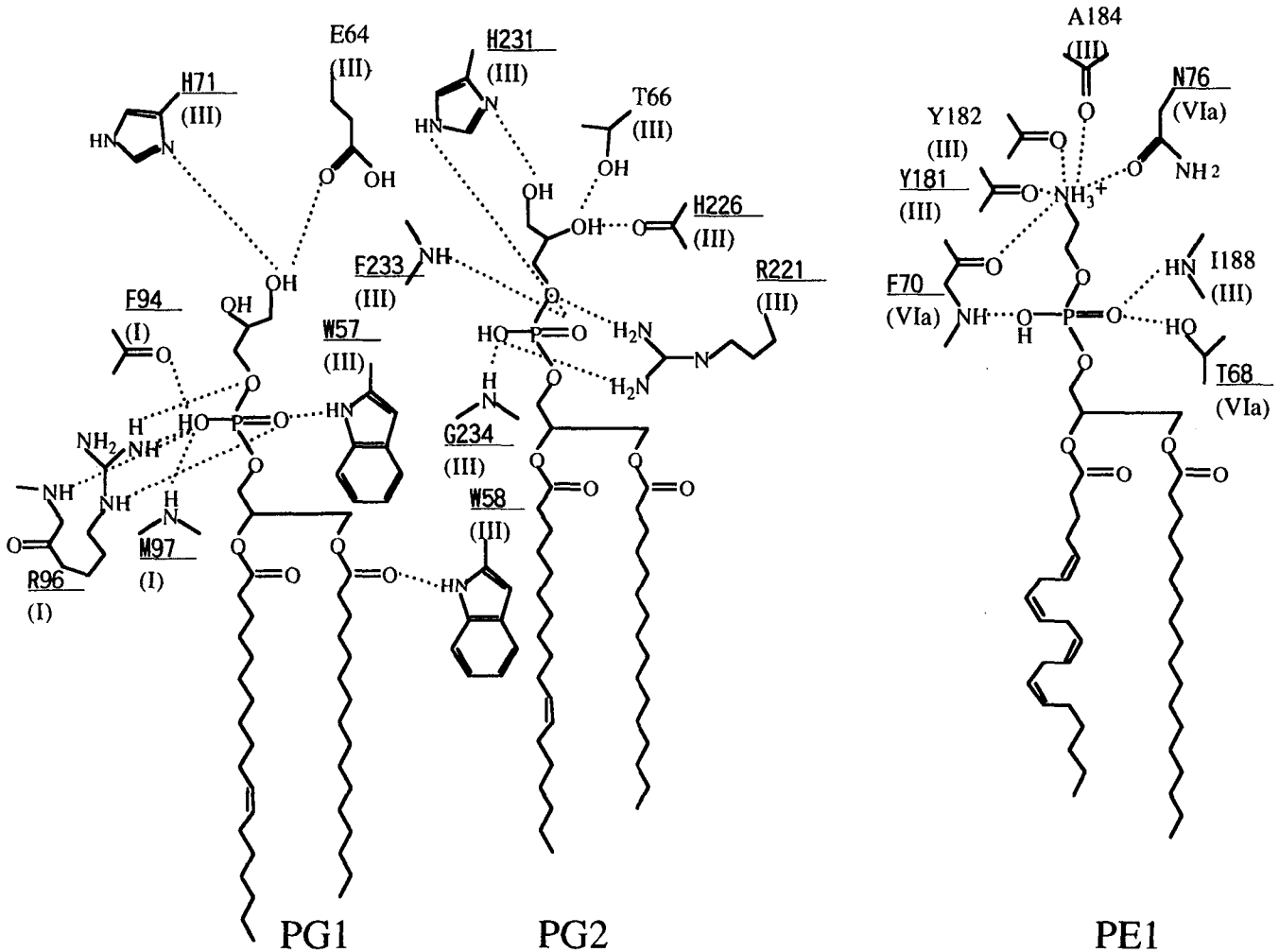

Figure 4.2. Hydrogen bonds between hydrophilic head groups including esters of three tightly bound phospholipids, PE1, PG1 and PG2, and protein residues are schematically drawn. Each hydrogen bonds is depicted by a broken line. The residues identical among all the species so far known are underlined.

center through one of three dioxygen channels to the heme a_3-Cu_B active center proposed previously (Tsukihara et al., 1996). The channel reaches to the reaction center from the phospholipid space to the reaction center along the amino acid residues of His151, Leu199, Phe67, Phe238, Phe235, Trp126, and Trp236. Since the hydrophobic channel is loosely packed, the dioxygen molecule could pass through to the oxygen binding site. This pathway is shown in Figure 4.3.

Out of 51 amino acid residues of subunits I and III interacting with PE1, PG1 and PG2, 34 residues were completely conserved among 30 species so far known. Four of five amino acid residues of subunit VIa interacting with these phospholipids were identical among four species. The identity scores were significantly higher than the averaged values of 0.55 for the subunits I and III, and 0.60 for the subunit VIa. Especially, amino acid residues, which interact with glycerol group of PG1 and PG2, were highly conserved. These amino acid residues bound selectively to glycerol group. The amino acid residues around tails of PE1, PG1 and PG2 highly conservative among molecular evolutions made specific interaction with these phospholipids.

4-3. Functional implications of cardiolipins in the respiratory enzyme complex.

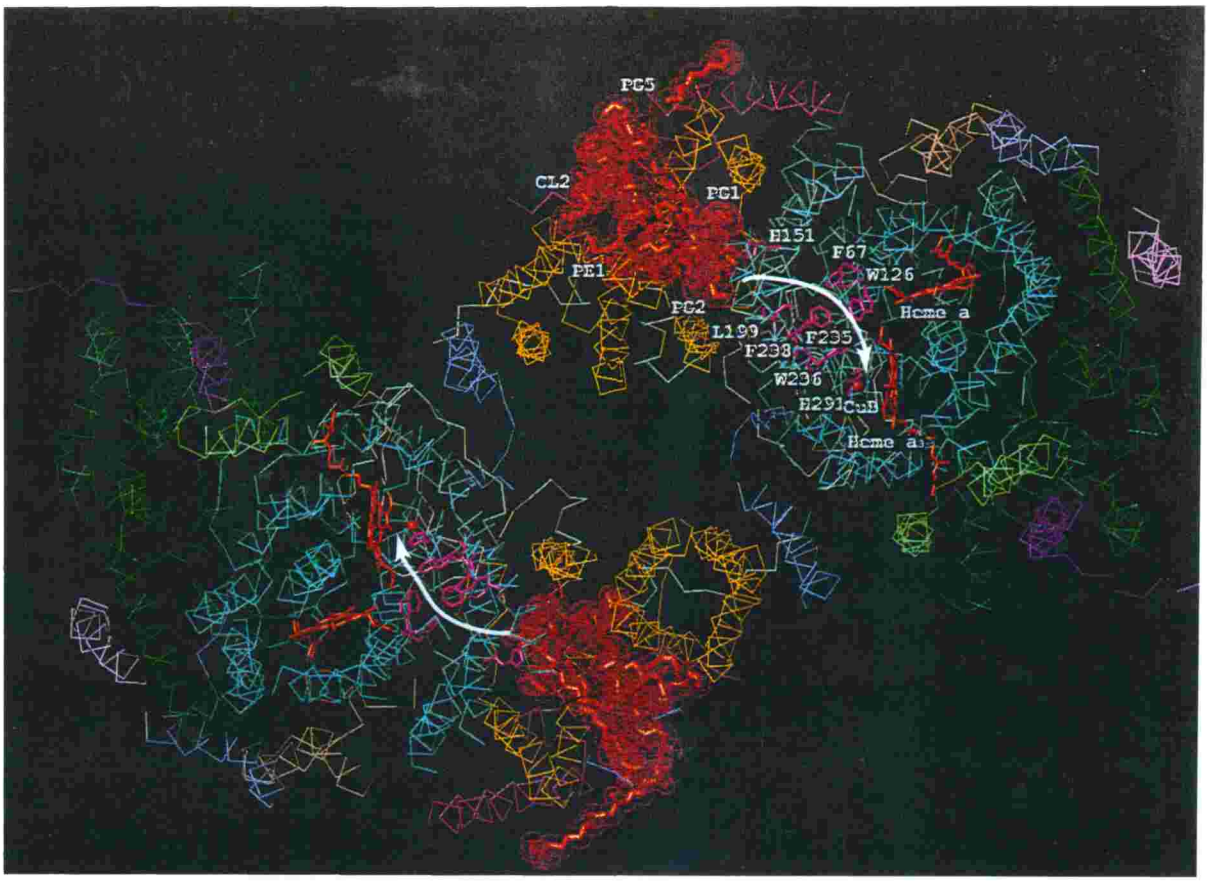

Figure 4.3. Dioxygen pool and a possible O_2 channel. PE1, PG1, PG2, PG5 and CL5 are depicated by heavy red sticks with dot surfaces of space filling models. Red sticks are hemes. CuB are red sphere. Aromatic and hydrophobic amino acid residues along the possible pathway of O_2 indicated by white arrows are represented by pink sticks. A cross section with 20 Å thickness of protein subunits.

Biochemical studies suggest that at least two CLs are required for full electron transport activity of the enzyme. Since CL1 bridged tightly two monomers of the dimer, removing the CL1 from the enzyme should lose the dimeric structure of the enzyme (Chapter 4.2). One of cardiolipins affects the rate of electron transport (Fry & Green, 1980; Robinson et al., 1980; Fry & Green, 1981; Vik et al., 1981). A cleft close to the CL1 could hold cytochrome *c* molecule (Banci et al., 1997) (Figure 4.4.a, b). This site was a possible lower affinity site of cytochrome *c* (Ferguson-Miller et al., 1976, 1978; Capaldi et al., 1984; Michel et al., 1982; Capaldi, 1996). Then Glu89 (sub II of B mol), Glu43 (sub VIa of A mol) and phosphate of CL1 were on the interface of cleft. These residues should make ionic interactions with lysine residues around the heme edge of cytochrome *c*. CL1 was necessary to keep the dimeric structure and it made the lower affinity site of cytochrome *c*.

A tail of CL4 took an unique structure among 14 phospholipids. The hydrocarbon tail extending into the protein with a parallel orientation to the membrane surface. Interacting with helices I, X and XII of subunit I and with a helix of subunit VIIc, the hydrocarbon tail of CL4 reached closely to the end of hydroxyfarnesylethyl group of heme a as schematically shown in Figure 4.5. The tail bent at

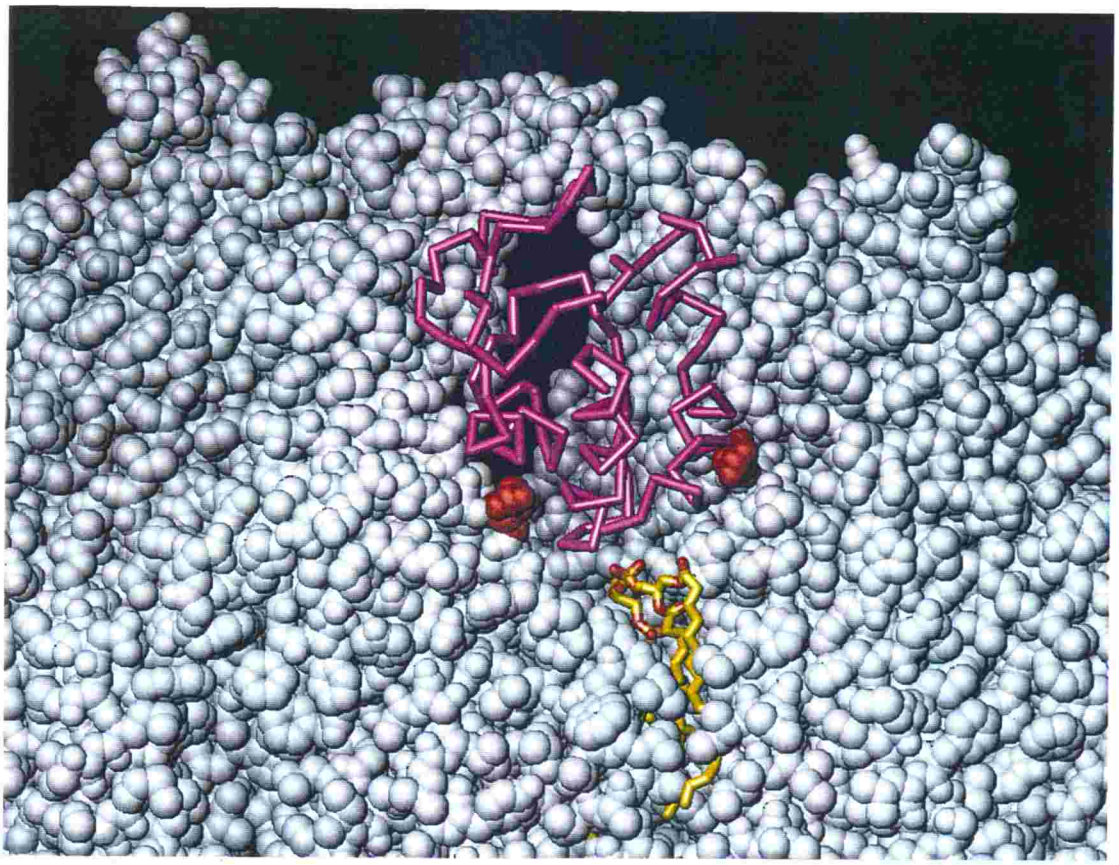

Figure 4.4. Lower affinity site of cytochrome *c* presumed by the surface structure of the enzyme.

a. A cave was found at the upper of the CL1. Pink wire model is a horse heart cytochrome *c* and sticks colored by yellow is CL1. Protein subunits are drawn by space filling models. Red models show E89 (sub II, right) and E43 (sub VIa, left).

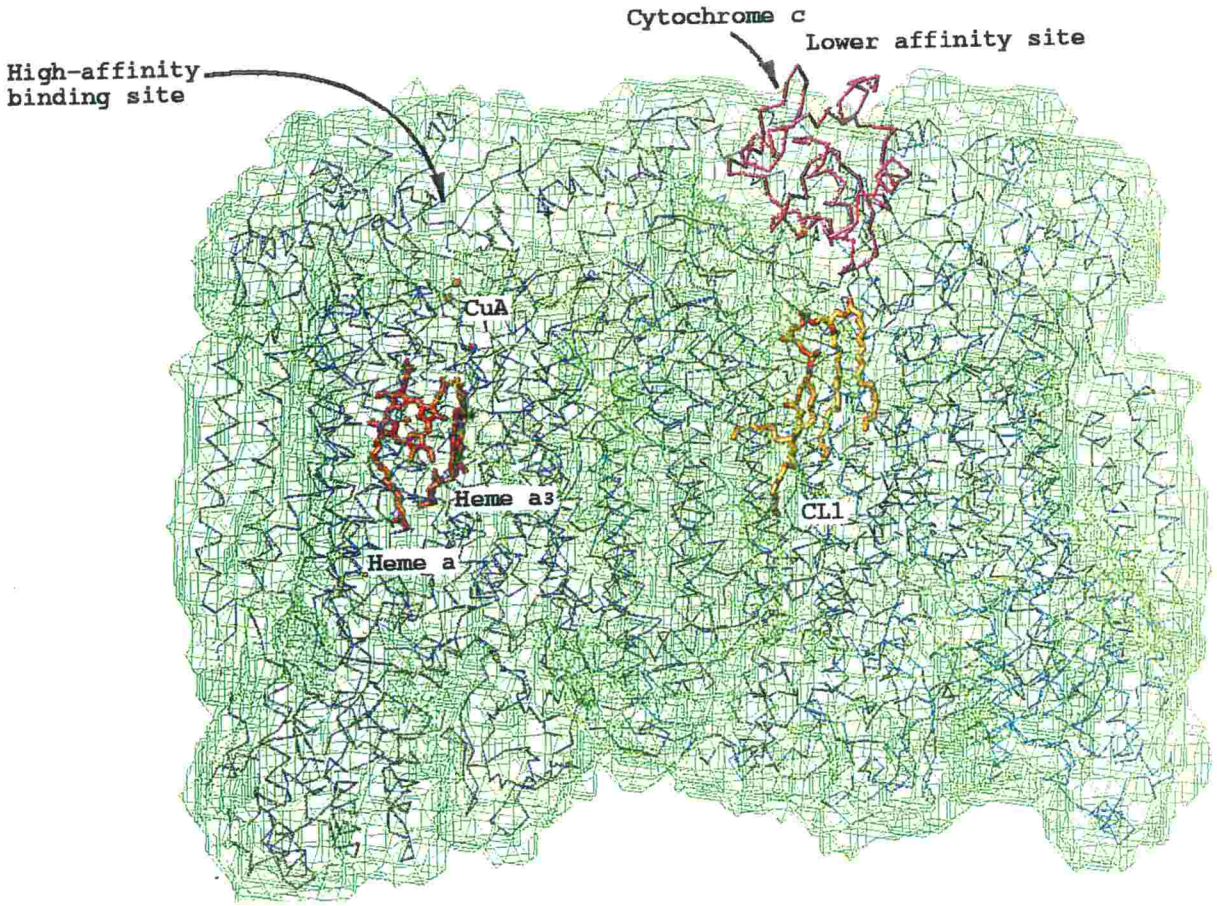

b. Lower affinity site and high affinity site of cytochrome *c*. Lower affinity site was placed the model of horse heart cytochrome *c*. High affinity site is electron entry site, which is close to the Cu_A site.

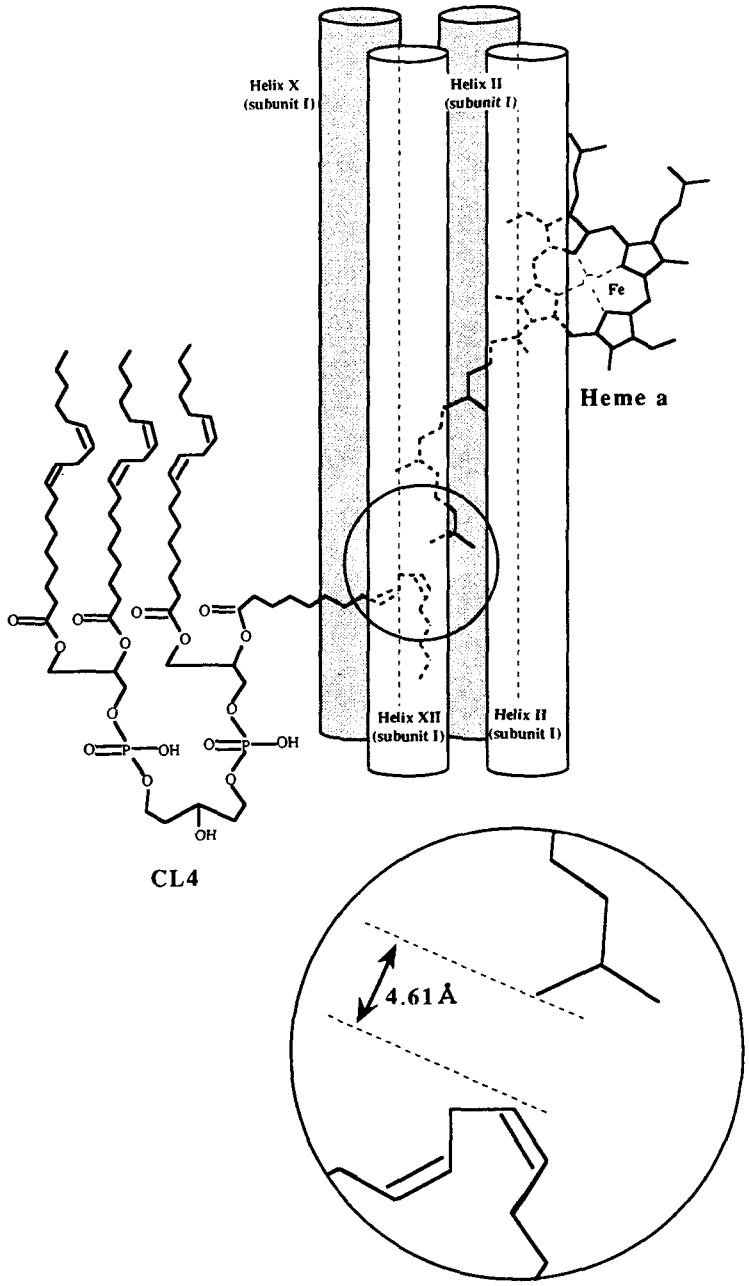

Figure 4.5. Schematic representations of interaction between farnesyl ethyl group of heme a and phospholipid. Heme a and CL4 corked cavities, which made from four α-helices.

a double bond C12-C13. The C12 of CL4 were located as closely as 4.61 Å from the end of farnesyl ethyl group of heme a. Phenylalanine residues (Phe393, Phe397 in subunit I) were close to this bending position. Phe393 prevented the fatty acid of CL4 from making a straight conformation. Phenylalanines (phe400, and 476 in subunit I, Phe13, 28, and 29 in subunit VIIc) as well as Phe393 and Phe397 around the fatty acid tail of CL4 were placed. Many C-H$\cdots\pi$ bonds were found between the fatty acid of CL4 and the aromatic groups. These phenylalanines were conserved among molecular evolution of cytochrome *c* oxidase.

The hydroxyfarnesylethyl group of heme a was located along a possible proton channel (Tsukihara et al., 1996) (Figure 4.6). If CL4 was removed from the enzyme, packing of farnesylethyl group and helices including helix XII of subunit I would be affected to perturb the structure of proton channel. Peroxidation of the double bond may prevent CL4 from residing in the proper site interacting with heme a. Thus the peroxidation of CL reduce the activity of this enzyme (Paradies et al., 1997, 1998).

Fatty acid tails of CL1 made the dimeric structure and the tail of CL4 extending to the farnesylethyl group of heme a prepared the possible proton channel, while the phosphate groups of CL1 forms the lower affinity site of

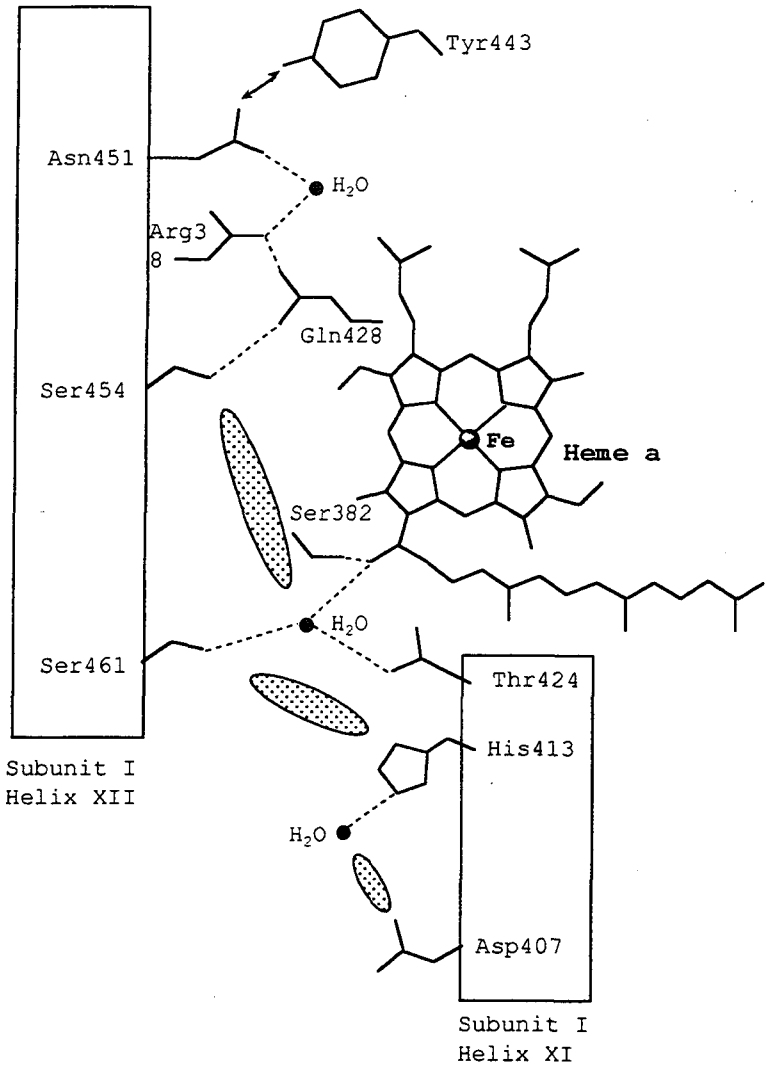

Figure 4.6. Schematic representation of candidates for proton channel.

Dark ovals, dotted lines, and dotted lines with arrows denote internal cavities, hydrogen bonds, and possible hydrogen bond structure, respectively.

This network contains Asp407 at the entrance of the network on the matrix side and only one possible hydrogen bond structure between Asn451 and Tyr443.

cytochrome *c*. Various phospholipid experiments show that cardiolipin influences the activity of the cytochrome *c* oxidase and the fatty acid is more important than the head group (Robinson et al., 1990). These biochemical experiments are consistent with the present CL studies.

Chapter 5. Conclusion

Structures of fourteen phospholipids included in membrane protein were determined by 2.3 Å X-ray structural analysis of cytochrome *c* oxidase from bovine heart. They included five cardiolipins, one phosphatidyl choline, three phosphatidyl ethanolamines, and five phosphatidyl glycerols. So many phospholipids were found in the membrane protein for the first time.

All phospholipids occupied designated sites in the enzyme complex and entered into specific interactions with amino acid residues as if they were co-factors. Then they bound to the protein by the hydrophobic interaction between the fatty acid and hydrophobic amino acid and also by salt bridges or hydrogen bonds between polar head groups and amino acid. A lot of C-H$\cdots\pi$ bonds existed between fatty acids and such aromatic residues as phenylalanine or tryptophan. Absolute configuration of any asymmetric carbon atom in glycerol moiety of each phospholipid was determined as R configuration.

Following functions of the phospholipids were implicated in cytochrome *c* oxidase. The first is the pasting role among proteins subunits within the monomer. Phospholipids stabilize the quaternary structure by binding

the α-helices of several subunits. The second function is assisting formation of dimeric structure. CL1, PE2, PE3 and PG3 are directly involved in the formation of the dimeric structure of the enzyme. The third role is a dioxygen pool. The V-shaped cavity of subunit III filled by PE1, PG1, and PG2 pools dioxygen molecules, which move to the Fe_{a3}-Cu_B active center.

Two cardiolipins among five cardiolipins were identified as molecules essential for enzyme activity. CL1 makes the dimeric structure and forms the lower affinity site of cytochrome *c*. Fatty acid tail of CL4 extending to the farnesylethyl group of heme a prepared the possible proton channel.

References

Ames, B.N., Shigenaga, M.K. & Hagen, T.M. (1995) *Biochem. Biophys. Acta.* **1271**, 165-170.

Anderson, S., Bankier, A.T., Barrell, B.G., DE Bruijn, M.H.L., Coulson, A.R., Drouin, J., Eperon, I.C., Nierlich, D.P., Roe, B.A., Sanger, F., Schreier, P.H., Smith, A.J.H., Staden, R., Young, I.G. (1981) *Nature* **290**, 457-465.

Anderson, S., DE Bruijn, M.H.L., Coulson, A.R., Eperon, I.C., Sanger, F., Young, I.G. (1982) *J. Mol. Biol.* **156**, 683-717.

Antalis, T.M., Palmer, G. (1982) *J. Biol. Chem.* **257**, 6194-6206.

Anthony, G., Reiman, A., Kadenbach, B. (1993) *Proc. Natl. Acad. Sci. USA* **90**, 1652-1656.

Awasthi, Y.C., Chuang, T.F., Keenam, T.W. & Crane, F.L. (1971) *Biochem. Biophys. Acta.* **226**, 42-52.

Babcock, H. & Wikström, M. (1992) *Nature* **356**, 301-309

Banci, L., Bertini, I., Gray, H.B., Luchinat, C., Reddig, T., Rosato, A., Turano, P. (1997) *Biochemistry* **36** 9867-9877.

Bisson, R., Jacobs, B., Capaldi, R.A. (1980) *Biochemistry* **19**, 4173-4178.

Bricogne, G. (1974) *Acta Cryst.* **A30,** 395-405.

Brünger, A.T. (1988) *J. Mol. Biol.* **203**, 803-816.

Capaldi, R.A. (1990) *Annu. Rev. Biochem.* **59**, 569-596.

Capaldi, R.A. (1996) *Nat. Struct. Biol.* **3**, 570-574.

Capaldi, R.A., Darley-Usmar V.M., Fuller S.D., Millett F. (1982) *FEBS Lett.* **138**, 1-7.

Cawtan, K. (1994) in *Joint CCP4 and ESF-EACBM Newsleter on Protein Crystallography* **31**, 34-38.

Cullis, P.R. & De Kruijff, B. (1979) *Biochem. Biophys. Acta.* **559**, 399-420.

Eilers, M., Endo, T. & Schatz, G. (1989) *J. Biol. Chem.* **264**, 2945-2950.

Endo, T., Eilers, M. & Schatz, G. (1989) *J. Biol. Chem.* **264**, 2951-2956.

Essen, L.O., Siegert, R., Lehmann, W.D., Oesterhelt, D. (1998) *Proc. Natl. Acad. Sci. USA* **95**, 11673-11678.

Ferguson-Miller, S., Brautigan, D.L., Margoliash, E. (1976) *J. Biol. Chem.* **251**, 1104-1115.

Ferguson-Miller, S., Brautigan, D.L., Margoliash, E. (1978) *J. Biol. Chem.* **253**, 149-159.

Fry, M., Blondin, G.A., Green, D.E. (1980) *J. Biol. Chem.* **255**, 9967-9970.

Fry, M. & Green, D.E., (1981) *J. Biol. Chem.* **256,** 1874-1880.

Gadaleta, G., Pepe, G., DE Candia, G., Quagliariello, C.,

Sbisa, E., Saccone, C., (1989) *J. Mol. Evol.* **28**, 497-516.

Gazzotti, P., Bock, H. & Fleischer, S. (1975) *J. Biol. Chem.* **250**, 5782-5790.

Grabau, E.A., Gengenbach, B.G. (1989) *Plant Mol. Biol.* **13**, 595-597.

Grigorieff, N., Ceska, T.A., Downing, K.H., Baldwin, J.M., Henderson, R. (1996) *J. Mol. Biol.* **259**, 393-421.

Harlos, K., Eibl, H., Pascher, I. & Sundell, S. (1984) *Chem. Phys. Lipids.* **34**, 115-126.

Hauser, H., Pascher, I. & Sundell, S. (1980) *J. Mol. Biol.* **137**, 249-264.

Hitchcock, P.B., Mason, R., Thomas, K. M. & Shipley, G.G. (1974) *Proc. Natl. Acad. Sci. USA.* **71**, 3036-3040.

Hoch, F.L. (1992) *Biochem. Biophys. Acta.* **1113**, 71-133.

Hunter, R., Haueisen, R.H. & Irving, A. (1994) *Angew. Chem. Int. Ed. Engl.* **33**, 566-567.

Iwata, S., Ostermeier, C., Ludwig, B., Michel, H. (1995) *Nature* **376**, 660-669.

Kabsch, W. (1976) *Acta. Cryst.* **A32** 922-923.

Kadenbach, B. & Merle, P. (1981) *FEBS Lett.* **135**, 1-11.

Kadenbach, B., Ungibaver, U., Jaraush, J., Buge, U. & Kuhn-Neurwig, L. (1983) *Trends Biochem. Sci.* **8**, 398-440.

Kobayashi, K., Asakawa, Y., Kikuchi, Y., Toi, H., Aoyama,

Y. (1993) *J. Am. Chem. Soc.* **115**, 2648-2654.

Krebs, J.J., Hauser, H. & Carafoli, E. (1979) *J. Biol. Chem.* **254**, 5308-5316.

Lee, S.J., Yamashita, E., Abe, T., Fukumoto, Y., Tsukihara, T., Shinzawa-Ito, K., Yoshikawa, S. (1999) *J. Biol. Chem.* (submitted)

Low, B.W., Chen, C.C.H., Berger, J.E. & Pletcher, J.F. (1966) *Proc. Natl. Acad. Sci. USA* **56**, 1746-1750.

Luzzati, V. (1952) *Acta Crystallogr.* **5**, 802-810.

Maeshima, M., Nakagawa, T., Asahi, T. (1987) *Seikagaku* **59**, 1040-1042.

Malmström, B.G. (1990) *Chem. Rev.* **90**, 1247-1260.

Meinecke, L., Buse, G. (1986) *Biol. Chem. Hoppe-Seyler.* **367**, 67-73.

Michel, B., Bosshard, H.R. (1984) *J. Biol. Chem.* **259**, 10085-10091.

Otwinowski, Z., & Minor, W. (1997) *Macromolecular Crystallography, part A*, 307-326.

Paradies, G., Ruggiero, F.M., Petrosillo, G., Quagliariello, E. (1997) *FEBS Lett.* **406**, 136-138.

Paradies, G., Ruggiero, F.M., Petrosillo, G., Quagliariello, E. (1998) *FEBS Lett.* **424**, 155-158.

Pascher, I. & S.Sundell. (1977) *Chem. Phys. Lipids.* **20**, 175-191.

Pascher, I., Sundell, S., Harlos, K. & Eibl, H. (1987) *Biochem. Biophys. Acta.* **896**, 77-88.

Pearson, R.H. & Pascher, I. (1979) *Nature* **281**, 499-501.

Prochaska, L.J., Bisson, R., Capaldi, R.A., Steffens, G.C.M., Buse, G. (1981) *Biochem. Biophys. Acta.* **637**, 360-373.

Raitio, M., Jalli T., Saraste M. (1987) *EMBO J.* **6**, 2825-2833.

Rand, R.P. & Sengupta, S. (1972) *Biochem. Biophys. Acta.* **255**, 484-492.

Read, R.J. (1986) *Acta Cryst.* **A42**,140-149.

Rees, D.C., Deantonio, L., Eisenberg, D. (1989) *Science* **245**, 510-513.

Robinson, N.C. (1993) *J. Bioenerg. Biomembr.* **25**, 153-163.

Robinson, N.C., Strey, F., Talbert, L. (1980) *Biochemistry* **19**, 3656-3661.

Robinson, N.C., Zborowski, J., Talbert, L.H. (1990) *Biochemistry* **29**, 8962-8969.

Rossmann, M.G. & Blow, D.M. (1962) *Acta Cryst.* **15**, 24-31.

Salamon, Z., Tollin, G. (1996) *Biophys J.* **71**, 858-867.

Schuller D. (1996) *Acta Cryst.* **D52,** 425-434.

Seelan, R.S., Grossman, L.I. (1992) *Biochemistry* **31**, 4696-4704.

Seelig, A., Seelig, J. (1985) *Biochim. Biophys. Acta.* **815**, 153-158.

Shigenaga, M.K., Hagen, T.M. & Ames, B.N. (1994) *Proc. Natl. Acad. Sci. USA* **91**, 10771-10778.

Soulimane, T., Buse, G. (1995) *Eur. J. Biochem.* **227**, 588-595.

Thalenfeld, B.E., Tzagoloff, A., (1980) *J. Biol. Chem.* **255**, 6173-6180.

Thiel, C., Kadenbach, B., (1989) *FEBS-Lett.* **251**, 270-274.

Tsukihara, T., Aoyama, H., Yamashita, E., Tomizaki, T., Yamaguchi, H., Shinzawa-Ito, K., Nakashima, R., Yaono, R. & Yoshikawa, S (1995) *Science* **272**, 1069-1074.

Tsukihara, T., Aoyama, H., Yamashita, E., Tomizaki, T., Yamaguchi, H., Shinzawa-Ito, K., Nakashima, R., Yaono, R. & Yoshikawa, S (1996) *Science* **272**, 1136-1144.

Vik, S.B., Georgevich, G., Capaldi, R.A. (1981) *Proc. Natl. Acad. Sci. USA* **78**, 3178-3187.

Visawamitra, M.A., Radhakrishnan, R., Bandekar, J., Desiraju, G.R. (1993) *J. Am. Chem. Soc.* **115**, 4868-4869.

Yoshikawa, S., Shinzawa-Ito, K., Nakashima, R., Yaono, R., Yamashita, E., Inoue, N., Yao, M., Fei, M. J., Libeu, C. P., Mizushima, T., Yamaguchi, H., Tomizaki, T. & Tsukihara, T. (1998) *Science* **280**, 1723-1728.

List of publications

1) Redox-Coupled Crystal Structural changes in Bovine Heart Cytochrome c Oxidase
S. Yoshikawa, K. Shinzawa-Ito, R. Nakashima, R. Yaono, E. Yamashita, N. Inoue, M. Yao, M. Fei, C.P. Libeu, T. Mizushima, H. Yamaguchi, T. Tomizaki, & T. Tsukihara
Science (1998) **280**, 1723-1728.

2) Structures and Functions of Phospholipids in a Membrane Protein Complex, Bovine Heart Cytochrome *c* Oxidase
T. Mizushima, R. Nakashima, E. Yamashita, M. Yao, T. Tsukihara, K. Shinzawa-Ito & S. Yoshikawa
Science (To be submitted)

Other related papers

1) Ordered structure of the crystallized bovine 20S proteasome
Y. Morimoto, T. Mizushima, A. Yagi, N. Tanahashi, K. Tanaka, A. Ichihara, T. Tsukihara
J. Biochem. (1995) **117**, 471-474.

2) X-ray structure of algal b-carbonic anhydrase reveals a novel catalytic center for CO2 hydration.

S. Mitsuhashi, T. Mizushima, E. Yamashita, M. Yamamoto, T. Kumasaka, H. Moriyama, T. Ueki, S. Miyachi & T. Tsukihara

EMBO J. (Submitted)